
# UHF RFID Tags Mountable on Metallic and Challenging Objects

by

**Abed Pour Sohrab**

Thesis submitted in accordance with the requirements for the award of the degree of Doctor of Philosophy of the University of Liverpool

November 2017

*To my dear parents and brothers.*

# Acknowledgements

First of all, I would like to express my deep gratitude to my supervisor, Professor Yi Huang for offering me this opportunity. His kind support and fruitful advices motivated me during the whole time of my studies. I would like to thank Dr. Paul Carter the founder of Aeternum LLC not only for providing financial support to this project but also for his supportive attitude and helpful ideas.

Special thanks to Dr. Zhirun Hu and his Ph.D student Mr. Ting Leng from University of Manchester for providing us with lab facilities for testing our designs.

Thanks to Alien Technology Corporation for providing us with RFID tag and chip samples.

Thanks to Elsevier Books and Cambridge University Press publication for offering the permission to reproduce some of the figures from their published books in Chapter 2 and Chapter 7.

I would like to thank Dr. Muaad Naser Hussein and Dr. Muayad Kod, for their contribution and collaboration in editing the published papers of this research and also for their friendly support. Thanks to all my friends and colleagues in the RF group for providing such a lovely environment for research.

Finally, thanks to my parents for their invaluable support. This journey would have never been possible without them.

# Abstract

Radio frequency identification (RFID) technology has been developing rapidly during the past years. It has been replacing optical barcodes and has found many applications beyond tagging and tracking objects. Despite their undeniable advantages, passive RFID tags working in the ultra-high frequency (UHF) band are sensitive to the host material and their performance is affected when attached to different materials. Although there are robust tag designs, the fabrication is costly. The motivation of this research is to study the effect of the challenging materials on the tags and find solutions for robust cost-effective designs.

Liquid bottles are one of the challenging objects for RFID tags. The study on the equivalent circuit of a typical tag which is basically a dipole antenna shows the liquid increases the loss resistance of the antenna and affects the impedance matching between the antenna and the chip. Two extra arms are added to the antenna in the suggested solution to alleviate the destructive effect of the liquid. The read range of the tag is improved without increasing the size of the design.

Study of the detuning effect shows that the capacitances in the antenna are the most sensitive elements. The presented theoretical analysis reveals that less capacitance in the feed point and more capacitance in the dipole arms lead to more robustness of the tag performance to the host material. Based on this finding a low cost 3D tag is designed.

The label-type dipole tags offer desirable uniform radiation pattern but are not functional on metallic objects. On the other hand the patch antennas are not efficient on non-metallic objects in terms of read range and radiation pattern. A novel hybrid tag is proposed which has the advantage of both types of antenna. The simple groundless design works in two modes. It acts as a dipole antenna in off-metal mode and a patch antenna in on-metal mode. The measurement result shows an outstanding performance on different materials.

Protecting the antenna from metallic background using an artificial ground plane composed of periodic structures is a practiced method. Mushroom unit cell is the most common structure used as artificial ground but the need for via increases the

fabrication cost. It is shown that the fabrication cost can be reduced by eliminating the via and having a uni-planar structure.

There has been many works in the literature proposing tag designs robust to the host material but what makes this works distinct from the previous works is in depth study on the effect of the challenging material on the performance of the tag antenna and identifying the main reason of the read range degradation for the first time. The findings of this study can be used for designing cost effective tags with improved read range. Analysis of the different parts of the tag antenna and their sensitivity to the host material is also performed for the first time in this thesis. The result of this study shows how the shape of the tag can determine the robustness to the host material. In addition to novel tag designs proposed in this thesis, a straightforward strategy for designing optimum tags is also introduced. This novel method helps the tag designers to modify the primary design step by step and reach the optimum result in a short time.

# Table of Contents

# Acronyms

| | |
|---|---|
| **ASIC** | Application Specific Integrated Circuit |
| **EBG** | Electromagnetic Band Gap |
| **EIRP** | Effective Isotropic Radiated Power |
| **EPC** | Electronic Product Code |
| **ERP** | Effective Radiated Power |
| **FET** | Field-Effect Transistor |
| **HF** | High Frequency |
| **HIS** | High Impedance Surface |
| **IFF** | Identification, Friend or Foe |
| **IoT** | Internet of Things |
| **ISO** | International Organization for Standardization |
| **LF** | Low Frequency |
| **NFC** | Near Field Communication |
| **PEC** | Perfect Electric Conductor |
| **PIFA** | Planar Inverted-F Antenna |
| **PMC** | Perfect Magnetic Conductor |
| **RFID** | Radio Frequency Identification |
| **UHF** | Ultra High Frequency |

# Chapter 1. Introduction

The evolution of new technologies and their application in modern societies is an undeniable fact nowadays. Using advanced automated systems are being part of our daily life. They facilitate providing different services to a large number of individuals which saves time and reduces the errors caused by human interferences. For example, it is not easy to imagine shopping in a store where the goods are not tagged with optical barcode or driving in a crowded highway where there is no automatic toll collection system. Radio frequency identification (RFID) is an evolving technology that has been replacing the optical barcode recently for tagging and tracking objects. The barcode system is suffering from a limited data capacity, a short read range which needs to be in the line of sight and a slow rate of read that means the objects need to be read one by one. On the other hand, the RFID system working in ultra-high frequency (UHF) band offers more data capacity with higher read range which does not necessarily need to be in the line of sight and it is possible to read more than one object at the same time. The strengths of the optical barcode are low production cost and reliability on different materials. Whereas, the UHF RFID tag is not able to offer the two mentioned factors simultaneously. The low cost tags are not reliable on different materials and the robust tags are costly. The motivation and objectives of the work in this thesis is explained in this chapter, followed by the achievements and the structure of the thesis.

# 1.1. Motivation and Objectives

The robustness of the tag to the host material is an important factor which determines the reliability in performance in any application of UHF RFID technology including tagging and tracking objects. As can be inferred from the title of the thesis "UHF RFID tags mountable on metallic and challenging objects", metallic objects are one of the challenging host materials for RFID tags. The other challenging materials that are studied in this thesis are liquid filled bottles and objects with high dielectric constant. There has been many works in the literature offering robust tags to the host material. The aim of this thesis is to propose new designs and analyse the details answering questions that are not covered by previous works. The objectives of this study can be summarized as follows:

- Identifying the effect of liquid bottle on the performance of a typical dipole tag from the equivalent circuit point of view and offering a solution to the problem of degrading the read range based on the findings.
- Identifying the most sensitive parts of a typical dipole tag to material with high dielectric constant and discovering the relation between the shape of the design and the robustness to host material.
- Proposing a novel design that offers an optimum performance for a different range of materials in terms of reading range and radiation pattern.
- Proposing a novel artificial ground plane for protecting dipole tags and offering a solution to the problem of existing complicated structures.

As the size and cost of the tag are two important factors, in all the proposed designs in this thesis the performance of the tag is improved without increasing the size and cost of the prototype.

# 1.2. Thesis Structure and Outcome

The structure of the thesis and the outcome and achievements of each chapter is discussed briefly in this section to give a better view about the work. The chapters are organized as follows:

- In **Chapter 2**, a brief introduction about the RFID technology and its applications is given. The history of the system, different types of tag, working frequency, and communication protocols are discussed.
- In **Chapter 3**, the contents are focused on the passive UHF RFID tag which is the main subject of this thesis. Different parts of a passive tag are introduced and some important principles and expressions in designing tags are explained. The effect of material with high dielectric constant on two commercial tags are simulated and analysed. Finally, a comprehensive literature review on tags working on liquid bottles and metallic objects is presented in this chapter.
- In **Chapter 4**, the effect of the liquid bottle on the performance of a tag is analysed and a novel design is proposed based on the findings to tackle the destructive effect of the liquid on the performance. The improvement in the read range is achieved without increasing the dimensions of the tag.
- In **Chapter 5**, the most sensitive parts of a passive tag are identified and based on the findings a simple design robust to host material is proposed. In another study, a dual-polarized antenna is designed which is mountable on metallic objects and is insensitive to the angle of the polarization.
- In **Chapter 6**, a novel hybrid robust tag is proposed which offers an optimum performance on a wide range of material. The tag is the first design which can be transformed from a dipole antenna to a patch antenna simply by putting it on a metallic object.
- In **Chapter 7**, a brief introduction of periodic structures in designing artificial ground plane for protecting dipole tags is given. These structures are analysed and a literature review of their application in tag design is presented. Finally, a novel design with simple structure for protecting dipole tags is proposed. The result of this study can also be used in antenna designs in other frequencies and applications.
- In **Chapter 8**, the conclusion of the study is summarized and the possible future work and future of the RFID technology is discussed.

# Chapter 2. Basics of RFID Technology

The contents of this chapter give a brief introduction to RFID technology. The main components of an entire system are introduced and the history of the evolution of this technology is reviewed. Different types of tags in terms of power consumption are introduced and their characteristics and applications are discussed. The regulated frequency bands used for RFID systems are presented. The application, advantages, and drawbacks of the systems working in different frequencies are presented. The communication protocol and code standards are reviewed. Finally, the relationship between the cost and market trend of RFID technology is reviewed in this chapter.

# 2.1. Introduction to RFID

Radio frequency identification (RFID) is a wireless communication technology that is used to uniquely tag and identify any object or target which can be a human as well. This technology has found various applications. The most common applications are:

- Supply chain and pallet tracking.
- Access control systems, such as keyless entry and employee identification devices.
- Automatic toll collection systems that is usually used at the entrance of tunnels, highways, and bridges.
- Animal tracking which is used for pets and also wild animals.
- Vehicle tracking and immobilizer.
- Wrist and ankle band for infant ID and security [1].

The application of RFID technology is not limited to the list above. By integrating some other technologies with RFID systems the application can be extended to:

- Car parking capacity management systems.
- Different types of sensor systems such as gas detector and container level indicator.
- Indoor positioning and navigation.
- Implantable devices and body centric wireless sensing [2].

Each application mentioned above demands different category of RFID technology in terms of working frequency band, read range, size and other characteristics.

## 2.1.1. Components of an RFID System

An RFID system is comprised of two main parts:

- The tag or transponder which is attached on the object that needs to be tracked.
- The reader or interrogator which is a read only or read/write device depending on the technology.

The main parts of an RFID system are depicted in Fig. 2.1.

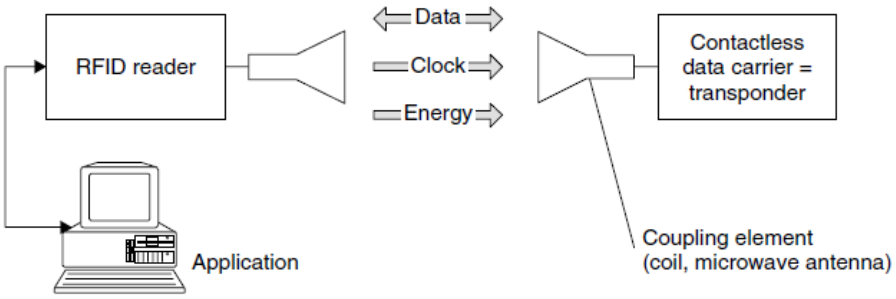


**Fig. 2.1. Main components of an RFID system [3].**

The system may employ a coupling element coil or a microwave antenna (depending on the technology) and the working frequency band. The tag (transponder) contains the identification data. This data is retrieved to the reader and analysed in the application unit. As can be seen in Fig. 2.1, the reader also sends energy to the tag. This energy is vital for running passive tags. Different types of tags and the details of the communication system and protocol are discussed in this chapter but a brief history of the technology will be given first in the following.

# 2.2. History of RFID Technology

Although RFID technology has been mostly developed recently, it has a long history which goes back to World War II. The basic principles of this technology such as modulated backscatter was defined during that time when the researchers were looking for a solution to identify the friend and enemy aircrafts using radar systems. This research led to development of the "Identification, Friend or Foe (IFF)" system later during the war.

The first basic example of passive modulated backscatter for identification was used by German air force in the late 30s. The pilots received an indication while their aircraft was illuminated by friend radar then they performed a manoeuvre by rolling the aircraft as illustrated in Fig. 2.2. This action changed the backscattered signal from their airplanes. The modulated backscatter signal caused a blip on the radar screen which helped the radar operators to identify the friend aircrafts. Although this method was simple and effective, it was not secure as any aircraft could roll and pretend to be friend. In other words, the data capacity of this method is just one bit.

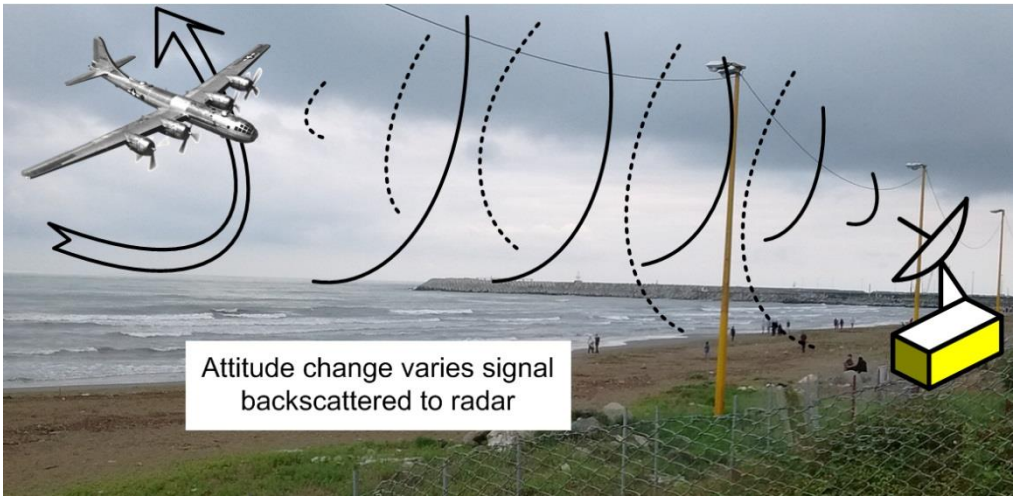


**Fig. 2.2. Backscattered radiation to communicate with a radar operator.**

More secure IFF systems were developed by United States and Britain later. An active beacon was employed on the airplane. The first systems of this generation were called XAE and Mark I which were used in 1937 and 1938 respectively [4]. The improved version Mark III was widely used by Britain, USA, and Soviet Union during the war had the capacity of six identification codes which is equivalent to 2.5 bits of data [5].

The first work about using of backscattered radiation for communication was published in 1948 by Harry Stockman [6]. The working principle of his device is depicted in Fig. 2.3.

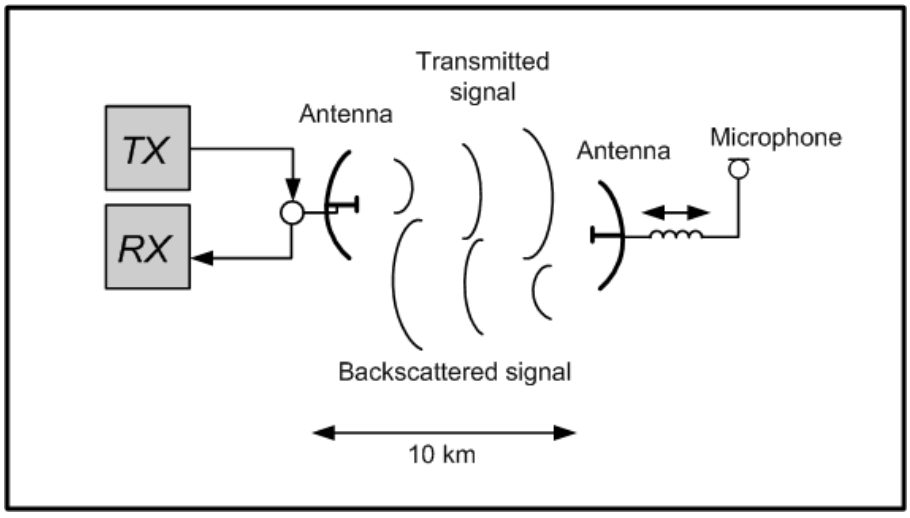


**Fig. 2.3. Communication by means of reflected power.**

The position of the receiving antenna is modulated by a typical microphone and speaker coil which lead to a backscattered modulation in the signal. The modulated signal can be detected at the other side of the link and the sound is reproduced.

The investigation on the passive backscattered continued in 50s. Methods for harvesting the energy of the received signal were proposed. Using a diode and capacitor circuit for rectifying and saving the energy of the received signal was proposed by Crump in the patent documented in 1956 [7]. The harvested energy is used to power an oscillator producing identifying signal in another frequency as depicted in Fig. 2.4.

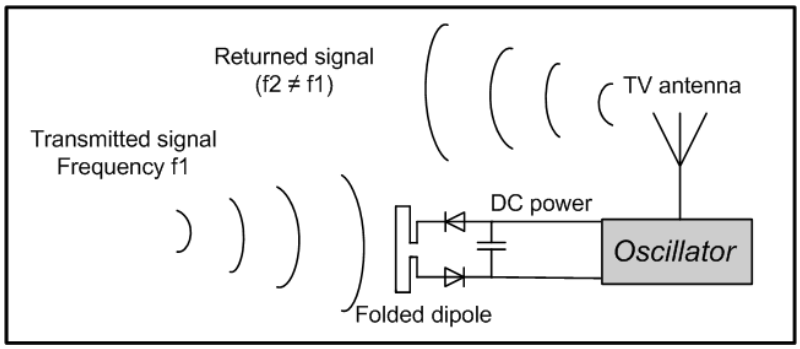


**Fig. 2.4. Passive retransmitting identification system using oscillator driven by DC power harvested from incoming RF.**

A long read range is not necessary in many applications such as door security systems where a close contact is suitable for identification. Investigation on inductively coupled RFID systems was developed in 60s. In the work patented by Walton in 1973 the RFID tag is inductively coupled to the reader coil [8]. The proposed system is shown in Fig. 2.5.

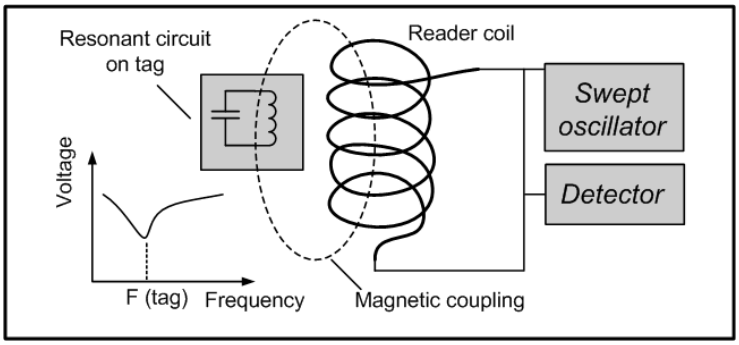


**Fig. 2.5. Resonant circuit coupled to a reader coil acts as an identifying tag.**

The reader performs a frequency sweep and detects the resonant frequency of the tag. The data capacity of this system is more than one bit because the resonant frequency of the tag can be changed by altering the coil length and also a tag can have more than one resonant frequency.

The investigation in 70s was mostly focused on developing RFID systems with more security and data capacity while consuming low power. The researchers applied the energy harvesting method with newer semiconductor technology and proposed the load modulation as a simple and efficient way to backscatter the signal. An early work was done by Koelle in 1975 [9]. The block diagram of his system is depicted in Fig. 2.6. The working principle of any passive RFID tag is similar to this since 1975. Several large and small companies began to emerge in 70s with commercial RFID products. Different organizations in public and private sectors showed interest in these products and the commercial RFID era began in late 70s [1].

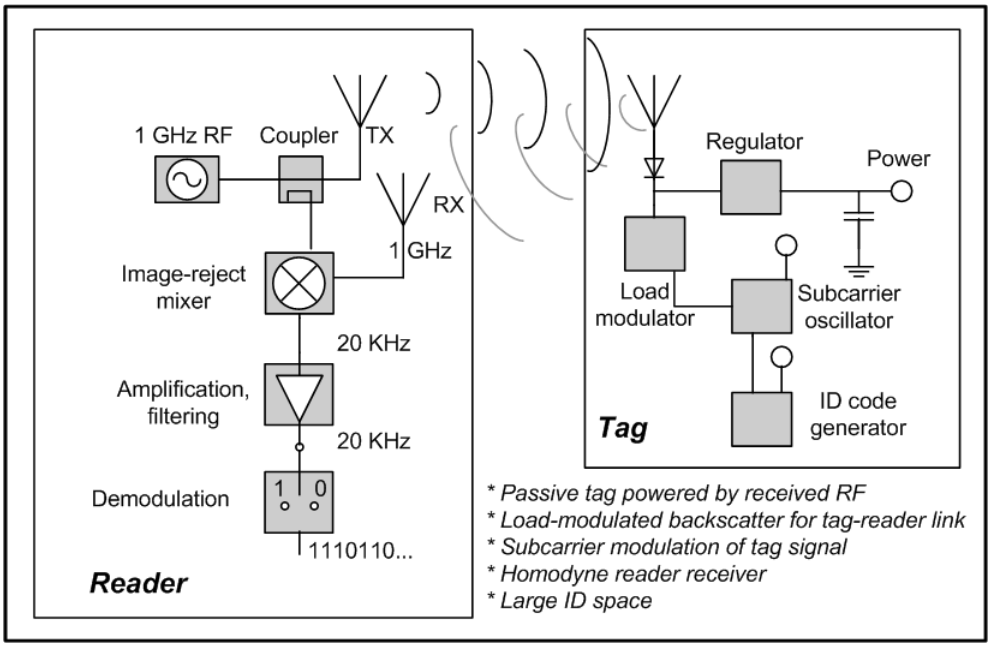


**Fig. 2.6. An early UHF passive tag system.**

The widespread commercial RFID systems evolved in 80s. Livestock management, keyless entry and personnel access systems were available in the market. The world's first toll application was installed in Norway and USA at that time. Despite this success, the growth of the technology was slow due to high cost of the system and lack of the competition between companies [1]. RFID transponders

were using CMOS digital circuitry at that time. However, the size of the circuits was still a limiting factor. Normally, half of the area of the tag was occupied by circuits. This restriction is evident in sample of tags shown in Fig. 2.7 (a), (b).

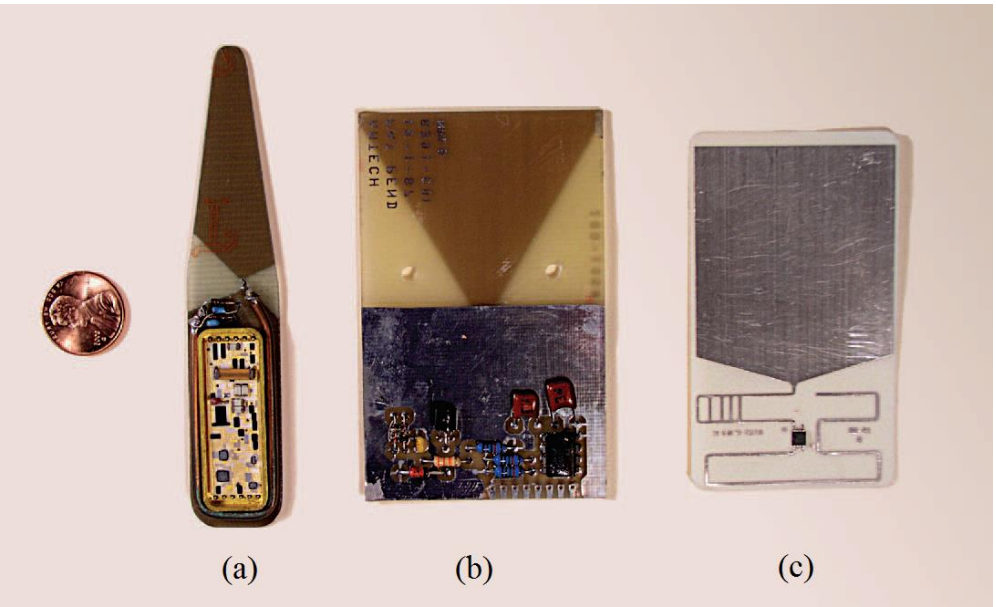


**Fig. 2.7. Evolution of RFID tags compared in size to a penny. (a) A 12-bit read-only tag from 1976. (b) A 128-bit read-only tag from 1987. (c) A 1024-bit read-write tag built using a single custom CMOS integrated circuit, 1999 [10].**

The application and development of RFID had significant growth in 90s. The technology entered the mainstream of business. The toll systems became common in most highways at that time and many regional toll agencies began to develop their own RFID systems. Many companies in the USA and Europe became involved in this technology. Development in information technology and internet enhanced the application data management of RFID. The cost of the system was still an issue until advances in material and semiconductor technology reduced the production costs. This increased the competition between companies and caused further growth in the technology [1]. It can be seen in Fig. 2.7 (c) that with the advances in CMOS technology all the circuitry are embedded in a tiny chip. This would save room for efficient antenna designs.

In the beginning of 21$^{st}$ century fabricating tags with the cost of only 5 cents became feasible. It was clear that the RFID technology can someday replace the barcode system. In 2003, the world's largest retailer and supply chain began to

employ RFID technology. All the coding protocols and standards converged to a unique standard in 2006 made the development and application of the technology easier. The interest has been shifting towards item-level tagging nowadays (2017). The outcome of this progress will be no checkout scenario at large supermarkets. Important goods which have high value or high risk such as wine bottles, pharmaceuticals and firearms would be the first to benefit from item-level tagging. Smart shelves for select categories of products and smart appliances with embedded RFID technology are other examples of recent applications. In the coming years the RFID technology will grow further and becomes part of the daily life [1].

# 2.3. RFID Tag Types

The source of power for running an RFID tag is an important factor in categorizing the tags. Depending on the source of the power and the method of transmitting signal to the reader the tags can be divided into three different groups: passive, semi-passive, and active tags as depicted in Fig. 2.8. As can be seen in the figure, both semi-passive and active tags are equipped with a battery. The difference between them is in the method of communication and the transmitter circuits. The three types of tags are reviewed in the following.

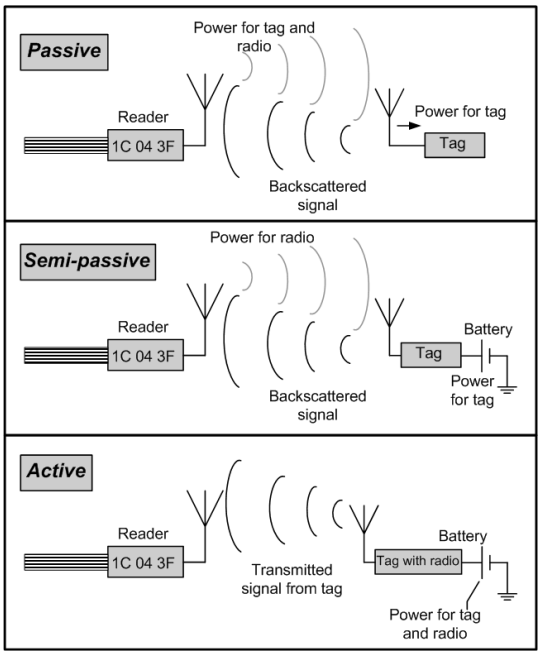


**Fig. 2.8. Communication in three different types of tags.**

## 2.3.1. Passive Tags

Passive tags have no independent source of power. The required power for running the circuits and reflecting back the signal to the reader is provided by rectifying the signal received from the reader. Thus, this type of tag is relying on the reader. The reader has to send a continuous signal to the tag over the whole time of the reading process. The diagram of a passive tag system is shown in Fig. 2.9 in more detail. The high frequency signal received by the antenna is rectified by a diode and the resulting signal is stabilized using a saving capacitor to create an approximate constant voltage as illustrated in top of Fig. 2.9. The captured voltage is used to power up the logic circuits and the memory. Since the tag power is temporary, the memory circuitry is always non-volatile. Another rectifying circuit is used in the tag for demodulation purpose. The capacitor of this circuit is usually smaller than the saving capacitor to allow the output voltage vary on the time scale of the reader data. This technique is known as envelope detection [5]. It is shown in Fig. 2.9 how the change in the level of the output voltage is interpreted into logic data. The backscattered modulation is done using a field-effect transistor (FET). The logic circuit changes the gate voltage of the FET which leads to changing the electrical characteristics of the antenna. This is similar to rolling the aircraft for changing the reflected signal used in WWII.

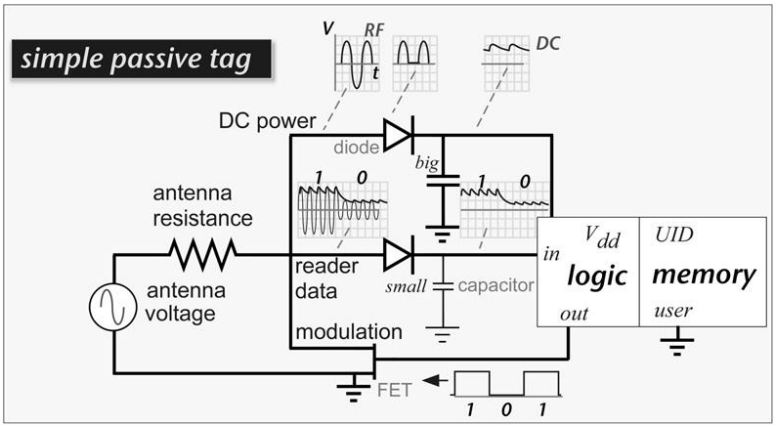


**Fig. 2.9. Schematic of a simple passive RFID tag [5].**

The main advantage of passive tags is the simplicity of the design and low fabrication cost. These are achieved at the expense of losing the read range. The read range of a passive tag relies on the reader power and the sensitivity of the circuits in

the tag and the reader and these factors are limited by the radio frequency regulations and semiconductor technology respectively. More details about this group are discussed in Chapter 3.

## 2.3.2. Semi-Passive Tags

Semi-passive tags are equipped with an assisting battery. They are also known as battery-assisted passive tags. A small battery is typically used to power up the tag circuits. The communication principle is the same as passive tags by backscattered signal as shown in Fig. 2.10. As can be seen, the energy harvesting rectifying circuit is replaced with a battery. Semi-passive tags offer more read range than passive tags which can reach up to 100 meters depending on the design and working frequency. This is achieved by increasing the size, cost, and maintenance requirements. They are reliable and usually used in automobile tolling and tracking high value targets such as airplane parts. Another application is in sensor integrated tags where constant measuring and saving of the data is required but the data can be transmitted to the reader without consuming the battery power. The battery life is saved by working in a low duty cycle and using a detector circuit which keeps the tag in a sleep mode until a signal is received from the reader.

A semi-passive tag used in automobile tolling is shown in Fig. 2.11. The tag is equipped with a printed circuit antenna, a 3.6 volt battery, and electronic circuitry as shown in the figure. The tag is placed in a plastic case with the size of 9.5×9.5×1.5 $cm^3$ and mounted inside the car. The large lithium battery provides 5 years of normal operation.

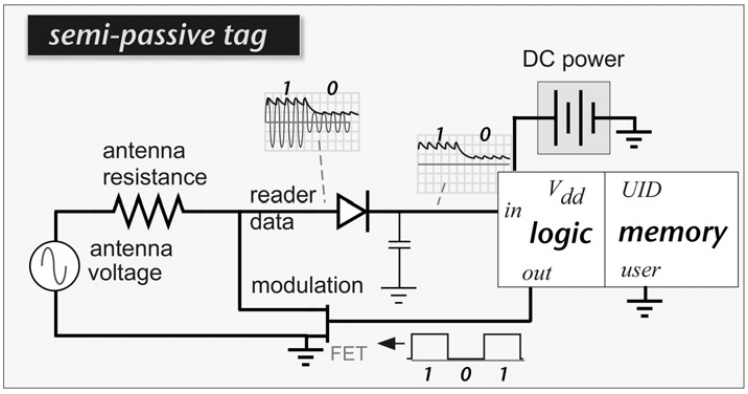


**Fig. 2.10. Schematic of a semi-passive RFID tag [5].**

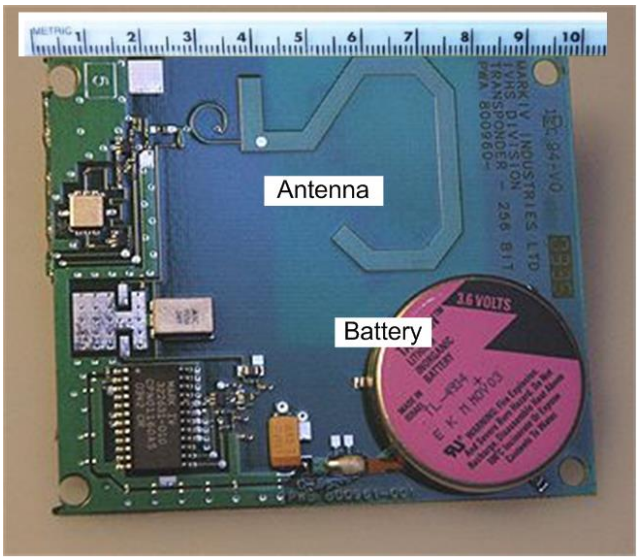


**Fig. 2.11. A semi-passive RFID tag used in automobile tolling.**

## 2.3.3. Active Tags

Active tags employ a battery for running the circuits similar to semi-passive tags but they also use the battery power to transmit the data to the reader. In fact, active tags use an independent transmitter for sending the identification information to the reader as shown in Fig. 2.12. Thus, they have local oscillator and other required components for a transmitter. A single antenna can be used for both transmitting and receiving as depicted in Fig. 2.12. However, some tags employ two antennas for this purpose.

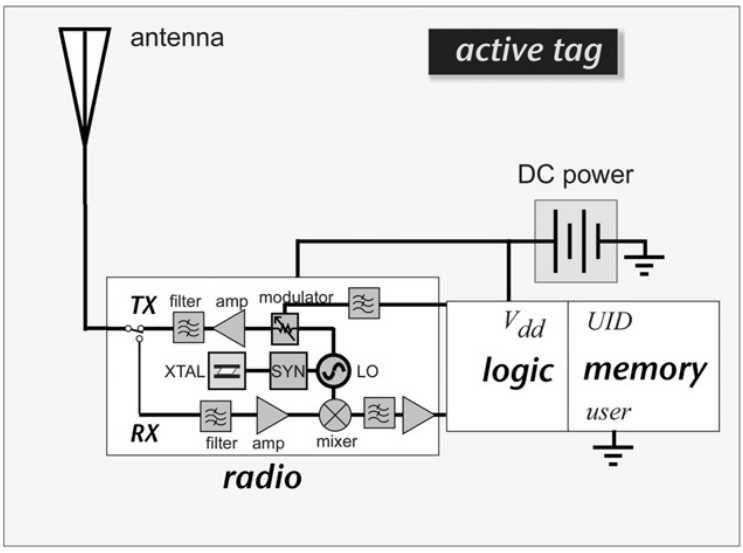


**Fig. 2.12. Schematic of an active RFID tag [5].**

The active tag can use amplitude modulation or any other digital modulation methods. Depending on the transmit power rand working frequency the read range of an active tag can reach up to hundreds of meter or even in kilometres. These tags are usually used in challenging conditions. For example, they are the best option for tracking large metallic container stored close to each other with no line of sight from reader to tag. The drawback is the size and the cost of fabrication and maintenance. A sample of an active RFID tag is illustrated in Fig. 2.13. This commercial tag is used for locating large assets such as shipping containers. The complexity of the internal circuitry and the large battery is evident in the picture. This tag produces an output power of 60 mW and provides about 900 m outdoor read range [5].

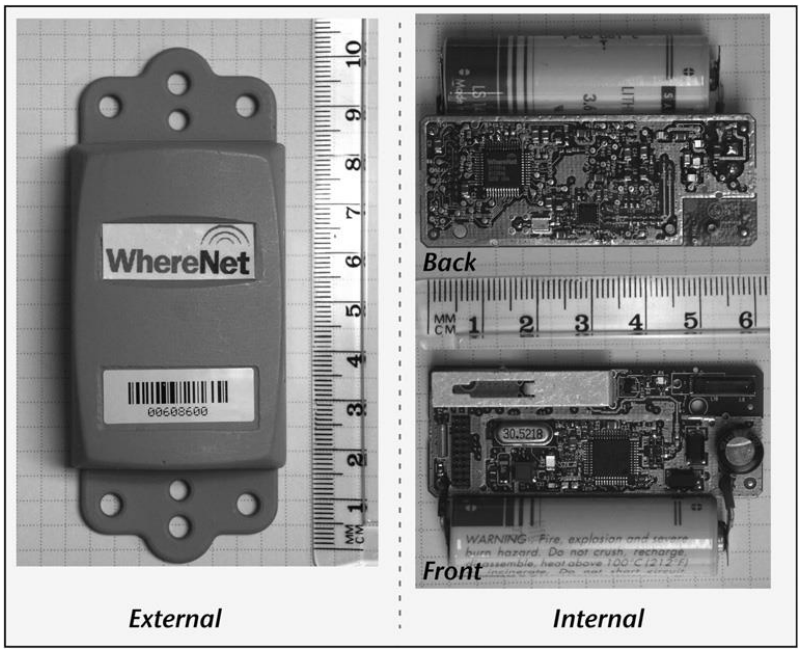


**Fig. 2.13. A commercial active RFID tag [5].**

# 2.4. RFID Operation Frequency

RFID systems work in a wide range of frequency bands from around 100 kHz to more than 5 GHz with almost the same working principles as explained so far. The used frequency bands are depicted in Fig. 2.14. The most common bands are in low frequency (LF), high frequency (HF), and UHF as shown in Fig. 2.14 which are explained in the following.

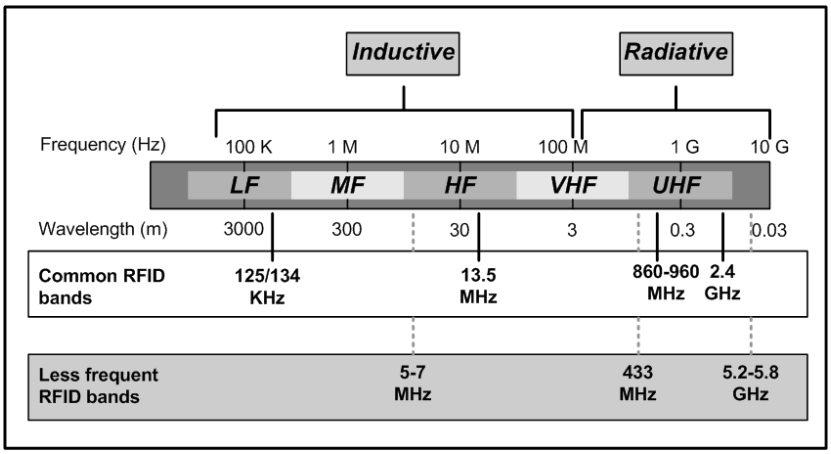


**Fig. 2.14. RFID frequency bands.**

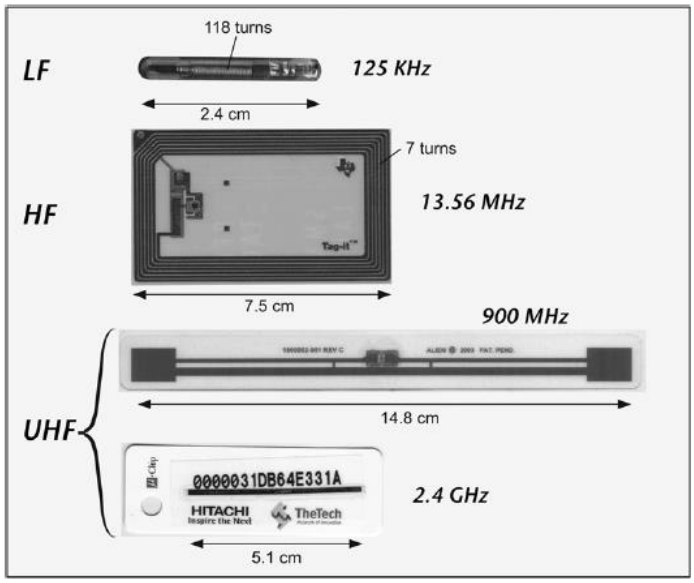


**Fig. 2.15. Tags working in three different frequency bands [5].**

**Low Frequency (LF):** The LF band is between 30-300 KHz. The two common frequencies in this band are 125 and 134 KHz. The tags in LF system are usually passive and they use inductive coupling for the communication. A coil with tens of turns around a ferrite core is used for this purpose. The magnetic field of the coil is barely affected by the surrounding material. Therefore, the LF tags are suitable for challenging materials when a short read range is desired. They are usually used for metallic objects, water containers and for medical implantable devices. The production cost of this type of tags is relatively high because the coil needs a winding machine. An implantable sample of LF tag used for animal tracking is shown in Fig. 2.15.

**High Frequency (HF):** The HF frequency band is between 3-30 MHz. The most common frequency in this band used in RFID is 13.56 MHz which ranges between 13.553-13.567 MHz. HF tags are also using inductive coupling and they are usually passive. The advantage of HF tags is higher working frequency than LF which reduces the number of the turns in the coil. A 5 turn flat coil and a small chip are the only components of a typical HF tag. Thus, the cost is quite less than LF tags. Working in HF, the tag offers longer read range compared to LF tags. The read range in some cases can reach up to one meter. This type of tag is robust to challenging objects but it is not applicable on metallic surfaces. The applications of HF tags are in near field communication (NFC), smart cards, airline baggage tagging, electronic ticketing and more. A flexible HF tag based on plastic substrate is shown in Fig. 2.15.

**Ultra High Frequency (UHF):** The UHF frequency band is between 0.3-3 GHz. The wavelength becomes shorter by increasing the frequency to UHF band and consequently the size of the antenna gets smaller. This makes the UHF band a suitable choice for designing tags which can radiate the electromagnetic waves and reach higher read range compared to inductive coupling method. Three different bands in UHF are usually used for RFID application. Most of the active tags work at 433 MHz (433.05-434.79 MHz) and 2.4 GHz (2.4-2.4835 GHz). Passive and semi-passive tags work from 860 to 960 MHz. Two samples of UHF tags working at 900 MHz and 2.4 GHz are shown in Fig. 2.15. There is an international allocation in working frequency for preventing the interferences. A summary of the allocated frequency in the globe is illustrated in Fig. 2.16.

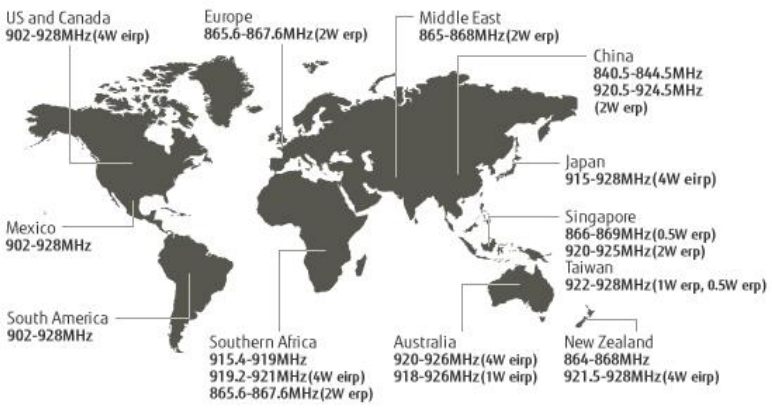


**Fig. 2.16. Summary of worldwide UHF RFID band allocations [11].**

The research in this thesis is focused on passive RFID tags working in UHF band and all the proposed designs are tuned to work at Europe frequency band at 866 MHz. According to the low production cost and reasonable read range, UHF tags are used for various applications including supply chain and inventory management, parking access control, baggage and asset tracking. More details about passive UHF tags is given in Chapter 3.

# 2.5. Communication Protocols

Assigning standard frequency bands for RFID tags used in different regions facilitates the application and prevents the interference. In addition to the frequency band, the communication protocol also needs to be standardized. There are a few organizations which has defined standards for RFID systems but the most significant bodies that made outstanding influence on the RFID industry are [1]:

- International Organization for Standardization (ISO).
- Electronic Product Code Global (EPC global).

The RFID systems that work in LF band do not have a standard usually as they are working in a closed-loop controlled environment and there is little need for inter-regional application. However, ISO has developed two standards for the animal tracking LF RFID systems. The ISO 11784 defines the identification code for animal tag. The animal can be identified by a country code and a national ID. The ISO 11785 defines the technical parameters of the communication between tag and reader. ISO has also released standards for identification cards and related devices. The three standards published in 2000 are: ISO 10536, ISO 14443, and ISO 15693. These are the most widely used and accepted RFID standards to date but they are specifically defined for HF systems [1].

The EPC Global standards are typically used for supply chain management and retailing. Most of the major retailing organization have adopted this standard for their RFID systems which means EPC Global will have a great influence over this technology and industry applications in future. This standard was firstly created in an academic research at MIT in 1999 with the goal of developing an “internet of things (IoT)” instead of internet of computers. They call this IoT Electronic Product Code (EPC) network. In fact, the EPC is the electronic version of UPC (the barcode

standard). The contents of an EPC code are shown in Fig. 2.17. It is comprised of four parts. The first part is called the header and it gives the EPC version or type which is 1 in the example. The second part is for identification of the product manufacturer. The third part represents the object class or the exact type of product. The serial number of the product is given by the fourth part finally. As can be seen, the total number of the bit in one code string is 96 bits which means it is capable to uniquely identify 268 million of companies, each of which could have up to 16 million different products and 68 billion unique serial numbers for each product.

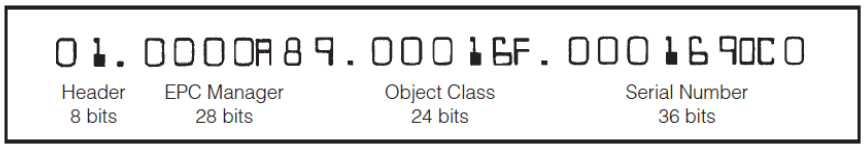


**Fig. 2.17. Example of an EPC tag numbering system [1].**

There are five different classes of EPC tags which define the programming capability of the tag and the type of it. It should be mentioned that all the proposed designs in this thesis are integrated with RFID chips that use EPC Class 1 Gen2 protocol. Gen2 refers to the second generation of EPC which is improved in terms of read and write speed and code security [1].

# 2.6. Cost and Market Trends

The cost of an RFID system is a determining factor in progress and growth of this technology. The overall cost of the system consists of the hardware and software cost including the tag production. The total RFID market is worth 11.2 US dollar billions in 2017 and the predictions suggest that the value exceeding 27 US dollar billions in 2024 [12]. The diagram of Fig. 2.18 shows the value of this market from 2014 to 2018. It can be inferred from the diagram that a big portion of the market belongs to passive RFID systems and the value is around 9 US dollar billions in 2017. Passive RFID tags have a significant share in this value which is around 4 US dollar billions in 2017. This result confirms the importance of the production cost of a passive RFID tag and its great impact on the total RFID market.

Since the tags are used to label any type of consumable objects, their cost should be fairly less than the cost of the object. The relation between the cost of the label-type RFID tags and the amount sold each year is depicted in Fig. 2.19.

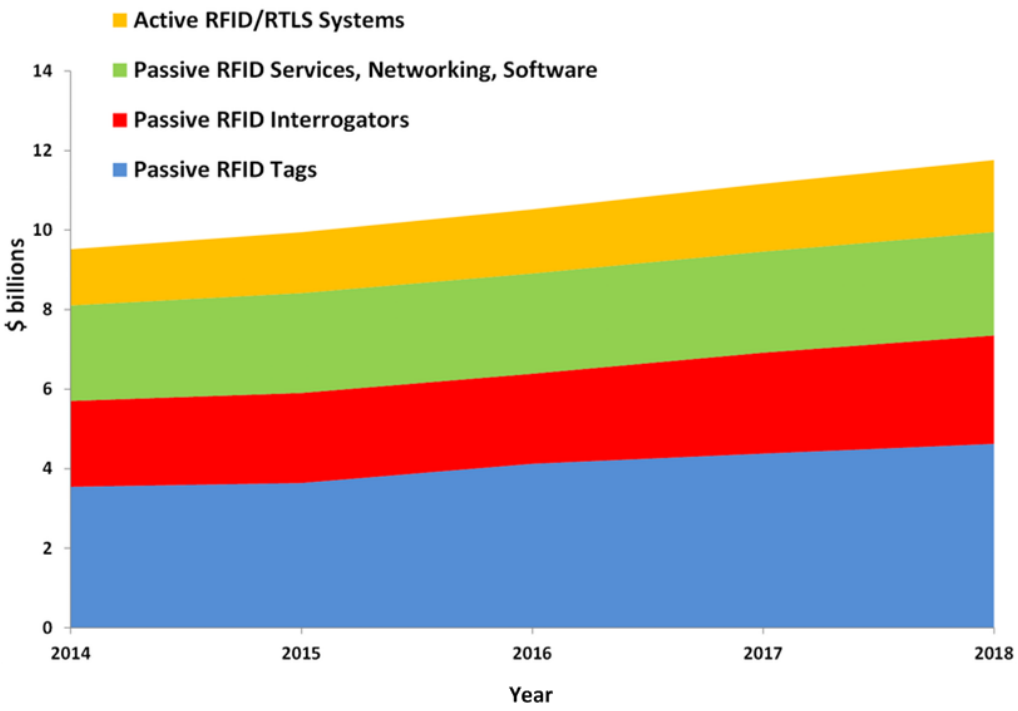


**Fig. 2.18. Total RFID market in US $ billions each year [12].**

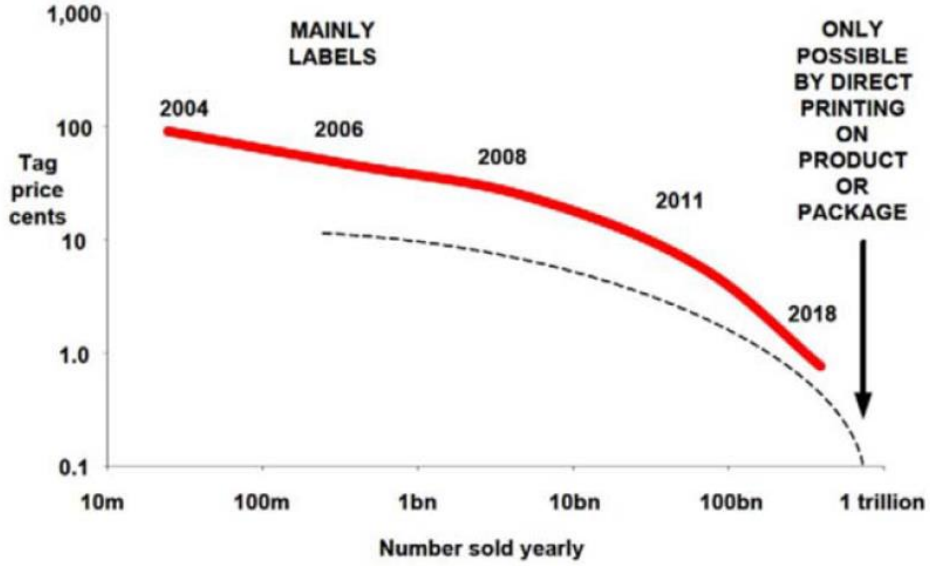


**Fig. 2.19. Relation of RFID tag price versus global sells from 2004 to 2018 [12].**

The plot shows that the number of sold tags has greatly increased by reducing the production cost of tags. The cost of a label-type tag is mainly determined by the RFID chip and the flexible substrate. The production cost of a typical tag is around a few cents of US dollar currently. According to the plot of Fig. 2.19, further reduction in the price is only possible by printing the tag directly on the object and eliminating the need of RFID chip which leads to chipless RFID tags. This technology employs passive resonating structures with multiple resonances in a certain frequency band. The binary data are determined on the presence and absence of the resonances by the RFID reader. However, the data capacity of this technology is far less than RFID tags with chip and it cannot satisfy the demands of the future market. Study on chipless RFID tags is beyond the scope of this thesis.

# 2.7. Conclusion

The RFID technology was reviewed in this chapter. It has been shown how the evolution of this technology started in World War II from a 1 bit identification system was reached to a 96 bit capacity nowadays. Advances in the semiconductor and material technology have reduced the production cost of RFID tags and was given the capability to substitute the optical barcode in many applications. RFID technology offers a wide range of solutions for different purposes; Low frequency tags for inductive coupling and short read range and UHF active tags for high read range. The communication and code standards have enhanced the progress of this technology worldwide by facilitating the data sharing and contributing to the internet of things criteria. Finally, the growth of RFID systems since World War II reflects a promising future for this technology.

# Chapter 3. Passive UHF RFID Tag: Overview and State of the Art

After reviewing the basics of RFID technology in Chapter 2, the main subject of the thesis is discussed in this chapter. The components of a passive UHF RFID tag are introduced first. Different types of tags available in the market are reviewed after that. The required principles for designing and measuring the tags are discussed. The detuning effect which is a common problem in label-type tags is introduced with two examples. Finally, a comprehensive literature review about the tag designs for challenging material such as liquid bottles and metallic objects is presented in this chapter which clarifies the advantages and drawbacks of the current solutions.

# 3.1. Structure of a Passive UHF RFID Tag

The structure of a passive UHF RFID tag is simply comprised of a chip as the transponder and the antenna. There are different types of antenna suitable for tag design but generally they can be categorized into two groups: dipole and patch antenna. There is an impedance matching part in dipole antenna usually, which is called T-match [13-15]. The matching part in patch antenna is not always necessary. By locating the chip in the proper position on the patch the suitable impedance matching could be achieved in some designs. However, using matching loop or stubs is also practiced in patch antennas [5]. The components of a typical dipole tag and patch tag is depicted in Fig. 3.1. These components are discussed in the following.

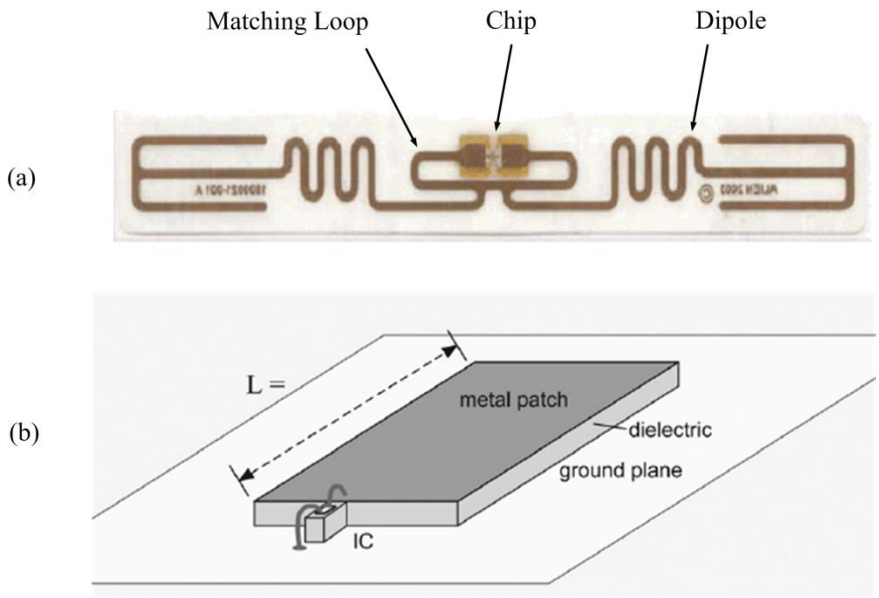


**Fig. 3.1. Components of a typical UHF RFID tag. (a) Label-type with dipole antenna. (b) Patch antenna tag [5].**

## 3.1.1. UHF RFID Chips

Application specific integrated circuit (ASIC) chip is the brain of a passive tag. With a high capacity rewritable memory, tagging, tracking, and managing a huge number of objects is possible nowadays. Different types of packaging, power and impedance characteristics of typical chips are discussed in this section and a dual port chip is introduced finally.

### 3.1.1.1. Packaging

The evolution of CMOS technology has made it possible to fabricate a tiny low cost application specific integrated circuit (ASIC) chip on a die area in order of a quarter $mm^2$. Low power consumption is a critical requirement in passive tags and these ASICs fulfill this by needing just few tens of μW of electric power [16].

According to the demand of the market, these ASICs are fabricated in different packages. A tiny unpackaged chip is usually applied directly on a label-type tag. This makes the fabrication process easier and faster but it requires sophisticated fabrication appliances. An alternative packaging type is a tiny chip applied to conductive strip ready to be attached to the port of the antenna. Another group of packaging is SOT323 which is bigger than the other groups and has an area around 5 $mm^2$. This type of packaging is suitable for prototype designs and lab works which is also used in the designs proposed in this thesis. The three groups of ASIC packaging are illustrated in Fig. 3.2.

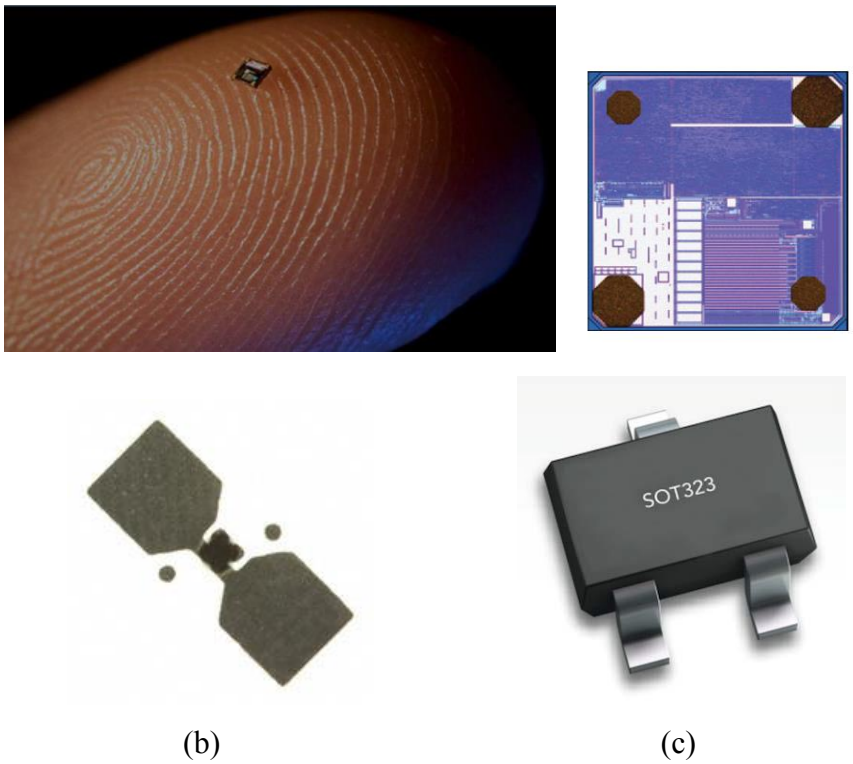


**Fig. 3.2. Different types of ASIC packaging: (a) Unpackaged chip (Higgs 3, Alien Technology). (b) Strap (RI-UHF-STRAP-08, Texas Instruments). (c) SOT323 (Higgs 4 SOT, Alien Technology).**

### 3.1.1.2. ASIC Characteristics

The internal circuitry of an ASIC is depicted in Fig. 3.3. As mentioned in previous chapter, the passive tag relies on the electromagnetic power received from the reader. The ASIC has energy harvesting parts for capturing, saving, and using this power. The main components of an energy harvesting part are capacitors and Schottky diodes. The level of voltage can be increased by using multiple components. This part plays an important role in determining the read sensitivity of the chip or threshold power ($P_{th}$). This is the minimum required power delivered to the chip for having a successful communication. The evolution of the CMOS technology in the past 15 years has reduced $P_{th}$ from -8 dBm to -20 dBm [17]. This guarantees an increase in the reading range of the passive tags. The diagram of Fig. 3.4 shows how this evolution has increased the read range during the past years.

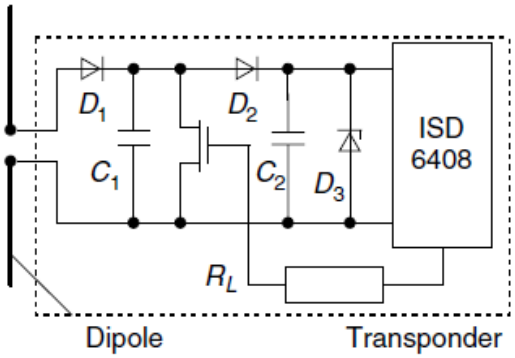


**Fig. 3.3. Sample internal circuitry of an ASIC (Integrated Silicon Design, 1996) [3].**

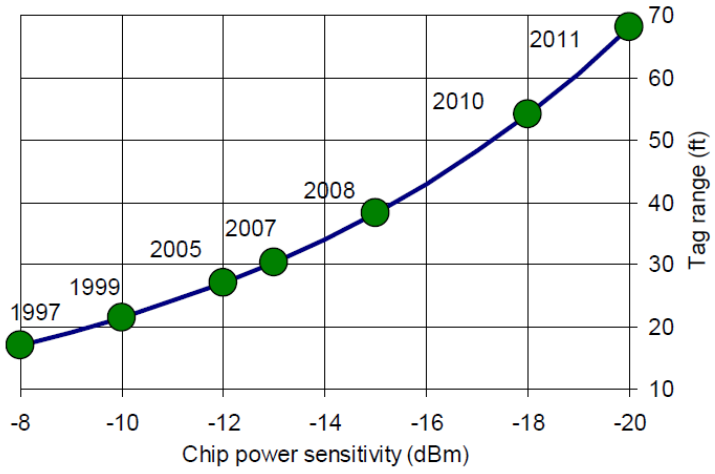


**Fig. 3.4. Tag read range versus chip sensitivity [17].**

The tag responds to the reader by backscattered modulation. The ASIC sends continuous signals to the FET switch shown in Fig. 3.3 and changes the impedance matching state of the system which leads to reflection of the signal to the reader.

Analysing the input impedance of the ASIC is important as the chip need to be properly matched to the antenna. Although the input impedance depends on the level of the received power and the frequency of the signal but it can be considered in the range of $P_{th}$ in practice. According to the internal capacitors for harvesting and saving the electric power, the input impedance of the chip is mostly capacitive. This impedance is usually modelled by a parallel combination of a resistance $R_c$ and a capacitance $C_c$ [18, 19]. The resistance represents all the power consumed by the active internal parts. Thus, the input impedance of a typical chip, $Z_c$ is usually a complex value with negative imaginary part. The characteristics of some commercial ASICs are tabulated in Table 3.1.

**Table 3.1. Power and impedance characteristics of several RFID chips [16].**

| | $P_{th}$ (dBm) | $R_c$ (Ω) | $C_c$ (pF) | $Z_c$ (Ω) at 915 MHz |
|---|---|---|---|---|
| **Alien Higgs 4** | -18.5 | 1800 | 0.85 | 23-*j*202 |
| **Alien Higgs 3** | -18 | 1500 | 0.85 | 27-*j*201 |
| **Alien Higgs 3 (SOT)** | -17 | 1500 | 0.9 | 25-*j*190 |
| **Monza 5** | -17.8 | 1800 | 0.825 | 24-*j*208 |
| **Monza 4** | -17.4 | 1650 | 1.21 | 12-*j*142 |
| **Monza Dura** | -17 | 1600 | 1 | 19-*j*172 |
| **NXP UCODE G2XM** | -15 | 1385 | 1.16 | 16-*j*148 |

### 3.1.1.3. Monza 4 Chip

Monza 4 made by Impinj is a dual port chip for passive RFID tags [20]. The principle of working in this chip is the same as the other commercial chips but it has two completely independent RF ports that enable the designer to attach it to a dual-polarized tag antenna as shown in Fig. 3.5. The advantage of this dual-polarized dipole is the omni-directional radiation pattern that makes the tag accessible from different angles using a dual-polarized or circularly-polarized reader antenna [5]. A conceptual mode of dual independent ports depicted in Fig. 3.6 shows each port has its independent rectifier circuits which makes the impedance of the ports isolated

from each other. Different configuration of the ports can be used in the design. For example a single port connection can be employed like any typical chip. A shunt port connection also can be used for achieving the desired input impedance. Monza 4 is used in the designs in Chapter 5 and Chapter 6.

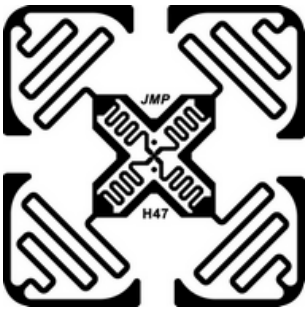


**Fig. 3.5. Dual-polarized tag (Impinj H47) [20].**

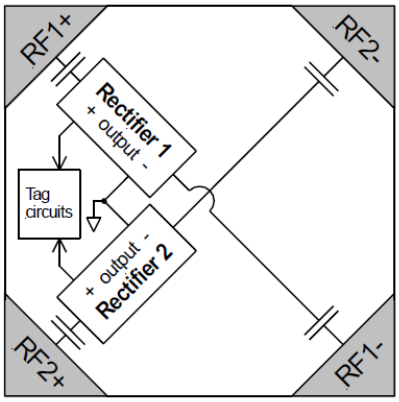


**Fig. 3.6. Conceptual model of dual independent ports [20].**

## 3.1.2. UHF RFID Antennas

The antenna is another main part of a tag which occupies almost the whole area of a typical passive tag. The characteristics of antenna and its effect on the performance of the tag are discussed in this subsection. The most common available tags in the market and their application, advantage, and drawbacks are also discussed.

The radiation efficiency of a tag, $\eta_{tag}$ is the ratio of the electromagnetic power radiated from the antenna to the power delivered to the antenna. The non-radiated power converts to the heat in the antenna body according to the ohmic loss in the antenna body and substrate. The designer's target is to reach the maximum possible radiation efficiency as this parameter has direct effect on the tag performance and

reading range. However, the size of the tag is another determining factor which affects the radiation efficiency. The radiated power from a dipole antenna is proportional to the square of the dipole length. Thus, the radiation efficiency and the radiation resistance can be increased by increasing the length of the tag antenna [21]. Therefore, there is a compromise between the size of the tag and the reading range. According to the application of the tag, the designer selects the optimum size and consequently the maximum available $\eta_{tag}$.

The radiation pattern of the tag is the factor that determines the orientations that the tag is readable depending on the polarization of the tag and reader antenna. An isotropic radiation pattern is usually desired as it makes the tag readable from different angles. The dipole type tags offer an omni-directional radiation pattern in the plane perpendicular to the dipole axis. However, in some applications involving metallic bodies it is better to have a non-uniform radiation pattern to improve the performance. In this case, the main lobe should be away from the surface of the metallic body to reduce the destructive effect of the conductive surface on the impedance matching and efficiency of the antenna. The tags employing a ground plane in the antenna design normally are suitable for this purpose.

The polarization of the tag and the reader antenna is also another factor that determines the orientation availability of the tag. In general, the two antennas polarization should be aligned for having the optimum power transfer. In modern RFID readers, the device is equipped with a circularly-polarized or dual-polarized antenna. A dual-polarized antenna is basically a dual-dipole structure with elongated arms in orthogonal directions. This structure will interact with electric fields in any direction in the plane of the antenna which increases the reliability of the reading process. However, some simple handheld readers still employ single polarized antenna. In this case dual-polarized tag antenna could be used to increase the reliability.

The most common passive tags can be categorized into two groups: label-type dipole tags and patch antennas employing substrate and ground plane. The most popular tags are the label-type dipole designs as they are reliable and low cost. The dipole antenna has to be usually half wavelength in practice but the half wavelength in 866 MHz is almost 16 cm which is too long for most passive tag applications. The designers apply different solutions for reducing the length of the tag with the cost of

losing radiation efficiency. One solution is meandered dipole which helps to bring down the length to less than 10 cm. However, just those parts of the meandered dipole that are in the direction of the polarization contribute to radiation and the other parts cause an ohmic loss. The radiation resistance and the ohmic loss contribute to impedance matching between the antenna and the chip [5]. Another solution to size reduction is applying capacitive loads at the tip of the dipole. The series capacitance in the antenna body is increased by this method which leads to a down shift of the resonant frequency. This would consequently lead to a size reduction [5].

There are a variety of label-type tags in the market for different purposes. The most common are the general purpose tags which can be attached on a wide range of non-challenging materials which are basically composed of a material with low dielectric constant. A few samples of this type are shown in Fig. 3.7(a). The performance of general purpose tags is seriously affected by materials with higher dielectric constant and challenging objects like liquid bottles due to detuning effect

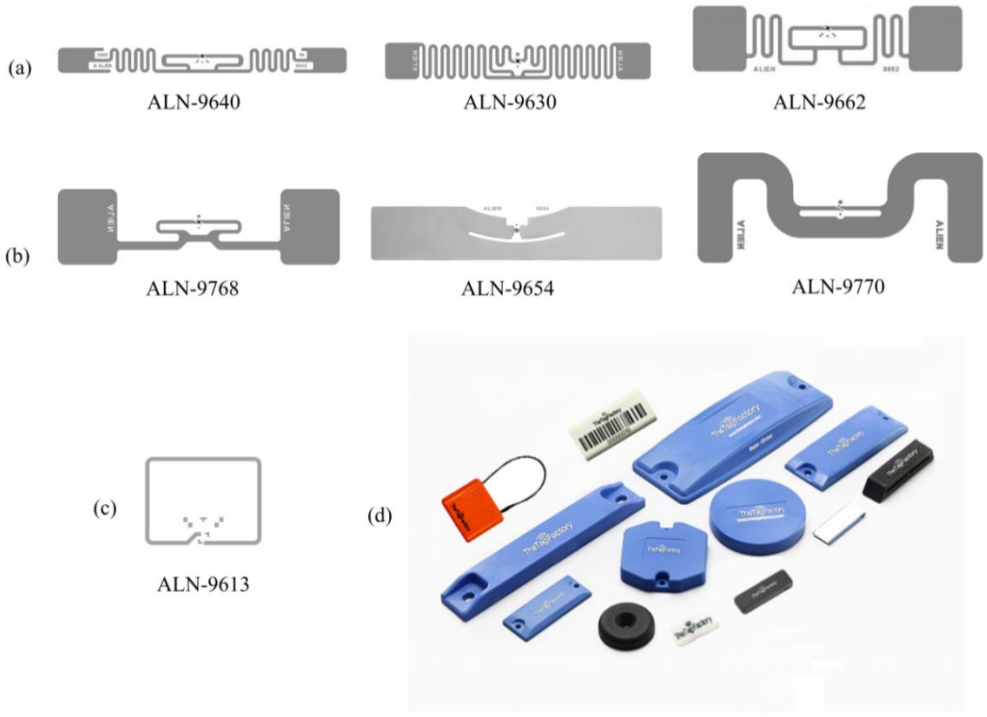


**Fig. 3.7. Different types of tags in market (not to scale). (a) General purpose tags by Alien Technology. (b) Robust tags for challenging material and high dielectrics by Alien Technology. (c) Near field loop tag by Alien Technology [22]. (d) Different types of metal mountable tags from The Tag Factory [23].**

which is discussed in Section 3.3. There are some tags available which are robust to challenging materials in some extent. A few samples of robust tags are depicted in Fig. 3.7(b). In some application, a short read range is required. In this case, an inductive loop would make it possible for having a near field tag. One sample is shown in Fig. 3.7(c). The label-type tags are not functional on metallic objects as the conductive body interacts with the radiation of the dipole and also surface currents [2]. Patch antennas are vastly used for this purpose. A few samples of metal friendly tags are illustrated in Fig. 3.7(d).

# 3.2. Designing and Measurement Principles

The most important principles and definitions in designing and testing the tags that are used throughout this thesis are introduced in this section. After reviewing these concepts, analyzing the common problems of tags and reviewing the state of the art in RFID tag design robust to host material is presented.

## 3.2.1. Conjugate Impedance Matching

It is important to deliver the maximum available power from antenna to chip. Particularly, in a passive system which is relying on the received power. The impedance matching between the chip and antenna plays a crucial role. It is learned in 3.1.1 that the input impedance of a typical chip is a complex number with negative imaginary part. On the other hand it is known that the input impedance of a dipole antenna is determined by its length and it is generally a complex number as well. A system of an antenna connected to an RFID chip can be translated as the equivalent circuit of Fig. 3.8. $V_{OC}$ is the open-circuit voltage source representing the received signal by antenna. The real part of the antenna in an ideal scenario can be the radiation resistance $R_{rad}$. The imaginary part of the antenna, $X_{ant}$ is zero when the antenna is resonating and this happens for a dipole with the physical length almost equal to half wavelength. The imaginary part is a positive value for a dipole equal or longer than half wavelength which means the input impedance is inductive and finally, the imaginary part is a negative value for a dipole shorter than half wavelength representing capacitive input impedance. The latter case is normally considered for tag antennas as the antenna needs to be short enough in practice.

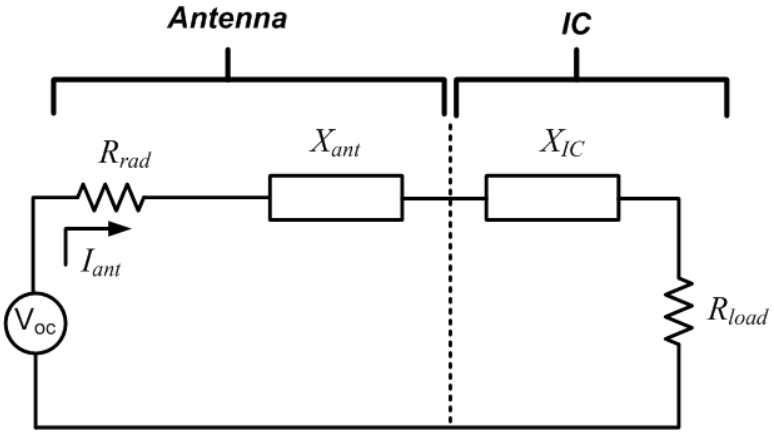


**Fig. 3.8. The equivalent circuit of RFID antenna and chip.**

For a system with minimum signal reflections the impedance of the chip should be exactly the same as the impedance of the antenna [24], but for having the maximum power transfer which is the target the conjugate impedance matching needs to be achieved. The current of the circuit $I_{ant}$ can be found by (3.1):

$$I_{ant} = \frac{V_{OC}}{(R_{rad} + jX_{ant}) + (R_{load} + jX_{IC})} \tag{3.1}$$

The real power transferred to the load or chip is calculated by (3.2):

$$P_{load} = \frac{|I_{ant}|^2 R_{load}}{2} = \frac{{V_{OC}}^2 R_{load}}{2\left[(R_{rad} + R_{load})^2 + (X_{ant} + X_{IC})^2\right]} \tag{3.2}$$

For having the maximum power delivered to the chip the denominator must be as small as possible. This condition is satisfied when the imaginary part is zero which means the reactance of antenna and chip has the same value with different sign and they cancel each other. The real parts also needs to be equal as proved in [5]. As an example, to have a conjugate impedance matching between a chip with impedance of (12-$j$142) and the tag, the input impedance of the tag should be equal to (12+$j$142) which is shown by: $(Z_{ant} = Z_{chip}^{*})$. This means the input impedance of the antenna should be inductive whereas, in a short dipole the input impedance is capacitive as mentioned before. The practical solution is to apply an inductive matching loop between the chip and the dipole. This loop cancels the capacitive part of the dipole [5, 25].

## 3.2.2. EIRP and ERP

The electromagnetic power emitted by the reader antenna has direct effect on the read range of the tag. The mentioned power is a function of the power transferred to the reader antenna by the active transmitter circuits and the gain of the antenna. The gain of the antenna is the product of the efficiency and directivity of the radiation pattern [26]. Different type RFID reader devices employ different type of antennas with different level of the power consumed by the transmitter. It is recommended to use a standard scale for reporting the emitted power by each reader antenna. The effective isotropic radiated power (*EIRP*) is usually used for this purpose. *EIRP* is the total power that would have to be radiated by a hypothetical isotropic antenna to give the same signal strength as the actual source in the direction of the antenna's strongest beam. As shown in Fig. 3.9, the gain of an isotropic emitter is equal to one. Sometimes instead of *EIRP*, effective radiated power (*ERP*) is used and it is the total power that would have to be radiated by a half wavelength dipole antenna to give the same signal strength as the actual source in the direction of the antenna's strongest beam. The gain of a dipole antenna is 2.15 dB more than an isotropic emitter as shown in Fig. 3.9. It can be expressed by (3.3):

$$EIRP(dB) = ERP(dB) + 2.15 \tag{3.3}$$

The amount of power can be also reported by dBm or Watts. The maximum regulated *EIRP* for an RFID reader is 4 W or 36 dBm.

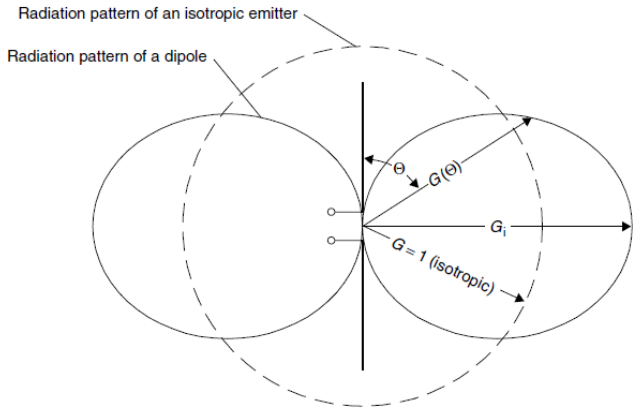


**Fig. 3.9. Radiation pattern of a dipole and an isotropic emitter [3].**

### 3.2.3. Read Range Measurement

The read range of a passive tag is the most important factor in determining the performance. It is defined as the maximum distance in which the reader is able to read information from the tag. The read range is directly influenced by the reader power and antenna. The sensitivity of the reader receiving circuits is higher than the sensitivity of the tag chip. Thus, the threshold of the tag is another parameter determining the read range. The read range of a tag, $d_{tag}$ can be calculated by the Friis formula:

$$d_{tag} = \frac{\lambda}{4\pi}\sqrt{\frac{\chi\tau e_{r,tag} D_{tag} EIRP}{P_{th}}} \tag{3.4}$$

$$\tau = 1 - \left|S_{11}\right|^2 = \frac{4R_{load}R_{rad}}{\left|Z_{ant} + Z_{load}\right|^2} \tag{3.5}$$

where $\lambda$ is the wavelength of the carrier tone, $\chi$ is the mutual polarization power efficiency between the tag and reader antenna, $\tau$ is the antenna-chip power transfer efficiency and it is equal to one when perfect conjugate impedance matching exist between the antenna and chip represented in Fig. 3.8, $e_{r,tag}$ is the radiation efficiency of the tag antenna, $D_{tag}$ is the tag antenna directivity, *EIRP* is the effective isotropic radiated power of the reader, and $P_{th}$ is the threshold power of the tag chip [2]. However, the calculated read range using this formula is not always accurate due to different errors in design simulation, fabrication, and testing process.

There are different methods for measuring the read range of a tag in practice. A simple way is to start reading a tag using a commercial reader and increase the distance between them constantly until the tag stops responding. The maximum distance in which the tag is still responsive can be measured finally. The same method is used for testing the designs in Chapter 4, and Chapter 5. It is recommended to measure the read range in an anechoic chamber because the reflections and noise affects the read range [25]. The mentioned method has two drawbacks. Firstly, the readers are usually working in a fixed frequency and the result of the test cannot give any idea about the read range in a frequency sweep. So, the designer cannot be sure about the maximum possible read range in the frequency

band. Secondly, the power is fixed in this method and the distance is changing. For large amount of the reader power a big testing room is required.

Another method for testing the tag that is common in the labs is to have a fixed distance between the tag and the reader and change the transmitter power until the minimum required power for waking up the tag is found. The maximum read range which is also called the theoretical read range is then calculated using the following equation derived from Friis formula:

$$d_{\max} = d_{ref} \sqrt{\frac{EIRP_{\max}}{EIRP_{ref}}} \tag{3.6}$$

where, $d_{max}$ is the maximum possible tag read range (theoretical read range), $d_{ref}$ is the reference read range measured in the lab, $EIRP_{max}$ represents the maximum regulated *EIRP* which is 4 Watts in most regions, and $EIRP_{ref}$ is for the equipment used to measure the reference read range in the lab. This method can be done using an RFID reader system connected to an antenna located inside an anechoic chamber as shown in Fig. 3.10. It is also possible to do this test in a transverse electromagnetic (TEM) cell. The RFID reader is equipped with a circulator and a signal analyser for receiving and analysing the reflected signal from the tag. There are testing kits available in the market which is consisted of the reader module and the antenna and a user-friendly software which can give the read range in the required frequency sweep. Tagformance from Voyantic is one of these products which has been used in the work presented in Chapter 6.

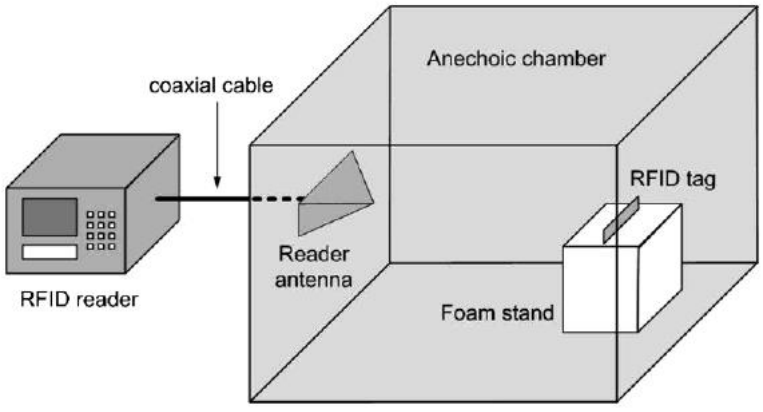


**Fig. 3.10. Measurement setup for finding the read range of a tag in anechoic chamber [25].**

# 3.3. Detuning Effect

The detuning effect occurs when a label-type tag is placed on a material with a high dielectric constant. The background material affects the electric characteristics of the tag antenna and changes its frequency response which deteriorates the impedance matching and affects the read range consequently. The tag stops responding to the reader in severe cases [27]. The detuning effect on two commercial label-type tags are analysed in this section. This gives better understanding about the mechanism of this effect and helps in finding solutions to overcome this phenomenon.

## 3.3.1. ALN-9640

The detuning effect on ALN-9640 that is a general purpose tag from Alien Technology is investigated using CST simulation software. The target of this simulation is to find the effect of the host material on the impedance matching between the tag antenna and the chip. The real physical dimension of the tag is designed in the software as shown in Fig. 3.11. The overall dimension of the tag is 95×8 $mm^2$. A Higgs-3 RFID chip is used in ALN-9640. The equivalent circuit of this chip is a 1500 Ω resistor in parallel with a 0.85 pF capacitor. A lumped element capacitor is used in the design and located in the center of the antenna attached to the matching loop. Instead of adding a lumped element resistor, the impedance of the feed port is changed from 50 to 1500 Ω.

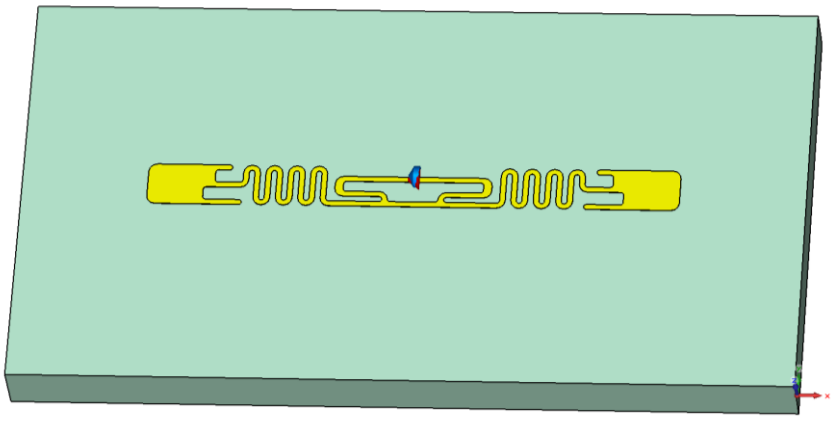

**Fig. 3.11. ALN-9640 designed in CST software.**

The impedance matching and S11 result is calculated between the feed port and the rest of the design. This makes the analyzing process straightforward. The tag is placed on a dielectric slab with size of 140×80×10 $mm^3$ and the relative dielectric constant of the slab is changed from 1 to 15 with step of 5. The result of the detuning effect is depicted in Fig. 3.12. There is a considerable frequency shift and detuning after increasing the relative dielectric constant from 1 to 5. The tag is normally out of order in practice when the reflection constant is more than -2 dB [28]. This means ALN-9640 is suitable for materials with low dielectric constant [22].

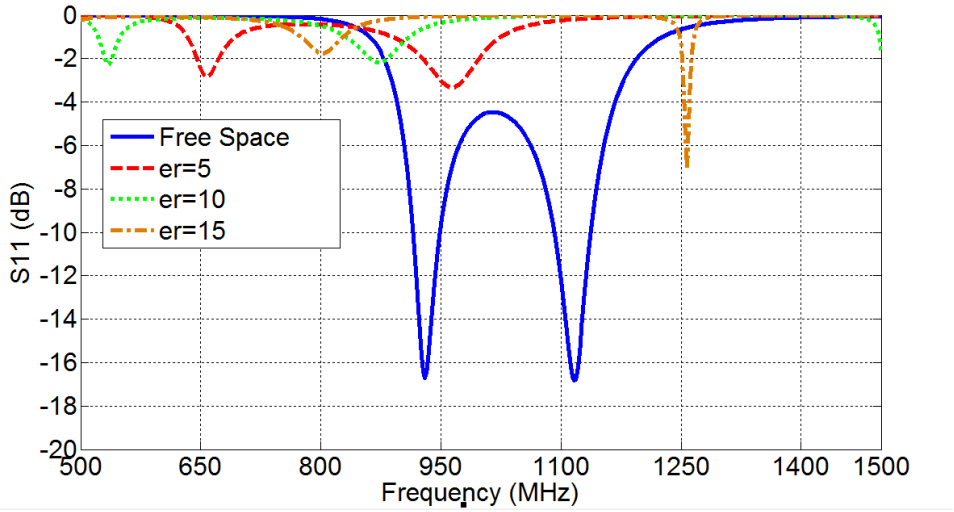


**Fig. 3.12. The detuning effect on ALN-9640 by changing the dielectric constant of the host material.**

## 3.3.2. ALN-9654

ALN-9654 is another product of Alien Technology. This tag is specially designed for high dielectric constant materials and is claimed to have more robustness compared with ALN-9640. The same process for designing and testing this tag is done using CST software. The design is shown in Fig. 3.13. This tag is using the same chip thus the arrangement of the port and lump element is the same as ALN-9640. The size of this tag is roughly 93×32 $mm^2$. The relative dielectric constant of the background slab is changed from 1 to 15 in steps of 5. The frequency response of the tag is recorded each time and the result is depicted in Fig. 3.14.

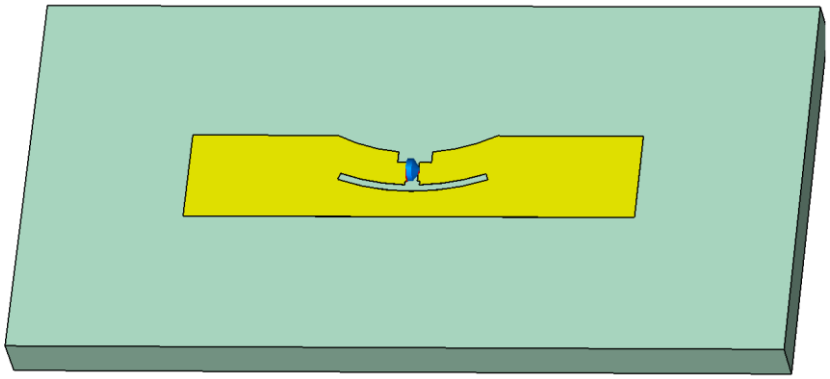

**Fig. 3.13. ALN-9654 designed in CST software.**

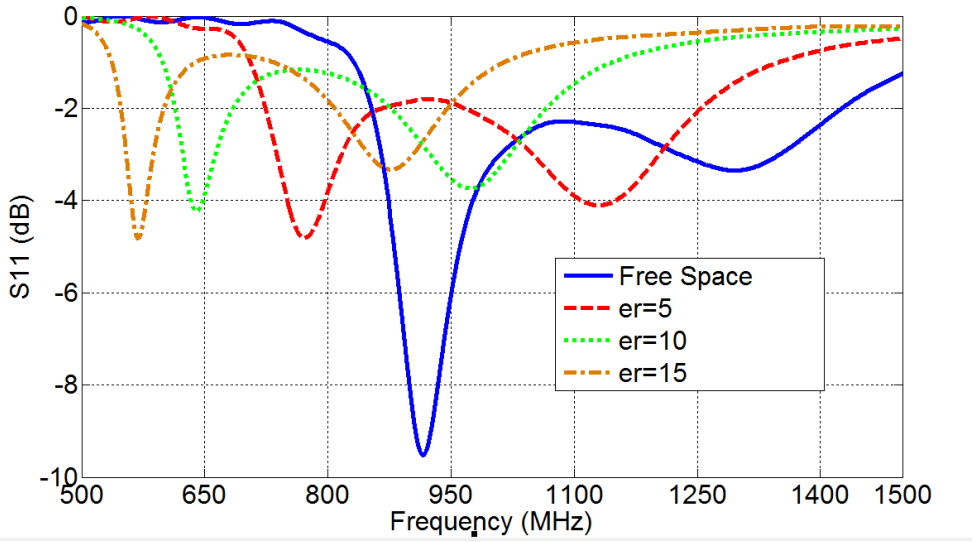


**Fig. 3.14. The detuning effect on ALN-9654 by changing the relative dielectric constant of the host material.**

By comparing this result with the result of Fig. 3.12, it can be seen that ALN-9654 offers a wider bandwidth in the working frequency. Of course, the level of the power reflection is consequently more than ALN-9640. This means ALN-9654 offers less read range in free space compared to ALN-9640. The advantage of ALN-9654 to ALN-9640 gets obvious when it is placed on a slab with a higher dielectric constant. As can be seen in Fig. 3.14, the detuning effect is less in ALN-9654 and the reflection is less than -2 dB in a wide range of frequency.

## 3.3.3. Equivalent Circuit Analysis

It is already known that the detuning effect is the result of change in the characteristics of the antenna. The target of this part is to find out what is exactly changed in the tag when it is placed on a material with higher dielectric constant. The equivalent circuit analysis of the tag can give the answer. In fact, this analysis finds the elements in the equivalent circuit which are affected by the background material. First, it is needed to find a suitable equivalent circuit for a conventional dipole tag with a matching loop. A dipole tag with the corresponding equivalent circuit is illustrated in Fig. 3.15. The physical structure of the tag is in symmetry according to the vertical axis leading to a symmetric equivalent circuit. Looking at the equivalent circuit from right to left, it starts with the chip. The internal resistance and capacitance of the chip are shown in a series topology. However it can be easily converted to a parallel circuit. The chip is connected to the matching loop from both sides. The matching loop is basically providing a series inductance as depicted in the circuit. The series inductance is terminated to a shunt inductance which actually closes the matching loop and provides the required inductance for the chip. The remaining part is the two arms of the dipole which is represented by a series *RLC* circuit. More accurate circuit for a dipole can be found in [29] but for a narrow dipole working in a narrow frequency band the *RLC* is simpler and sufficient.

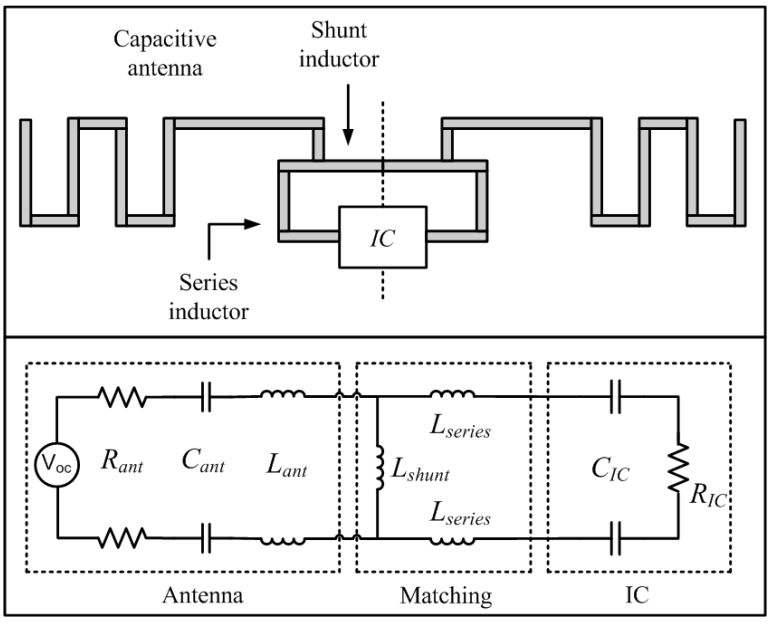


**Fig. 3.15. A typical matched RFID dipole tag and its equivalent circuit.**

The inductance and capacitance of the dipole are influenced by the shape of the dipole arms. The capacitance has a relationship with the dielectric constant of the environment. Thus, this element is expected to be vulnerable to any change in the dielectric constant of the host material. The radiation characteristic of the dipole is represented by the radiation resistance in the circuit and finally the received electromagnetic signal is translated into a voltage source in the circuit. Applying the electric wall theory, the balanced circuit of Fig. 3.15 can be transformed to the unbalanced circuit shown in Fig. 3.16 [13, 30].

The equivalent circuit of Fig. 3.16 is designed and simulated in ADS software. The target of this simulation is to find the impact of increasing the dipole capacitance $C_{ant}$ on the impedance matching. The result of this simulation is presented in Fig. 3.17 (b).

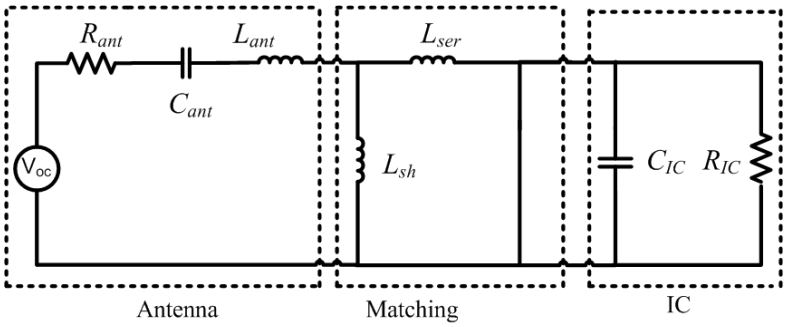


**Fig. 3.16. Unbalanced equivalent circuit of a typical tag.**

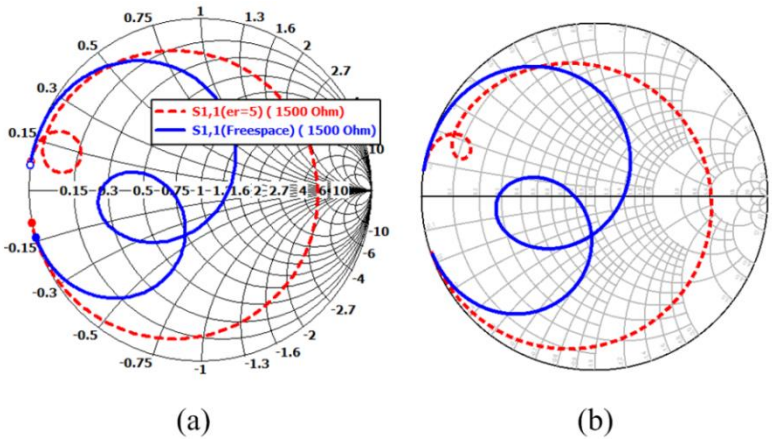


**Fig. 3.17. Detuning effect illustration in Smith chart. (a) Increasing the relative dielectric constant of ALN-9640 host material from 1 (solid line) to 5 (dashed line). (b) Increasing the capacitance of the dipole arm in the equivalent circuit from 1 pF (solid line) to 1.75 pF (dashed line).**

The plot in the Smith chart shows how increasing the capacitance can cause a mismatch. This plot is compared with the plot of detuning effect in ALN-9640 in Fig. 3.17 (a) in which the relative dielectric constant is increased from 1 to 5. The plots in the two Smith charts are quite similar. It is concluded that the detuning effect is basically caused by increasing the value of the antenna capacitance. The antenna capacitance is increased from 1 pF to 1.75 pF in the simulation. More details about calculating the values of each element in the circuit are discussed in Chapter 4. An analysis on the relationship between the dielectric constant of the host material and the capacitance is done in Chapter 5 and a solution for increasing the robustness of the dipole tag is proposed.

# 3.4. State of the Art

The latest achievements in robust tags in the literature are reviewed in this section. Based on the application and the structure of the design, the works are divided into three groups. First, the tags applicable on liquid bottles are reviewed. Second, the most important tags employing ground plane are discussed. Finally, some label-type and groundless tags are reviewed. Studying the advantages and drawbacks of each group determines the common challenges in designing robust tags.

## 3.4.1. Tags for Liquid Bottles

Liquid bottles are one of the most challenging objects for RFID tags. There are a variety of bottles made of different material and filled with different liquids in the market that need to be tracked by RFID technology. The producers of wine are one of the costumers of this technology as they want to have a track of the expensive wine bottles from factory to the consumers. Liquid bottles seriously affect the performance of label-type tags placed on them. High permittivity and conductivity of water are the main reasons for this effect [27, 31]. Although the designs with a ground plane can tolerate liquid bottles, they are costly and bulky compared to label-type tags. In addition, in many applications like tagging goods in stores it is required to hide the tag from the surface of the object for security and appearance reasons. There has been some work in the literature to solve the problem of tags used on liquid bottles. They are reviewed in this part.

One solution is to avoid the liquid by placing the tag on the neck of the bottle. The proposed design in [32] is depicted in Fig. 3.18. The structure of the antenna is quite similar to the conventional T-match tags but the arms of the dipole are connected together with an extra inductive loop. The authors didn't give any details about the theory of the design. However, this tag only works when the bottle is in a standing position because the performance of the tag would be dramatically affected when it is backed by the liquid.

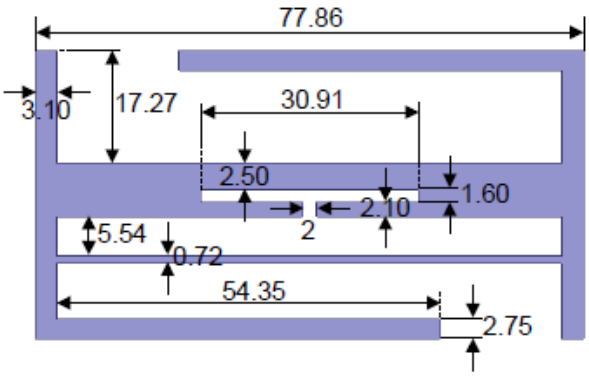


a) Tag antenna layout (unit: mm)

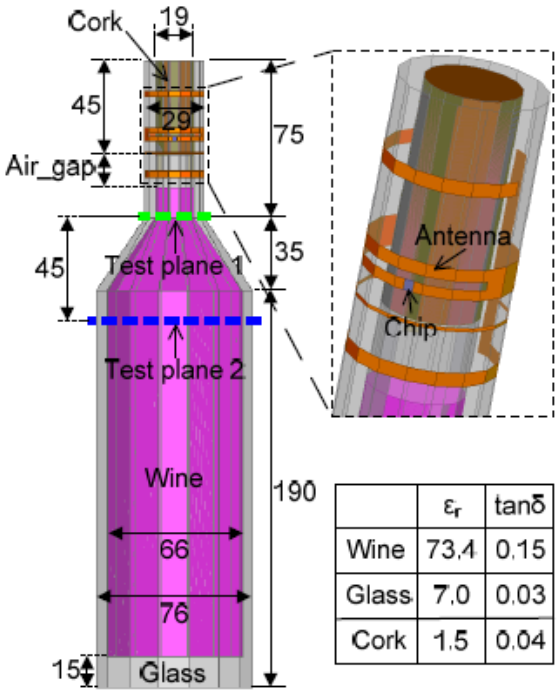


b) Simulation model (unit: mm)

**Fig. 3.18. Tag for neck of the bottle proposed in [32].**

Another solution is to embed the tag inside the cork as suggested in [33]. The proposed design and the fabricated prototype embedded inside the cork is illustrated in Fig. 3.19. The design is a typical meandered dipole matched with an inductive loop. The advantage of this design is that the tag stops working after opening the bottle. This works as a safety lock which prevents opportunists who change the contents of the bottle. However, due to the complicated design, the fabrication process would be costly. In addition, many liquid bottles do not have cork stoppers.

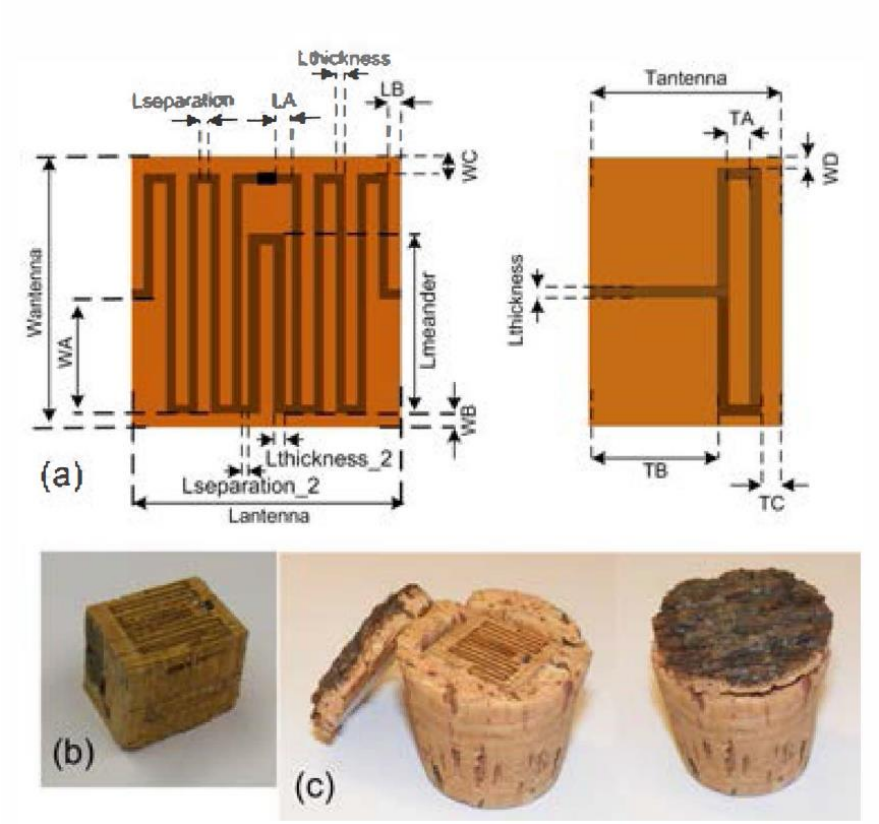


**Fig. 3.19. Cork embedded RFID tag [33].**

Another effort for improving the performance is done with the cost of using a combined reflector plate on the back of the bottle [34]. The work is shown in Fig. 3.20. The tag is a simple dipole with inductive matching loop. The metallic plate at the back of the bottle increases the directivity and gain of the antenna which can somehow compensate the detuning effect of the liquid bottle. The drawback of the design is that the tag is not omni-directional. Furthermore, it is not possible to use the conductive patch on all bottles for appearance reasons.

**Fig. 3.20. Reflector backed tag for liquid bottles [34].**

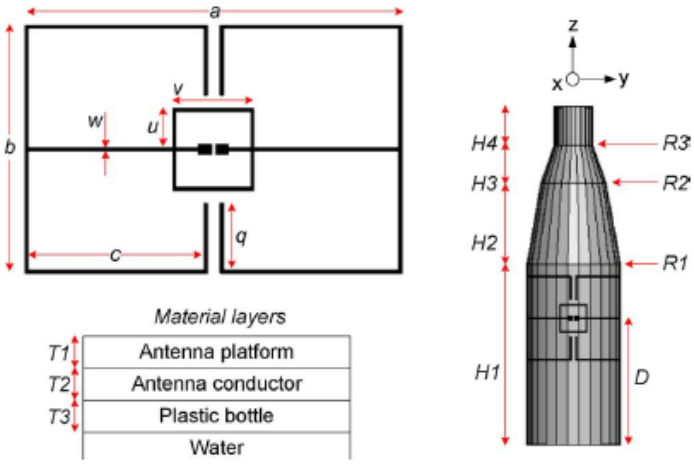


**Fig. 3.21. Folded dipole tag design for liquid bottles [31].**

Another practiced solution in the literature is to fold the tip of the dipole as proposed in [31] or having a dipole with spiral tip [35]. The length of the dipole gets longer by folding the dipole arms. This improves the radiation efficiency of the antenna which is critical on the bottle. It is reported in [31] that by bending the folded dipole shown in Fig. 3.21, around the water filled bottle the null in the dipole E-plane radiation pattern can be removed and the tag can be readable from different angles. The high dielectric constant of the water is the main cause of this phenomenon. The whole bottle becomes part of the antenna in this case and changes the radiation pattern. It is shown in Fig. 3.22 that the nulls in the antenna directivity which represents the radiation pattern disappear after placing the antenna on the water filled bottle.

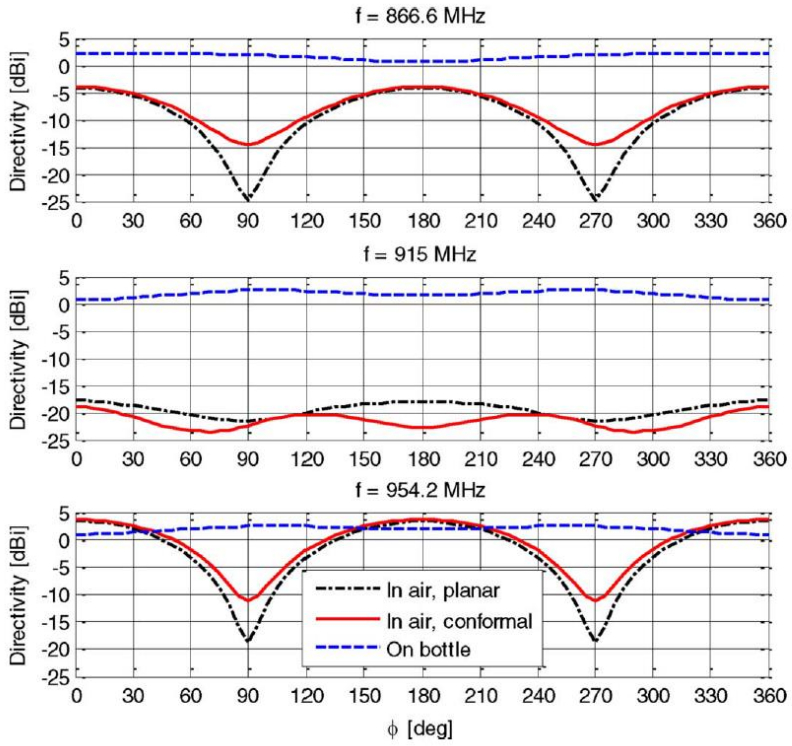


**Fig. 3.22. Directivity of the antenna design of Fig. 3.21 in xy-plane at three different frequencies [31].**

The disadvantage of the design is that the radiation pattern of the tag changes by attaching it on bottles with different shape and size. Thus, the proposed design is only useful on cylindrical bottles with certain size. The inductive matching loop in this design is used as well. However the thin conductive parts of the antenna restricts the bandwidth of the tag [5]. It is proved in Chapter 5 that thin parts make the tag even more vulnerable to the host material as they have less capacitance in the antenna body.

There has been interesting solutions for the problem of tagging the liquid bottles as reviewed here but what is missing in the previous works is a deep study about the effect of the liquid on the performance of the tag in terms of impedance matching and detuning. A comprehensive study is conducted about this issue which is reported in Chapter 4.

## 3.4.2. Tags for Metallic Objects

Metallic objects are the most challenging host for RFID tags. The performance of a typical dipole tag becomes seriously affected in the vicinity of a metallic object

[27, 36, 37]. A metallic plate with a distance of quarter of a wavelength from the dipole tag improves the gain and performance of the antenna but this length in 866 MHz is approximately 86 mm which is not acceptable in most applications. The tag needs to be close to the host metallic objects in a distance much smaller than quarter wavelength. In this condition the currents of the antenna induce almost the same current with reverse phase on the surface of the metallic object [38]. The negative effect of this currents increases when the tag gets closer to the object. It is clear that the tag stops working when the distance from metallic body reaches to zero. The existence of these surface currents can be explained by electromagnetic boundary condition.

It is known that the tangential electric filed on the surface of the metallic host should be zero. Therefore, it is necessary to have the surface currents with reverse phase to cancel the electric field of the antenna on the surface. The image theory can also be used for describing this effect. The metallic surface is removed in image theory while keeping the boundary condition satisfied. Thus, an image antenna is needed in the other side of the plate with reverse phase of currents. The superposition of the electric field of the two sources cancels out each other on the boundary of the metallic plate. The radiation of the two sources also cancels out each other in the far field which leads to a low radiation efficiency of the antenna. The input impedance of the antenna is also influenced by this metal interaction. The change in the input impedance deteriorates the impedance matching with the chip which is another important factor in tag performance. In summary, the radiation efficiency and the input impedance are the two important factors that get affected by a metallic host as a function of the distance [39].

The impact of the presence of a metallic plate in close distance to a quarter wavelength dipole working at 866 MHz is studied in [2]. The radiation efficiency of the antenna as a function of the distance with the metallic plate is plotted in Fig. 3.23 (a). The radiation efficiency increases from a low value up to 25% when the distance is increased to 3 mm. This radiation efficiency at the mentioned thickness is acceptable in practice but the problem is with impedance matching. The input impedance of the antenna remains very low as shown by the plot of Fig. 3.23 (b). Thus, dipole tags are not a suitable candidate for metallic objects.

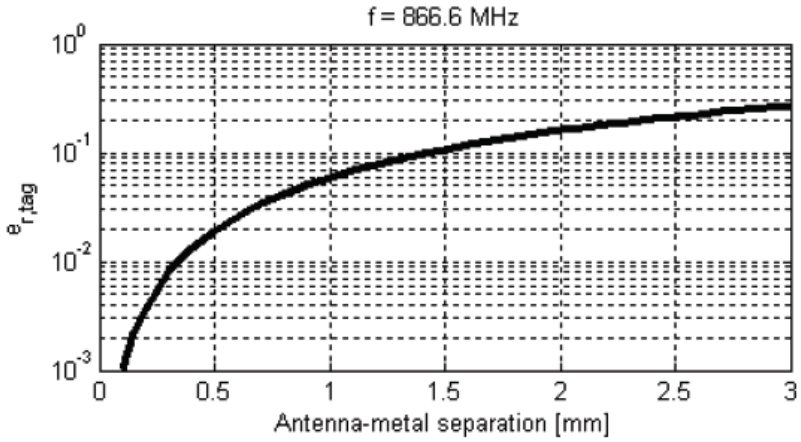


(a)

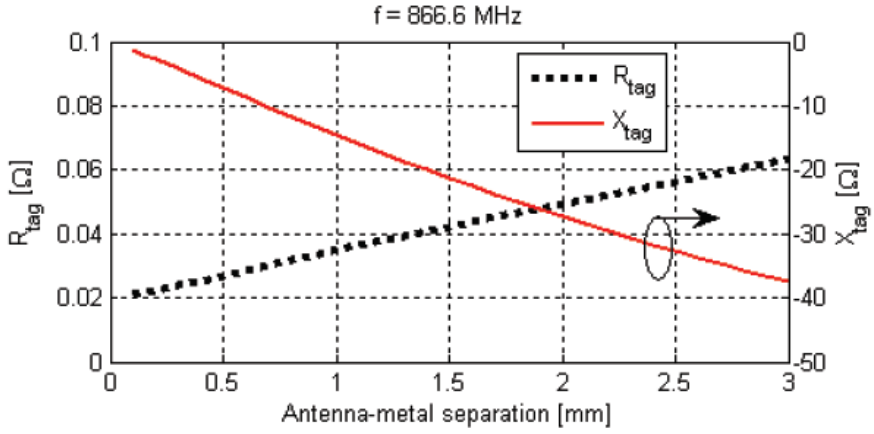


(b)

**Fig. 3.23. The effect of changing the distance of a dipole antenna from the metallic plate on (a) Radiation efficiency and (b) Input impedance [2].**

There has been an extensive amount of studies about metallic mountable tags in the literature. The most significant designs are reviewed in this part. The ground plane seems to be a crucial part in the antenna for protection from the metallic host material. Thus, most of the designs can be categorized as patch antennas. A typical patch antenna is comprised of a ground plane, dielectric substrate, and the conducting patch. In transmitting mode, the patch is excited by a time varying signal. This induces a time varying electric field between the patch and ground plane companied by the surface currents on both of them. The radiation occurs at the two edges of the patch perpendicular to the surface currents. According to the skin effect, the surface currents just exist on the surface of the ground plane facing the dielectric

substrate. Thus, the patch antenna is isolated form the host metallic object while it is working. The thickness of the substrate is normally between $0.01\lambda$ and $0.05\lambda$ [40]. These characteristics make this antenna the best choice as a low profile planar design for metallic mountable tags.

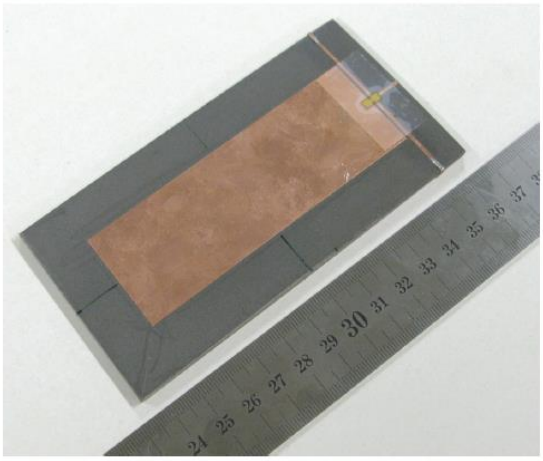

**Fig. 3.24. Long read range patch studied in [41].**

There is no size limit for tags in tracking large metallic objects used in heavy industries. The gain and read range of the tag can be improved by increasing the dimension of the prototype. The work presented in [41] is an example of long read range tags. The designed prototype is shown in Fig. 3.24. The tag is designed on a substrate with relative dielectric constant of 2.2. The overall dimension of the tag is $131\times68\times3.3$ mm$^3$. The authors found that a 16 mm gap between the edge of the patch and substrate can effectively suppress the fringing effect. The reported radiation efficiency of the tag is 89%. The chip is located at the edge of the patch as can be seen in the figure. The other side of the chip is connected to the ground via three sides. The perfect impedance matching can be achieved by adjusting the dimension of these conductive arms. The read range of the tag on a $20\times20$ cm$^2$ metallic plate with *EIRP* = 4 W is 25 m. A similar work is reported in [42].

There is always a compromise between the size of the tag and the offered read range. In many applications the designers have to sacrifice the read range in favour of the size. However there are some size reduction techniques. Applying slots on the patch is a practiced method for size reduction. The presence of slots on the patch forces the surface current to travel a longer distance which basically increases the

length and lowers the resonant frequency of the antenna. A multi-slotted tag design is proposed in [43]. The structure of the tag shown in Fig. 3.25 is comprised of an inductive loop connected to the chip. The currents on the loop excite the slotted patch. The patch is connected to the ground at two corners for impedance matching reasons as authors reported. The overall dimension of the tag is 50×50×1.6 $mm^3$ and the read range is 5 m. The slot is also applied to the designs reported in [44-46].

**Fig. 3.25. Multi-slotted tag reported in [43].**

Employing a high dielectric substrate is another method for reducing the size of the design. By increasing the permittivity of the substrate the electrical length of the system increases which leads to a reduction in the resonant frequency and miniaturization. A ceramic substrate with relative dielectric constant of 48 is used in the work reported in [47]. In addition to the substrate, this design also has slots for size reduction as shown in Fig. 3.26. The overall size of the tag is 25×25×3 $mm^3$ and the read range is 10.1 m.

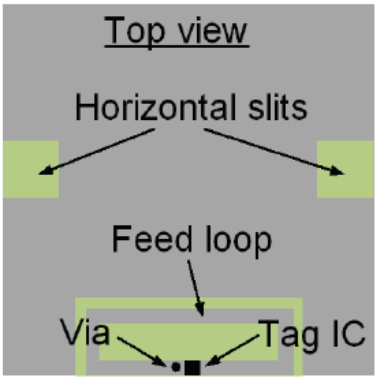


**Fig. 3.26. Miniaturized tag designed in [47].**

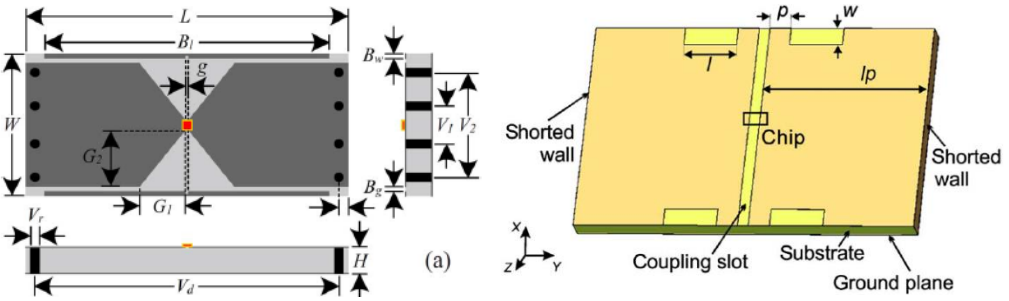


**Fig. 3.27. Center fed tags: (a) Bowtie tag reported in [48]. (b) Stepped impedance tag reported in [49].**

The chip is connected to the edge of the patch in all the tags reviewed so far. There are several designs in which the chip is located in the center of the structure and connected to two patches. The two patches are usually connected to the ground with either conductive wall or vias.

A bowtie shaped tag is reported in [48]. The chip is located in the center of the symmetric patch as depicted in Fig. 3.27 (a) and each patch is connected to the ground plane via holes. The analysis given by the authors define the tag as a parallel *RLC* circuit. The resistance *R* represents the radiation of the tag. The *LC* components behave as a high impedance circuit at resonant frequency. This makes the resistance of the chip be matched to the resistance of the antenna. The resonant frequency is related to the value of *L* and *C* which can be adjusted by changing the dimensions of the tag and number of the via holes. The overall dimension of the tag is 68×30×3 $mm^3$ and the read range reaches up to 3.3 m with *EIRP* = 0.4 W.

A similar design is presented in [49]. The two patched are connected to ground plane using shorted wall instead of vias. This makes the design simpler. The patches are loaded with slots. However the authors call it stepped impedance patch and they use transmission line model to analyse the design. This geometry enables the designer to easily tune the antenna and do the impedance matching. The overall dimension of the tag is 88×60×0.76 $mm^3$ and the read range is 5.4 m with *EIRP* = 4 W. Other similar designs in which the center fed patch is connected to the ground at the edges are reported in [50-54].

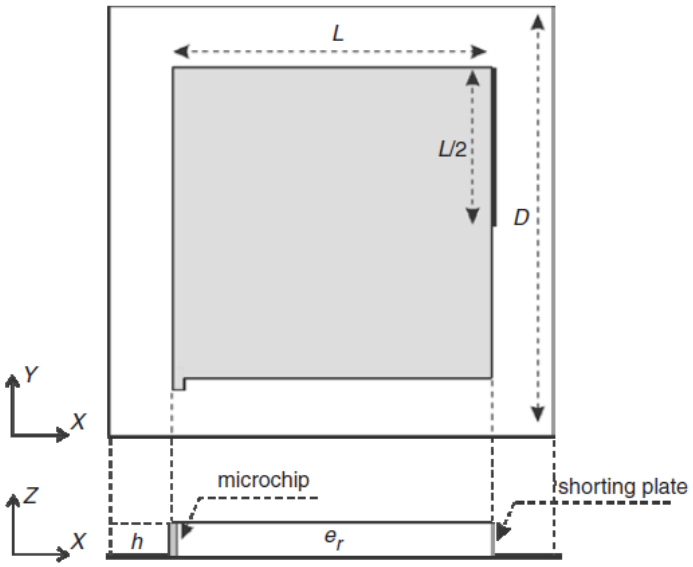


**Fig. 3.28. PIFA design for RFID tag proposed in [55].**

Planar inverted-F antennas (PIFA) are a special type of patch antenna which has low profile and multi-resonant characteristics. These features have made it popular in cell phone antenna designs [56, 57] and RFID tags [2]. A PIFA in its standard shape is a patch antenna which is shorted to the ground at one edge by either conductive wall or vias. Thus the radiation just occurs at the opposite edge of the patch. There is an extra connection between the patch and the ground in standard PIFA design which makes the cross sectional view of the antenna similar to letter F. However, for achieving the desired antenna characteristics in tag designs, the traditional shape of a PIFA needs to be modified usually. For example, the PIFA proposed in [55] is shown in Fig. 3.28. The chip is located at the corner of the design connected to the patch and ground as depicted in the picture. A shorting plate located at the opposite side of the patch connects the patch to the ground plane. The design has the overall dimension of 59×59×3 $mm^3$ and the read range is 4.3 m on a 60×60 $cm^2$ metallic plate with *ERP* = 0.5 W.

The authors of [58] showed by applying an open end stub to the design it is possible to eliminate the connection of the chip to the ground and also achieve a dual band antenna that can cover the two common frequency band in UHF RFID tag protocol. The proposed design is depicted in Fig. 3.29. The overall size of the design is 62×51.3×3 $mm^3$ and the measured read range with *ERP* = 2 W is 10.9 m. Other work that can be categorized as PIFA designs are reported in [59-61].

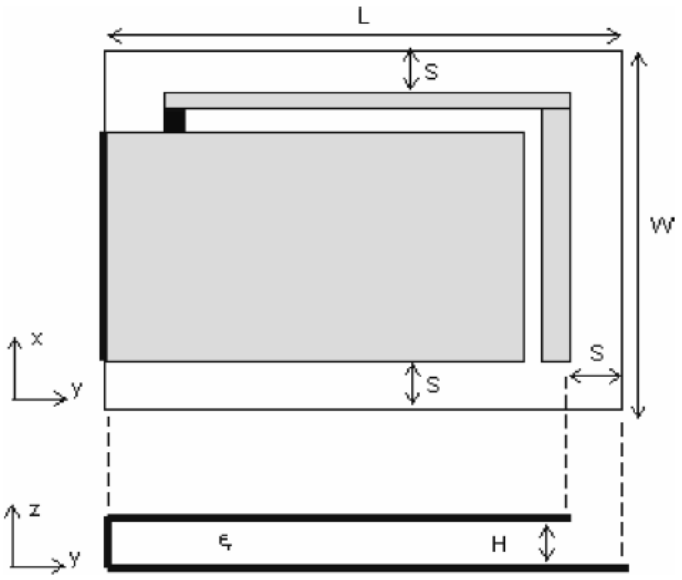


**Fig. 3.29. Dual band modified PIFA reported in [58].**

Not all the designs in the literature are limited to patch antenna. In some works a dipole antenna is used and the destructive effect of the ground plane is controlled by adding extra components and protecting the dipole. The design introduced in [62] is depicted in Fig. 3.30. An intermediate de-coupling layer is applied between the ground and dipole for protection. The overall size is 95×25×3.6 $mm^3$ and the read range with *EIRP* = 4 W is 6.2 m. Parallel bars are used as intermediate layer in the work proposed in [63]. The bars protect the tag and also excite the multi-resonant modes.

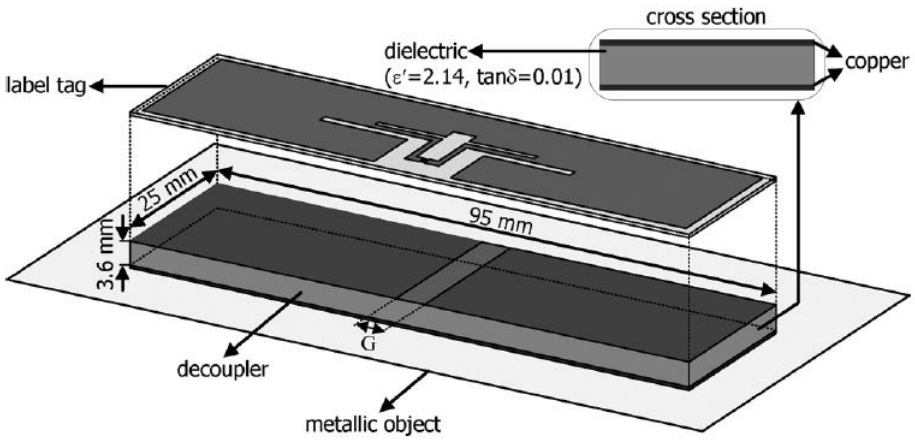


**Fig. 3.30. Dipole tag protected by de-coupler proposed in [62].**

Another practiced method for protecting the antenna from the metallic object is to support the antenna with a cavity. The radiating part of the system is usually a slot [64, 65] or patch antenna [66, 67]. The cavity backed tag antenna proposed in [68] is reviewed here. The structure of the design is illustrated in Fig. 3.31. The overall size of the tag is 127×90×5 $mm^3$. The structure is comprised of three parts: The cavity, the dipole, and the slotted cover. The chip is located in the middle of the dipole. Looking at the system as a transmitting antenna, the dipole excites the cavity and the radiation take place at the two U-slots on the cover face of the cavity as can be seen in the figure. According to the size of the structure which is bigger that the most reviewed works a long read range is expected. The antenna reached a 5.7 dBi gain and 23 m of read range. Another similar work in the literature is a cavity backed bowtie antenna reported in [69].

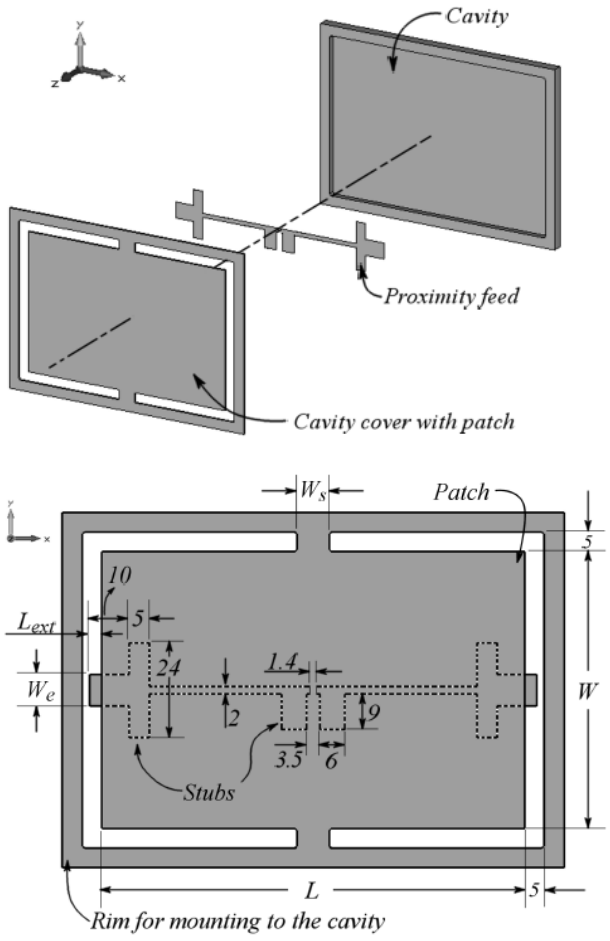


**Fig. 3.31. Cavity backed tag proposed in [68].**

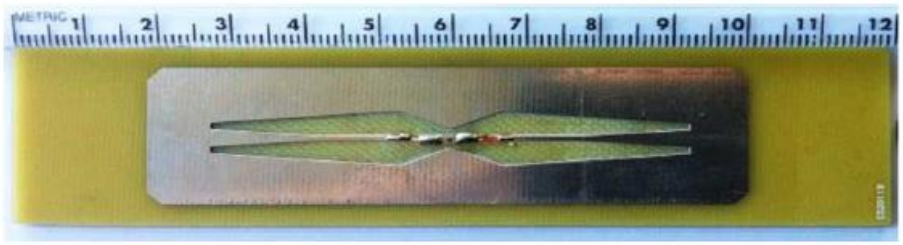

**Fig. 3.32. The antenna proposed in [70].**

Connection to the ground or having extra layers increases the cost of the prototype. All of the tags reviewed so far consist of costly and complicated structures. Here, some tags with simpler design are reviewed. The design shown in Fig. 3.32 is introduced in [70]. It is comprised of an FR-4 substrate with 1.5 mm thickness. One side of the substrate is the ground plane and the other side is the slot patch shown in the figure. As can be seen there is no need for connection between the two layers. The overall dimension is 120×23×1.5 $mm^3$. The read range of the tag in free space is 3.5 m with *EIRP* = 4 W. There is no study about the performance on large metallic plates. Another slot design tag is proposed and analysed in [71].

The input impedance of a dipole antenna reduces dramatically when it is close to a metallic plate as mentioned earlier in this section. The reduction of the input impedance increases the mismatch loss and decreases the radiation efficiency of the antenna [72]. There has been some effort to tackle this problem by improving the impedance of the antenna when it is close to a perfect electric conductor (PEC). It is known that the input impedance of a dipole can be increased by having a folded dipole [64]. It was shown in [72] that by designing a multiple-arm folded dipole the radiation efficiency and impedance matching of a dipole located at a distance less than 0.05 λ from the PEC can be improved. Following this finding, the authors in [73] proposed a three arm folded dipole designed to be matched to RFID chip. The prototype of the design is depicted in Fig. 3.33 (a). The overall size of the design is 125×14×1.5 $mm^3$ and the achieved read range is around 5 m with *ERP* = 2 W. The authors managed to reduce the length of the antenna by cutting one of the dipole arms and connecting that side to the ground via holes as shown in Fig. 3.33 (b). However, this method increases the cost of the fabrication. Similar multiple-arm folded dipole tags are suggested in [74, 75].

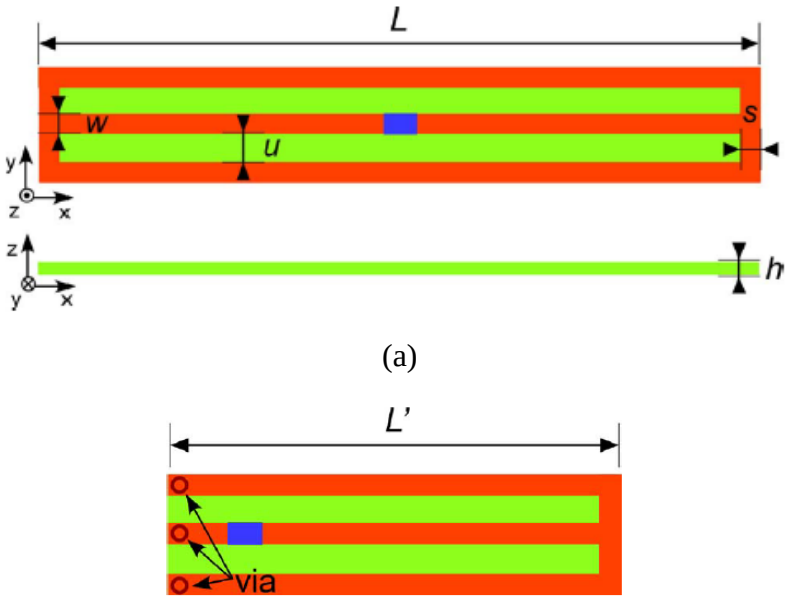


**Fig. 3.33. Multiple-arm folded dipole proposed in [73]. (a) Basic design. (b) Compact design.**

Following the trend to make the tag design as simple as possible, there has been some groundless tag designs. This type of tag is simply comprised of a substrate and a radiator patch on top. The surface of the metallic host material plays the role of the ground plane when the tag is attached on it. A sample of this type of tag is proposed in [76]. The structure of the fabricated prototype is depicted in Fig. 3.34.

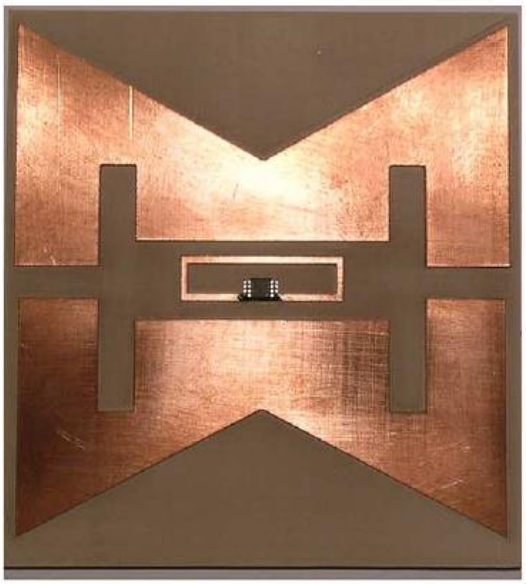

**Fig. 3.34. Ground less tag proposed in [76].**

The chip is connected to a matching loop which provides the required inductance for matching. The patch is inductively coupled to the loop. The loop excites the two patches which provide a dual band frequency response for working at the desired UHF RFID frequencies. The overall size of the design is 80.5×74.5×1.5 $mm^3$. The tag is basically designed and tuned to work on metallic objects. However, it can still work on non-metallic material but with limited read range. The measured read range on metallic plate with *EIRP* = 4 W is 7.9 m and in free space is 4.4 m.

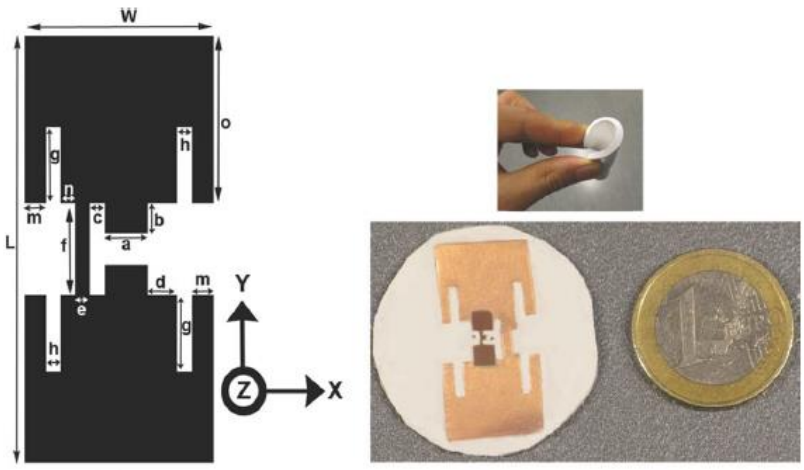


**Fig. 3.35. Miniaturized groundless tag reported in [77].**

In order to achieve low cost conformal tags, flexible substrates can be used in the design of groundless tags. The thin flexible design is a suitable choice for tagging metallic cans and containers. A miniaturized groundless tag is introduced in [77]. The design is employing a high permittivity ceramic ($BaTiO_3$) polymer substrate with 1.5 mm thickness. The relative dielectric constant of the polymer is 12 which helps in miniaturizing of the antenna by increasing the electrical length of the design and reducing the resonant frequency. The overall size of the design is 28×13×1.5 $mm^3$ which makes it suitable for tracking small metallic objects. The structure of the design is depicted in Fig. 3.35. The two halves of the tag are connected by the thin track (f). This creates an inductive loop for impedance matching. The slots (g) in the design help to lengthen the path of the surface currents. This lowers the resonant frequency and contributes in further miniaturization of the design. The resonant frequency of the tag antenna can be tuned by altering the length of the slot (g). The flexible substrate makes the tag attachable on conformal objects. The tag was

measured with *EIRP* = 4 W and the achieved read range on metallic object is 2.65 m. The performance on non-metallic objects is not reported. Other groundless tag designs can be found in [78, 79].

# 3.5. Conclusion

The basics of passive UHF RFID tags have been introduced in this chapter. Some designs in the literature for liquid bottles were reviewed. It is learned that there is a lack of study in the literature on the effect of liquid bottle on the performance of the tag antenna in terms of equivalent circuit and impedance matching. All the reviewed efforts were about increasing the directivity of the tag on the bottle or avoiding close contact between the liquid and the tag. Tags for metallic objects were also reviewed in this chapter. It is learned that long read range tags are available with the cost of complicated and bulky designs. Different types of patch antennas were introduced. Patch antennas offer a low-profile tag with outstanding performance but the need for conductive wall or via is a negative point. Patch antennas are functional on non-metallic objects but the performance is limited in terms of read range and radiation pattern. A multiple-arm folded dipole was introduced as a simple design with acceptable performance in vicinity of the metallic objects but the performance on non-metallic objects is limited as the tag is tuned and matched for working on the metallic plate. Simpler patch designs were introduced by eliminating the need for a ground plane. However, the performance on non-metallic objects is limited again.

# Chapter 4. A UHF RFID Tag with Improved Performance on Liquid Bottles

The literature review in Chapter 3 showed there is a lack of study on the effect of liquid bottle on the performance of the tag. In this chapter, the performance of one of the latest commercial tag designs on a thin liquid bottle is investigated. The effect of water on the frequency response is studied from the equivalent circuit point of view. It is found the effect of the liquid bottle is a reduction in radiation resistance and an increase in the loss resistance. This destructive effect is compensated by adding two arms to the dipole without increasing the size of the tag and a new design with an improved reading range and bandwidth is then proposed. Finally, the performance of the proposed prototype is tested and compared with the commercial tags.

# 4.1. Analysis of ALN-9768

ALN-9768 which is known as "Wonder Dog" is one of the latest products of Alien [22]. It is a general purpose tag particularly designed for RF reflective and absorbing materials such as metals and bottled liquids. The performance of this tag in free space and on a thin liquid bottle is studied by simulation and circuit analysis in the following subsections.

## 4.1.1. Structure Simulation

The physical structure of ALN-9768 is analysed and simulated by using CST software. The passive tag is composed of a chip and an antenna which are connected together by a matching loop as shown in Fig. 4.1.

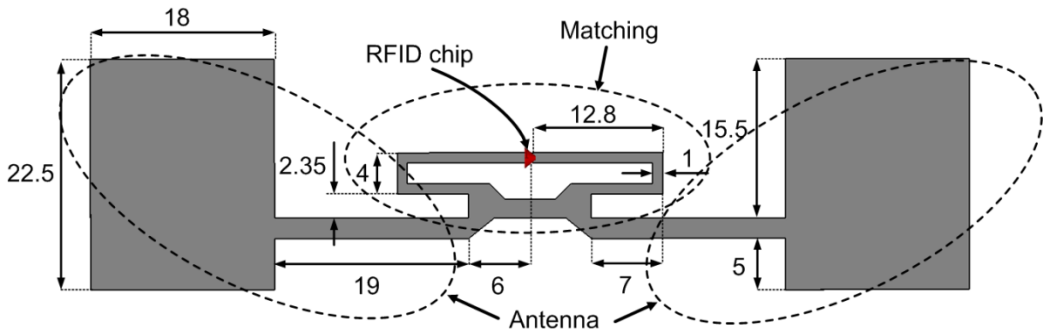


**Fig. 4.1. Physical structure of ALN-9768 with dimension details. All values are in millimeters.**

The matching loop provides the required inductive impedance for conjugate matching to the capacitive impedance of RFID chip. This is to achieve the maximum power transfer [25]. The short dipole antenna is loaded with capacitive plates at both ends. This facilitates the impedance matching and also increases the average current on the radiating wire leading to an improvement in the radiation efficiency of the tag [21]. It is known that the radiation efficiency of the tag is severely limited by the presence of water [31]. Thus, perfect impedance matching with a sufficient bandwidth plays an important role in having a reliable universal tag that covers UHF RFID EPC Gen 2 band (860-960 MHz, but most countries use either 865-868 or 902-928 MHz bands). The reflection coefficient S11 parameter of the tag in free space and on a plastic bottle with relative permittivity of 2.3, thickness of 1 mm and dimensions of 80×80×200 $mm^3$ is simulated and the result is plotted in Fig. 4.2.

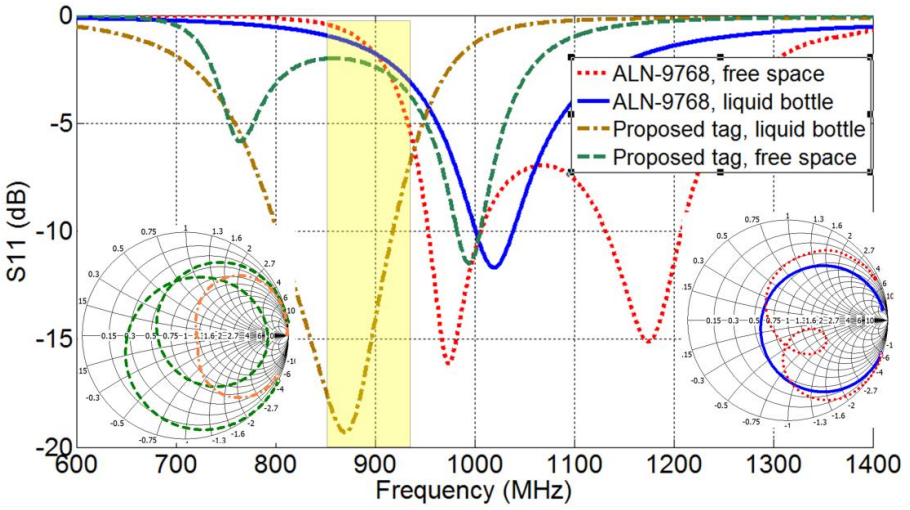


**Fig. 4.2. S11 and the Smith chart of ALN-9768 and the proposed tag in free space and on a plastic bottle filled with water.**

The S11 is at the chip input port and matched to the chip impedance. It is observed that the tag is out of tune. In general purpose tags, the antenna is usually designed to resonate slightly higher than the various international band. This compensates for the effect of the dielectric material on the tag [5]. As can be seen in Fig. 4.2, the frequency response of the tag is affected by the liquid bottle with a smaller bandwidth and smaller return loss. This not only affects the reading range but also makes the tag sensitive to any changes in the material and thickness of the bottle and also the environmental temperature. The permittivity of the tag substrate is altered by changing the environmental temperature. This leads to detuning of the tag. The study in [80] shows the resonant frequency of a tag with paraffin wax substrate can be shifted up to 30 MHz by increasing the temperature from 30º to 60º C. The role of the liquid bottle in changing the frequency response of the tag can be clarified by studying the equivalent circuit of the tag in the next subsection.

## 4.1.2. Equivalent Circuit Analysis

The physical structure of the tag in Fig. 4.1 can be translated into the equivalent circuit of Fig. 4.3 by applying the electric wall concept [5], [30]. Due to the mutual inductance and radiation from the matching part it is difficult to have an accurate prediction on the values of the elements in the circuit. However it is possible to have an approximate estimation on the values. The inductance can be found by (4.1):

$$L = \frac{\mu_0}{2\pi} l \left( \ln\left[ \frac{l}{w} \right] + \frac{\pi}{2} \right);\ \mu_0 = 4\pi \times 10^{-7}\, H/m \tag{4.1}$$

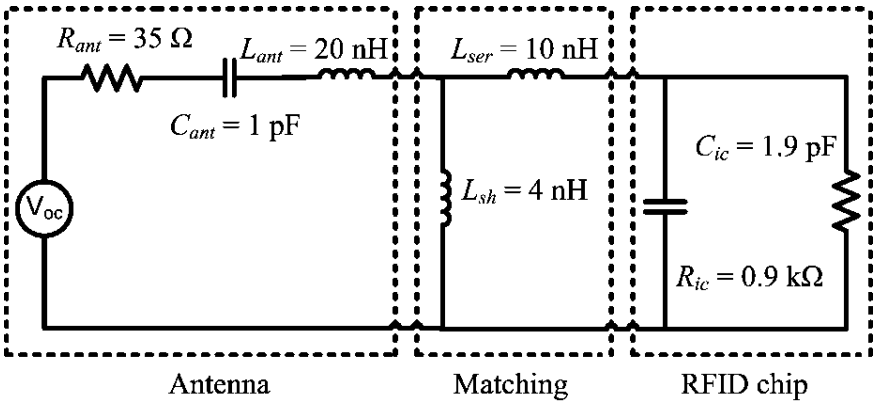


**Fig. 4.3. Equivalent circuit of ALN-9768. The values are for the tag working in free space.**

where *l* and *w* are respectively the length and width of the conductive trace [5]. The calculation of the inductance for the antenna divided by the electric wall results in: $L_{ser}$ = 10.5 nH, $L_{sh}$ = 3.2 nH, and $L_{ant}$ = 19.3 nH. The antenna capacitance is mostly provided by the plates at the end of the dipole. A study done in [5] shows that a disk with radii of around 1 cm provides capacitance of about 1 pF. The antenna resistance is the sum of the radiation and loss resistance ($R_{ant} = R_{rad} + R_{loss}$). The loss resistance is usually negligible in comparison to radiation resistance at the working frequency of UHF RFID tag in free space. The radiation resistance for a small dipole can be approximated by (4.2):

$$R_{rad} = 80\left( \frac{\alpha \pi l}{\lambda} \right)^2 \tag{4.2}$$

where *l* is the length of the antenna and $\alpha$ is a factor between 0.5 and 1 depending on the current distribution along the antenna. For example, the factor $\alpha$ is equal to 1 for a dipole antenna with uniform current distribution and it is equal to 0.5 for an open-ended short dipole [21]. By considering the working frequency of the tag at 866 MHz, the radiation resistance is supposed to be between 12.17 Ω and 48.66 Ω. The equivalent circuit for Higgs-4 RFID chip is a 1.8 kΩ resistor in parallel with a 0.95 pF capacitor. These values are respectively divided and multiplied by 2 after

applying the electric wall concept. ADS software is used to simulate the equivalent circuit and the value of elements that achieved by fine tuning is given in Fig. 4.3. They are in good agreement with the predicted values by calculation. These values are for the tag working in free space. It is observed that by increasing the value of $R_{ant}$ from 35 Ω to 125 Ω the frequency response of the circuit resembles the effect of the liquid on the tag. The result is depicted in Fig. 4.4 which is similar to Fig. 4.2. As shown in Fig. 4.5, the directivity of the tag is increased from 1.92 dBi to 3.29 dBi in presence of liquid but the total radiation efficiency is decreased from -0.17 dB to -22.17 dB. Thus it can be concluded that the liquid causes an increase in $R_{loss}$ leading to a total increase in $R_{ant}$. This results in the impedance mismatch and reduced bandwidth.

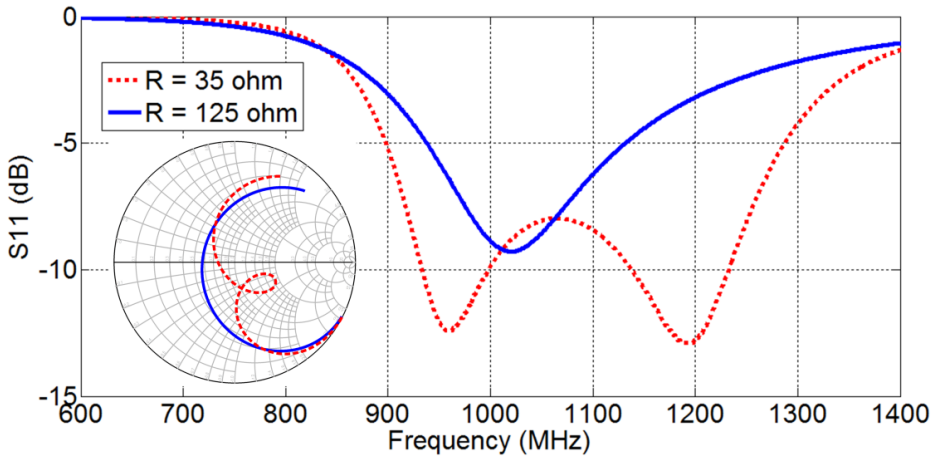


**Fig. 4.4. The frequency response of the equivalent circuit for $R_{ant}$ = 35 Ω and $R_{ant}$ = 125 Ω.**

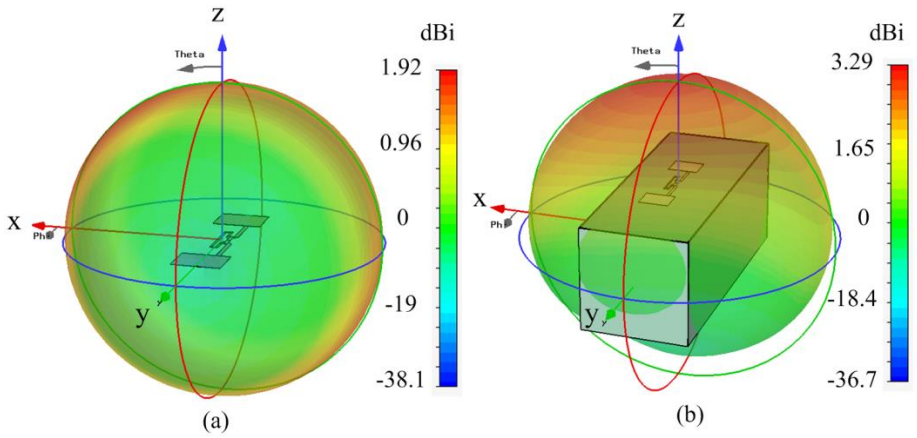


**Fig. 4.5. The radiation pattern of ALN-9768 in: (a) free space and (b) on a plastic bottle filled with water.**

# 4.2. Equivalent Circuit Modification

Having identified the problem, a novel solution is proposed in this section by compensating the effect of the liquid: a smaller resistance in parallel to $R_{ant}$ is added. In this way it is possible to correct the total resistance in the antenna body in order to create the optimum impedance matching with the chip. The parallel resistance is added to the circuit in the form of another series resonant *RLC* circuit as shown in Fig. 4.6. The resonant frequency of the added *RLC* circuit should be close to the resonant frequency of antenna body. To show the effect of the new added resistance, a high value of about 1 kΩ is considered first. Such a high resistance in parallel to 125 Ω should not make a significant change on the frequency response. For the next step, the value of resistance is set to be about 35 Ω. Compensation takes place at this point as depicted in Fig. 4.7.

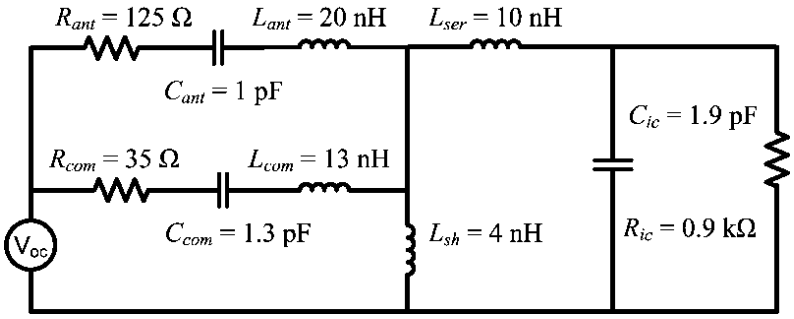


**Fig. 4.6. Modified equivalent circuit of the tag for compensating the effect of liquid on the frequency response.**

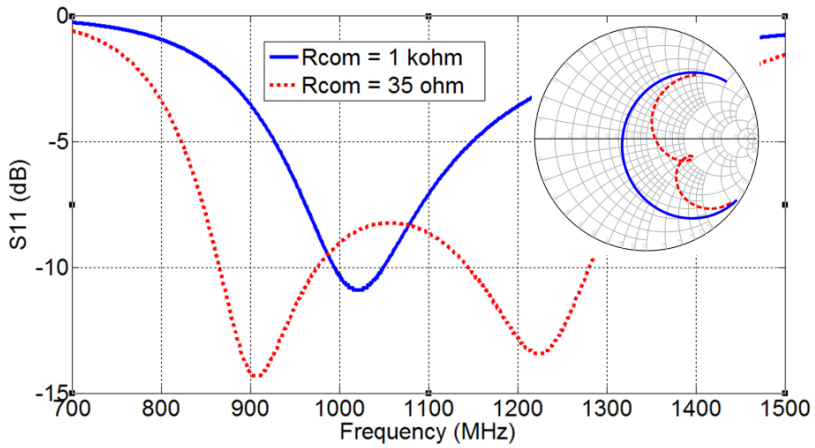


**Fig. 4.7. Determining the effect of $R_{com}$ on the frequency response by changing the resistance from 1 kΩ to 35 Ω.**

In an optimum tag design the impedance of antenna should be matched at the working resonant frequency. The circuit of Fig. 4.3 is simply translated from the physical structure and it cannot clearly reflect the manner of the system in resonance. This circuit can be transformed to a simpler form by using the method introduced in [13]. For the proposed circuit in Fig. 4.6, another stage of transformation is needed. It is found that the proposed circuit can be simplified to the circuit shown in Fig. 4.8. The parameters $\beta$, $x$, and $y$ can be found by following equations:

$$\beta = \frac{L_{sh}}{L_{sh} + L_{ser}} \tag{4.3}$$

$$x = 1 + \frac{Z_{ant}}{Z_{com}} \quad , \quad y = 1 + \frac{Z_{com}}{Z_{ant}} \tag{4.4}$$

$$Z_{ant} = R_{ant} + j\omega L_{ant} - \frac{j}{\omega C_{ant}} \tag{4.5}$$

$$Z_{com} = R_{com} + j\omega L_{com} - \frac{j}{\omega C_{com}} \tag{4.6}$$

where $Z_{ant}$ and $Z_{com}$ are the input impedances of the antenna body and the added part for compensating the effect of liquid. The derivation of equation (4.4) is proved in Appendix A. The transformed circuit depicted in Fig. 4.8 is comprised of two series resonators and one parallel resonator.

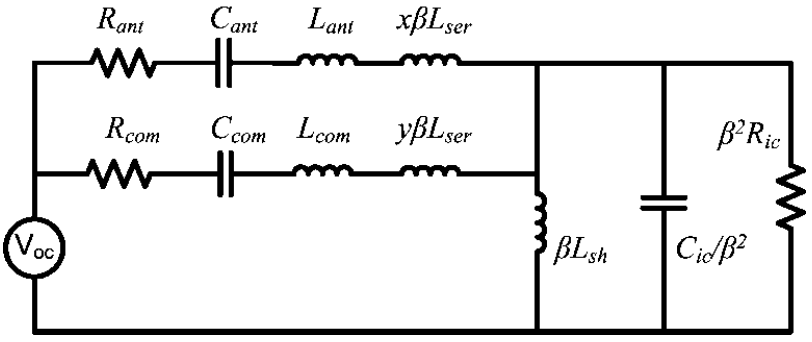


**Fig. 4.8. The modified equivalent circuit transformed into a simple circuit consisting of parallel and series resonators.**

The series resonators act as a short circuit at the resonant frequency and the parallel resonator acts as an open circuit. So, the circuit simply converts to a new arrangement of resistors. The maximum power transfer occurs when $R_{ant}$ in parallel to $R_{com}$ is equal to $\beta^2 R_{ic}$.

# 4.3. Tag Design and Measurement

The proposed equivalent circuit of Fig. 4.6 is translated into the physical structure shown in Fig. 4.9. The structure is designed and simulated using CST software. The overall structure of the proposed tag is based on the dimensions of ALN-9768 shown in Fig. 4.1. The dimension of the matching loop is increased in the proposed design to shift the resonant frequency of the tag down to the required band when it is on the bottle. The added series *RLC* circuit is translated into two arms in symmetry as can be seen in Fig. 4.9. The short gap of the arms provides enough capacitance and low loss resistance needed for impedance matching as discussed in the preceding section. The frequency response of the proposed design is depicted in Fig. 4.2 as well for easy comparison with the reference tag. The added arms increase the return loss and bandwidth of the tag in the working frequency. The -10 dB bandwidth is increased from 3.7 % to 13.5 % for the tag on the bottle. This is achieved without increasing the dimensions but using the available space in an efficient way. In general, if the size is limited in one or two dimensions, the performance can be improved by using more of the remaining space [21]. The S11 of the proposed design in free space is around -2 dB in the desired band as can be seen in Fig. 4.2. According to the high radiation efficiency of the tag in free space, this value is sufficient for most RFID applications in practice [81].

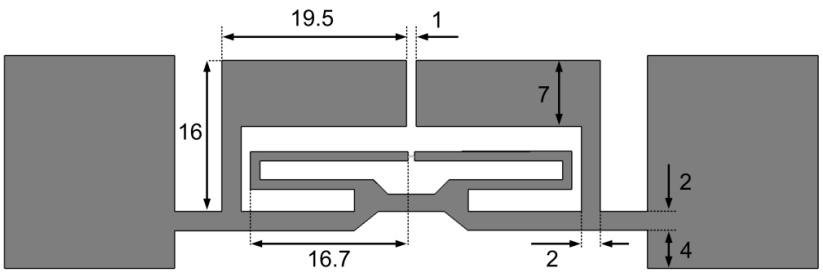


**Fig. 4.9. Proposed modified structure of the tag for compensating the effect of liquid on the frequency response. All values are in millimeters.**

A sample of the proposed tag is made by etching the structure of Fig. 4.9 into a copper sheet. A Higgs-4 SOT RFID chip is soldered to the tag. Please see Appendix B for more information about this chip. The reading range of the tag is measured in an anechoic chamber using Nordic ID PL3000 UHF RFID reader which is a handheld device with 630 mW equivalent isotropic radiated power (*EIRP*). The performance of the tag is compared with ALN-9768 and ALN-9770 (another tag from Alien known as BAT). This tag is specially designed for automotive batteries and other challenging metal, plastic, and fluid containers [22]. Three different types of water bottle are used for the experiment. The measurement setup and the tags on the bottles are illustrated in Fig. 4.10. The maximum reading range is measured in each case and the results are listed in Table 4.1. The proposed design offers the longest reading range in all cases.

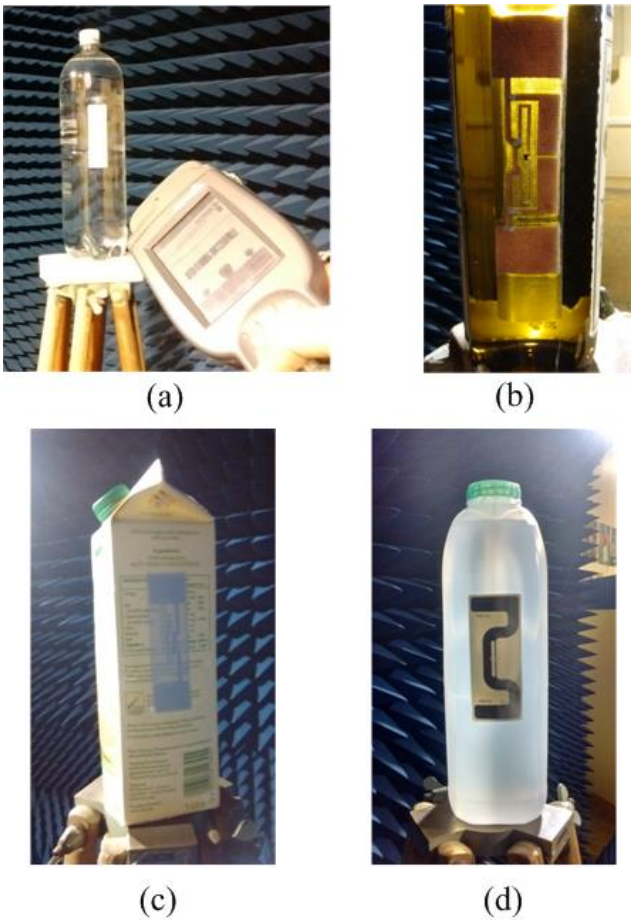


**Fig. 4.10. (a) Determining the reading range of the tags in an anechoic chamber. (b) Proposed design on a glass bottle. (c) Wonder Dog on a paper carton. (d) BAT on a plastic bottle.**

**Table 4.1. Reading range of the tags in centimeters.**

| Material | BAT | Wonder Dog | Proposed design |
|---|---|---|---|
| Free space | 110 | 150 | 220 |
| Paper bottle | 29 | 45 | 79 |
| Glass bottle | 13 | 22 | 31 |
| Plastic bottle | 16 | 23 | 54 |

# 4.4. Conclusion

One of the latest commercial UHF RFID tag designs on liquid bottles has been analysed in this chapter. Equivalent circuit analysis of the tag working on a liquid bottle showed the liquid dramatically affects the impedance matching between the tag and the RFID chip by changing the input impedance of the tag antenna. The result of the analysis confirmed the liquid bottle causes an increase in the real part of the input impedance of the tag antenna which is basically the loss resistance as the liquid bottle absorbs the energy of the tag. This change in the input impedance of the antenna limits the amount of power delivered to the chip and consequently reduces the read range of the tag working on liquid bottle.

The proposed solution to overcome the destructive effect of the liquid bottle is to add two extra arms in the antenna body. The extra arms reduce the real part of the input impedance of the antenna and help to reach an optimum impedance matching between the tag antenna and the chip. Both the simulation and experimental results have shown that the proposed solution can increase the read range of the tag on different liquid bottles and also in free space. This improvement is achieved without increasing the overall dimensions of the designs compared to similar commercial tags. The proposed solution in this chapter can be used as a general idea in designing novel robust tags.

# Chapter 5. RFID Tags Mountable on Metallic and Non-Metallic Objects

After studying and improving the performance of a tag on liquid bottles in previous chapter, more general designs are proposed in this chapter which can tolerate a range of materials. This chapter is comprised of two main sections. In the first section, a study is performed on the main circuit elements of a typical label-type tag with the target of finding the most vulnerable parts to host material. It is found that the capacitance in parallel to the feeding point of the tag is the most sensitive element in the circuit. The capacitance of the antenna body is also found to be an important element. A bigger antenna capacitance leads to less sensitive tag designs. Based on these findings a low profile and low cost label-type tag design is proposed.

In the second section, a dual-polarized tag supported by substrate and ground plane is introduced. It is known that by supporting the slot antenna with a shallow cavity, the robustness of the tag to metallic objects can be achieved. Applying this method, a dual-polarized thin cavity-backed slot antenna for RFID tag is proposed in this section. The simple single layer design with no via enables a low cost production. Dual-polarized symmetric shape is another advantage of the proposed tag. Small handheld RFID readers have a linearly polarized antenna that needs to be aligned in polarization with ordinary tags while the proposed design guarantees a reliable connection regardless of the orientation of tag and reader.

# 5.1. Label-Type 3D RFID Tag Mountable on Metallic and Non-Metallic Objects

Cost and reliability in performance are two prominent factors in RFID tags. Label-type tags made with flexible thin material are reliable and cost effective for tracking purposes but they fail on challenging materials like water and metals [27]. The target of this section is to investigate a way to eliminate the need for substrate in the design and have a label-type tag with reliable performance. The equivalent circuit of a common design of tag is studied first and the most sensitive elements of the circuit are identified and analysed. A novel design of the tag is proposed after that and the performance is studied by performing simulation and experiment.

## 5.1.1. Capacitance Analysis

As mentioned earlier, metallic and high dielectric objects are the most challenging materials for tags. Metallic objects induce a short circuit on both sides of the chip and the tag eventually stops working but high dielectric materials have different effect on the circuit. By attaching the tag on a high dielectric material all the capacitances in the circuit undergo a change [28]. This affects the impedance matching between the chip and the antenna. Consequently, the reading range is reduced and the tag can even be out of order in severe cases. This phenomenon is called detuning which was studied in Section 3.3. Analysing the role of the capacitances in the equivalent circuit can be helpful for producing new robust designs.

### 5.1.1.1. Capacitances in the Equivalent Circuit

The equivalent circuit of a common RFID tag is illustrated in Fig. 5.1. There are three capacitors in the circuit as shown in the figure. $C_{ic}$ is the internal capacitance of the chip that is fixed and cannot be affected by the adjacent material. $C_{sh}$ is the shunt capacitance in the matching loop which is normally negligible when the tag is in free space and $C_{ant}$ is the antenna capacitance [5]. The sensitivity of $C_{sh}$ and $C_{ant}$ is studied in the following.

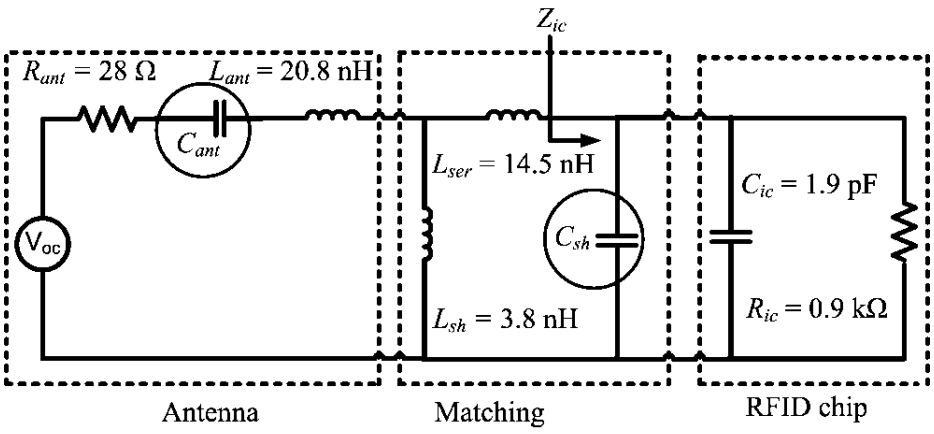


**Fig. 5.1. Equivalent circuit of a typical RFID tag.**

To study the role of $C_{ant}$ the input impedance of the dipole can be considered first by (5.1):

$$Z_{in} = R + j\omega L - \frac{j}{\omega \varepsilon_e C_0} \tag{5.1}$$

where $R$ is the radiation resistance of the antenna, $L$ is the inductance, $\varepsilon_e$ is the effective relative dielectric constant of the background material, and $C_0$ is the primary capacitance of the dipole in free space. Now, the input impedance in a certain fixed frequency can be considered as a function of $\varepsilon_e$. By calculating the derivative of the input impedance of $\varepsilon_e$ it can be determined how the impedance is influenced by the effective relative dielectric constant:

$$\frac{\partial Z_{in}}{\partial \varepsilon_e} = \frac{j}{\omega C_0 \varepsilon_e^2} \tag{5.2}$$

For making the input impedance independent of $\varepsilon_e$ , the term $j/\omega C_0$ should be close to zero as much as possible. One way is to increase the working frequency but it is not practical as UHF RFID band is limited to 860-960 MHz. Another solution is to increase $C_0$. The practical way to increase this capacitance is increasing the surface area of the dipole which reduces the inductance $L$ as well. This balance between $L$ and $C_0$ helps to maintain the resonant frequency of the dipole in the desired band.

A straightforward way to analyse the effect of $C_{sh}$ is to add it to $C_{ic}$ and calculate $Z_{ic}$ as shown in Fig. 5.1. This impedance can be found by (5.3):

$$Z_{ic} = \frac{R_{ic}}{1+\omega^2 R_{ic}^2 (C_{ic}+C_{sh})^2} - j\frac{\omega R_{ic}^2 (C_{ic}+C_{sh})}{1+\omega^2 R_{ic}^2 (C_{ic}+C_{sh})^2} \quad (5.3)$$

$C_{sh}$ exists in the denominator of both real and imaginary part of $Z_{ic}$. This means a small change in the value of this capacitance can dramatically affect the impedance matching between chip and antenna. The impact of changing the capacitances on the impedance matching is studied in the next subsection.

### 5.1.1.2. Capacitance and Impedance Matching

The equivalent circuit of Fig. 5.1 is analysed using ADS software. The optimum value of elements for having a perfect impedance matching is mentioned in Fig. 5.1.

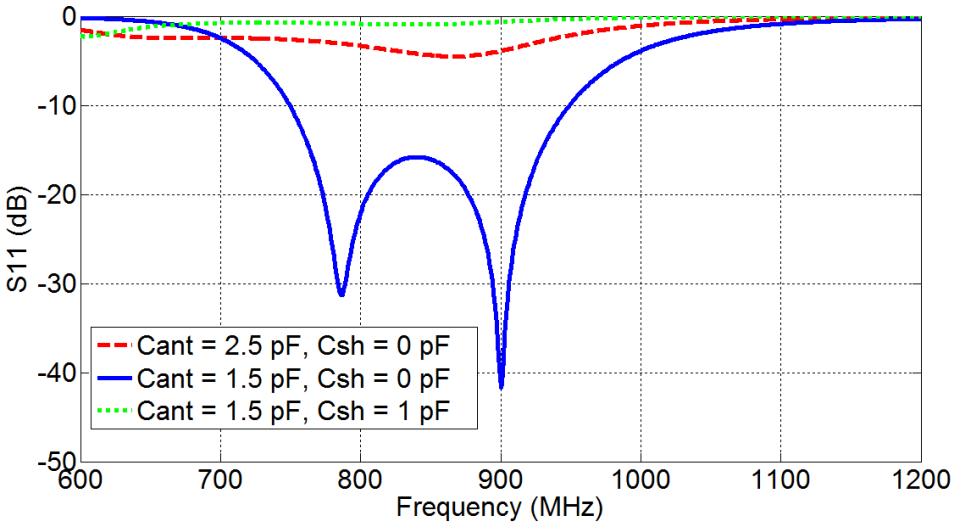


**Fig. 5.2. Effect of increasing the capacitances of equivalent circuit by 1 pF on the return loss.**

The primary value of $C_{sh}$ and $C_{ant}$ is 0 pF and 1.5 pF respectively. The effect of increasing the value of each capacitance by 1 pF is illustrated in Fig. 5.2. As can be seen in the figure, the resonant frequency does not shift by increasing the $C_{ant}$ but the return loss is degraded. There is still acceptable impedance matching after the change as the S11 is less than -2 dB which is sufficient for delivering required power to the chip in practice [28]. Note that to have this condition the primary value of $C_{ant}$ should be big enough as concluded in preceding subsection. The same change in $C_{sh}$ makes a destructive effect on the impedance matching. This means $C_{sh}$ is more sensitive than $C_{ant}$. A solution to reduce the sensitivity of $C_{sh}$ is proposed in the next section.

## 5.1.2. Proposed Design

The matching loop in ordinary label-type tags is in close contact with adjacent materials that leads to a change in the value of $C_{sh}$. The proposed solution to protect this capacitance is to design a 3D shape antenna as depicted in Fig. 5.3. The matching loop connected to the chip is in parallel with the antenna body and protected by the underneath conductive patch. In other words, the matching loop is in a standing position compared to the flat matching loop of ALN-9768 as depicted in Fig. 5.3. By this way the matching between the chip and antenna maintains in an acceptable condition over a wide range of the dielectric constant and also the conductive materials.

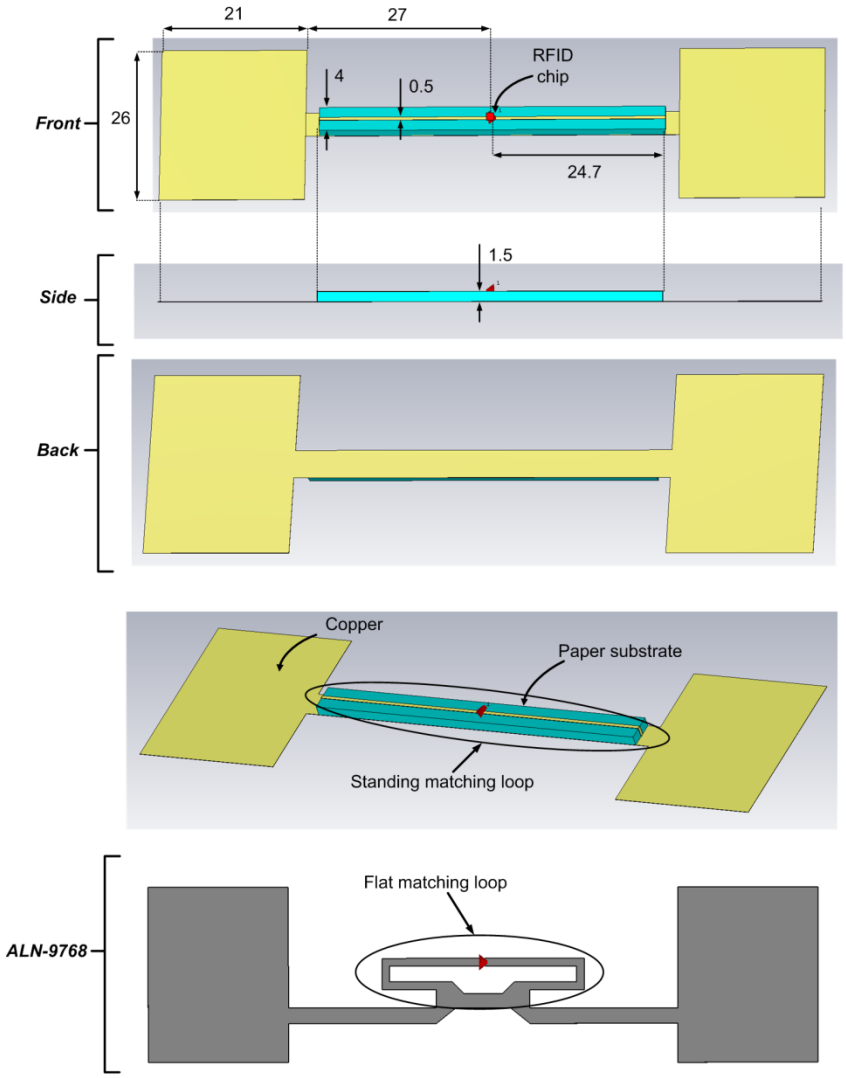


**Fig. 5.3. Structure of the proposed design. All the dimensions are in millimeters.**

### 5.1.2.1. Simulation Results

The structure of Fig. 5.3 is designed and simulated using CST software. The tag is placed on a material with dimension of 200×200×10 $mm^3$ and the relative dielectric constant of this slab is changed from 1 to 20. The effect of this change on the return loss of the tag is depicted in Fig. 5.4. As can be seen, there is no frequency shift in the resonant frequency. Of course there is degradation in the level of S11 over different values of $\varepsilon_r$ but in all of them the S11 is below -2 dB which is sufficient as mentioned in previous section. The S11 for a metallic background is also depicted in Fig. 5.4. The value is below -1 dB which means the read range is limited in this case.

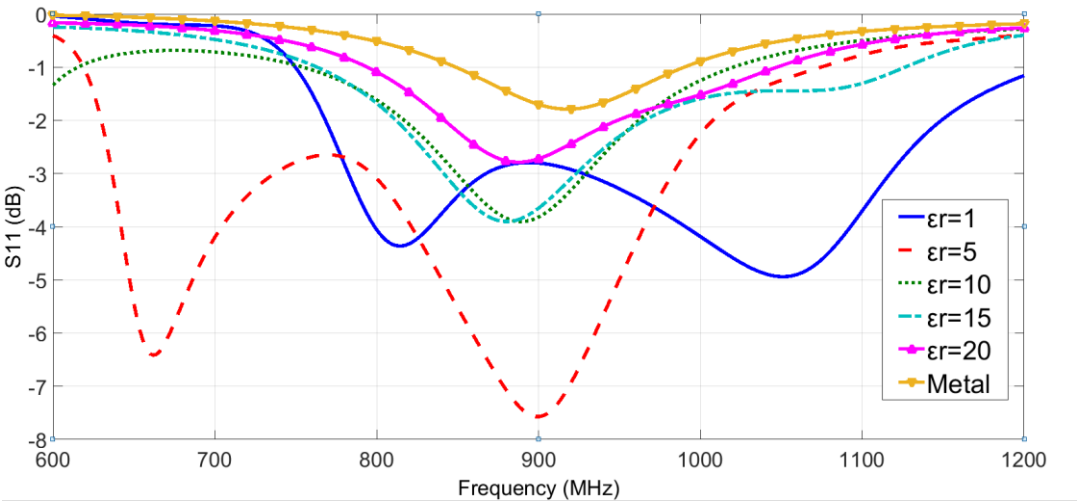


**Fig. 5.4. S11 of the proposed design when the background material is a metallic slab or a dielectric material with different relative dielectric constant.**

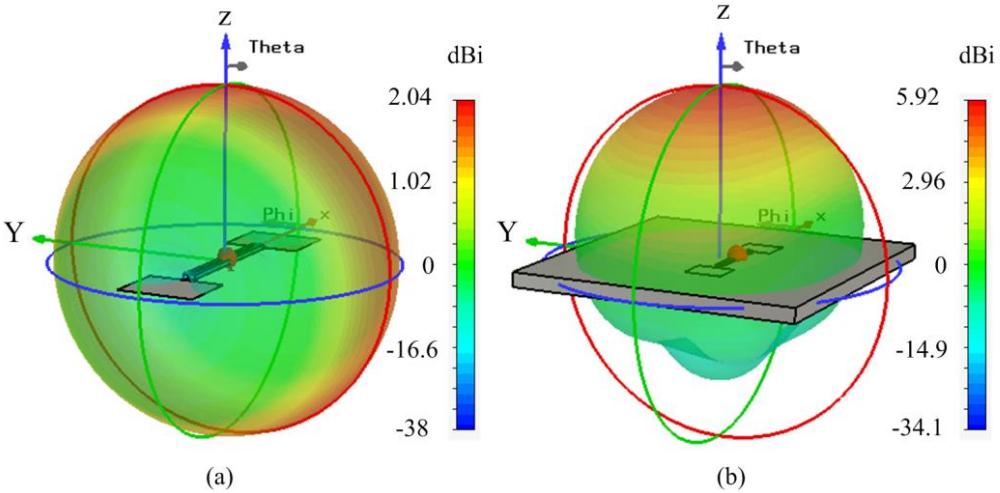


**Fig. 5.5. Radiation pattern of the proposed design in: (a) free space and (b) on a metallic slab.**

However, this can be alleviated by the increased directivity as a natural effect of the metallic background. The radiation pattern of the tag in free space and on a metallic slab is depicted in Fig. 5.5. The directivity increases from 2.04 dBi to 5.92 dBi when the tag is attached to a metallic slab. This contributes to maintain an acceptable reading range on metallic objects.

#### 5.1.2.2. Measurement Results

A prototype of the tag is fabricated using copper sheet and paper as substrate. A Higgs-4 SOT RFID chip is soldered in the center part of the tag as shown in Fig. 5.6. The reading range of the tag when attached on different materials is compared with ALN-9768 and ALN-9654 which are two products of Alien that are known to be tolerant to high dielectrics [22]. The measurement is done using Nordic ID PL3000 UHF RFID reader in an anechoic chamber. This handheld reader has 630 mW equivalent isotropic radiated power (*EIRP*). The result of the measurement is tabulated in Table 5.1. The dimension of the background material is 200×200×10 $mm^3$. The proposed tag offers the longest reading range on glass material. This could be predicted by comparing the result of Fig. 5.4 where the best impedance matching is for material with relative dielectric constant of 5. The relative dielectric constant of glass is typically close to this value. The tag shows acceptable reading range in lower relative dielectric constants like free space and Teflon.


**Fig. 5.6. Reading range measurement of the proposed design by a handheld reader.**

**Table 5.1. Measured reading range of the tags in centimeters.**

| Material | ALN-9768 | ALN-9654 | Proposed design |
|---|---|---|---|
| Free space | 216 | 220 | 127 |
| Metal | 0 | 0 | 50 |
| Glass | 250 | 250 | 295 |
| Water bottle | 6 | 6 | 36 |
| Teflon | 280 | 280 | 228 |

Although this reading range is less than the commercial tag samples but in high dielectric constants and challenging materials like water bottle and metallic slab, the proposed design overcomes the rivals. The proposed tag offers 50 cm reading range on metallic slabs while the commercial samples are useless in this condition.

# 5.2. Dual-Polarized UHF RFID Tag for Metallic and Non-Metallic Objects

A dual-polarized RFID tag supported by ground plane is proposed in this section. The presence of the ground plane in the design provides robustness to the host material and the values of the circuit elements are not determining factors. Most of the advanced UHF RFID readers employ circularly polarized or dual-polarized antenna but a linearly polarized antenna is used in small handheld devices. A dual-polarized tag design can provide a reliable communication with the small readers. The details of the design, simulation and measurement results are discussed in this section.

## 5.2.1. Antenna Design

A cavity-backed slot antenna is a common way of protecting the slot from background materials [64]. However, as the depth of the cavity needs to be a quarter of wavelength, this solution is not applicable in passive tags where a thin layer antenna is required. Reduction of the depth of the cavity is successfully done by modifying the topology and spreading the depth into the surface of the slot [65]. Applying this method, a dual-polarized thin cavity-backed slot antenna for RFID tag is proposed in this section. The antenna structure and details of the dimensions is

depicted in Fig. 5.7. It is printed on a 1.5 mm thick FR-4 substrate with relative dielectric constant $\varepsilon_r$ = 4.3. The symmetric arrangement of triangle conductive patches creates the dual-polarized V-shaped slots in front layer. While the back of the design is covered with the ground plane, all the edges are covered with conductive walls to make the thin cavity filled with FR-4. Monza 4 RFID chip is used for the design. It has two independent ports for connection to the dual-polarized antenna as discussed in Chapter 3. Please see Appendix C for more information about this chip. Dual port connection increases the read sensitivity of the chip up to -20 dBm that makes it useful in challenging environments. The chip is located in the centre of the tag and each port is connected to two triangle patches in symmetry according to the origin.

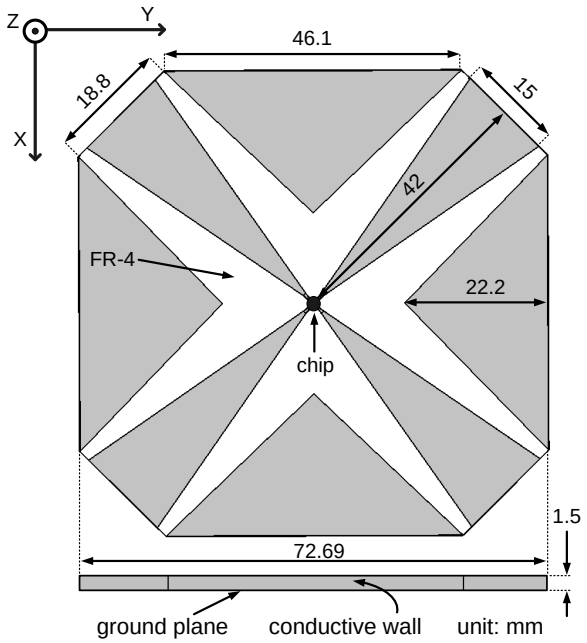


**Fig. 5.7. Structure and dimensions of proposed design (top view and side view).**

## 5.2.2. Simulation Results

In conventional antenna design the antenna port is usually matched to 50 ohm but in passive RFID tag designs the antenna needs to be conjugate matched to the chip as discussed in Chapter 3. Due to internal capacitive components for saving energy, RFID chips have capacitive input impedance which demands antenna design with inductive input impedance.

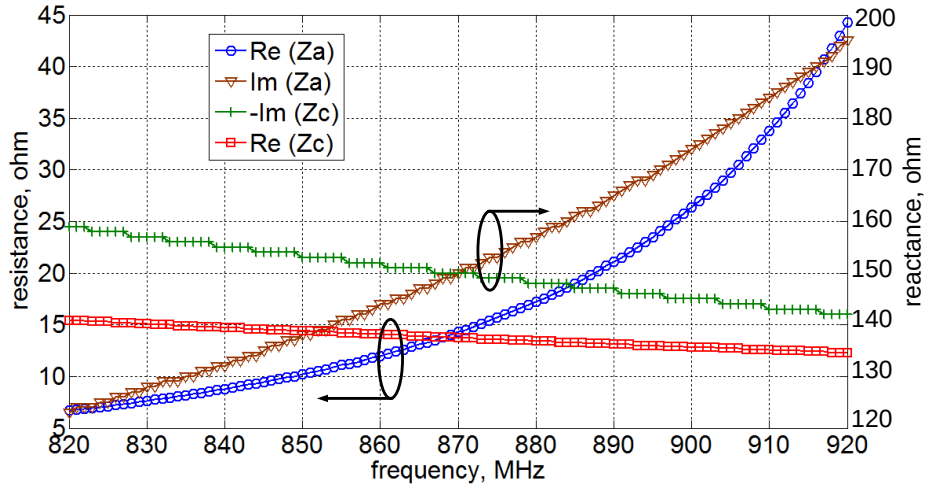


**Fig. 5.8. Simulated input impedance of antenna and Monza 4 chip.**

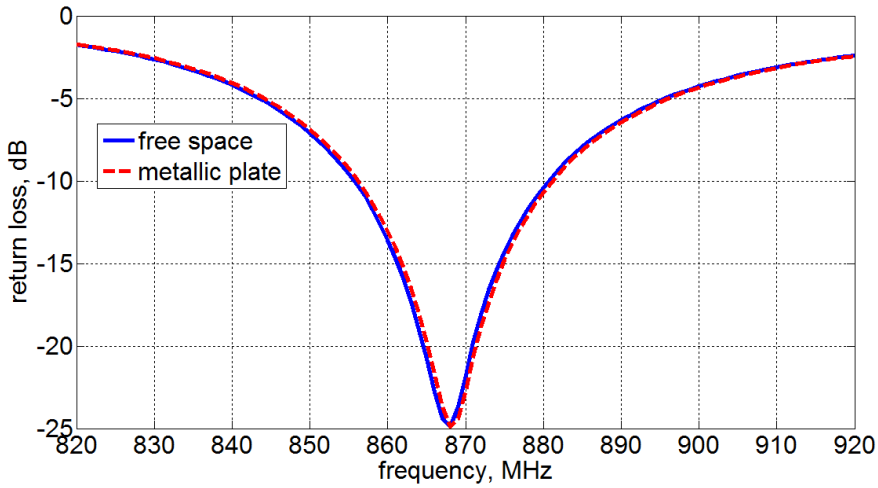


**Fig. 5.9. Return loss of the antenna in free space and on a 20×20 cm$^2$ metallic plate.**

The complex input impedance of Monza 4 is ($Z_c$ = 13-j151) at 866 MHz, thus the input impedance of the antenna should be ($Z_a$ = 13+j151) for perfect matching.

CST and ADS software are used for simulation. The real and imaginary parts of the input impedance of the antenna and RFID chip are illustrated in Fig. 5.8. As can be seen the real and imaginary parts of the impedances intersect around 866 MHz. This means that the maximum power transfer exists between antenna and chip at this frequency. This deduction can be confirmed by studying the return loss of the design. The return loss in free space and on a 20×20 cm$^2$ metallic plate is plotted in Fig. 5.9. As can be seen, the presence of the metallic plate does not leave any effect on the resonance frequency. This means the cavity-backed antenna is completely isolated

from background material and the input impedance of the antenna is not affected by the host material. A metallic host material can only affect the radiation pattern of the antenna in a constructive way. The directivity of the antenna increases by placing it on a metallic object. The result of simulation shows that the directivity of the antenna increases from 2.86 dBi to 6.1 dBi after placing it on a 20×20 $cm^2$ metallic plate.

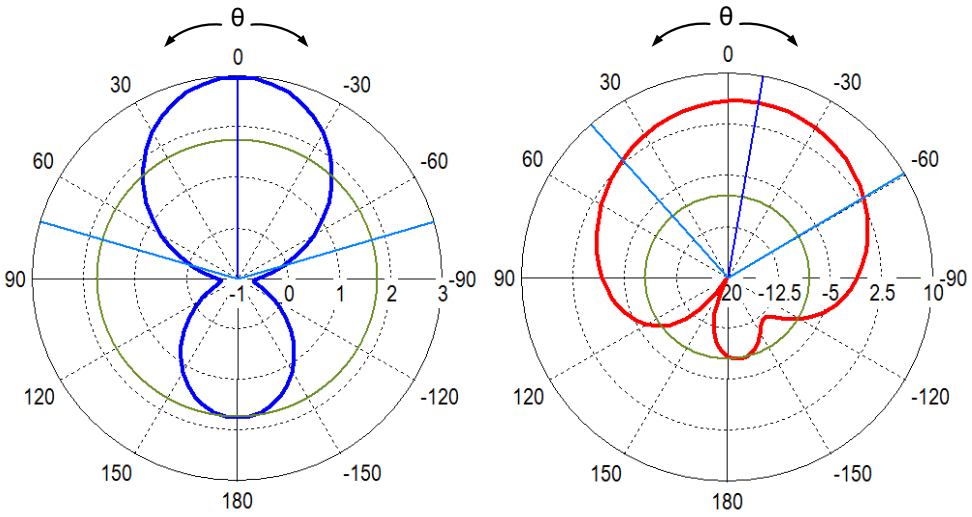


(a) (b)

**Fig. 5.10. Directivity of proposed antenna (dBi). (a) Free space. (b) Metallic plate with dimension of 20×20 $cm^2$.**

The directivity of antenna in XZ plane (φ = 0°) for the two cases is plotted in Fig. 5.10. The back lobe of the radiation pattern is comparable to the main lobe as can be seen in Fig. 5.10 (a). This is expected as the ground plane of the antenna has a finite dimension. By placing the antenna on a metallic plate which is equivalent to increasing the dimension of the ground plane, the radiation pattern gets reflected from the back to the front of the antenna. This improves the antenna gain and consequently the reading range which is investigated in the following section.

## 5.2.3. Performance Measurement

According to Friis formula, the reading range of a passive tag can be found by (3.4) as discussed in Chapter 3. Three parameters in Friis formula are usually affected by placing the tag on a metallic plate. These parameters are: $D_{tag}$, $e_{r,tag}$, and $\tau$. The simulation result of Fig. 5.9 shows that $\tau$ remains unchanged for the proposed

design. As the radiation takes place at slots, $e_{r,tag}$ would also remain stable. Therefore, the only varying parameter is the directivity of the antenna represented by $D_{tag}$. Thus, the ratio of reading range on metallic plate to reading range in free space for the proposed design can be found using (3.4) which leads to:

$$\frac{d_m}{d_f} = \sqrt{\frac{D_m}{D_f}} \tag{5.4}$$

where, subscripts *m* and *f* denote metallic plate and free space respectively. Using the values of directivity given in preceding section (6.1 and 2.86 dBi), the calculated reading range ratio is 1.46 which needs to be compared with the result of practical tests.

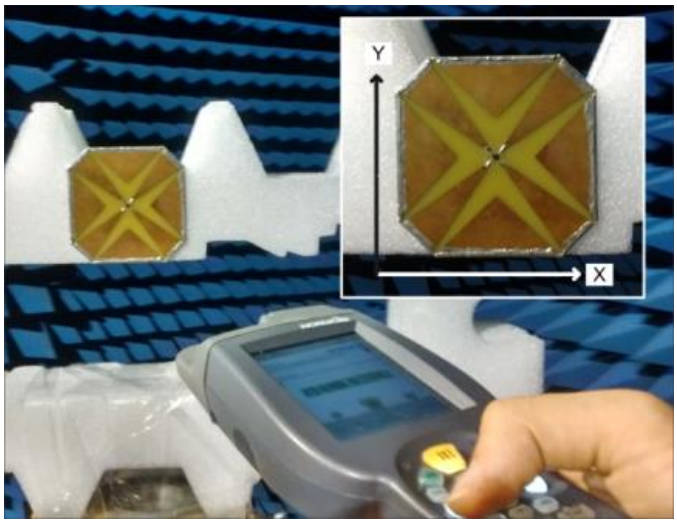


**Fig. 5.11. Fabricated tag under test in an anechoic chamber.**

Practical measurement of the tag is done in an anechoic chamber using Nordic ID PL3000 UHF RFID reader which is a handheld device with 630 mW *EIRP* and linear antenna. The setup for the test and the fabricated prototype is illustrated in Fig. 5.11. The reading range of the design in free space and on a 20×20 $cm^2$ metallic plate is determined. The sensitivity of the design to the polarization angle is also tested by keeping the tag in XY plane and changing the φ angle from 0° to 90° in 15° steps. The position of the tag in Fig. 5.11 is for $\varphi$ = 0°. The value of $\chi$ changes between 0 and 1 by changing the $\varphi$ angle for an ordinary tag with linear antenna but the result of measurement in Fig. 5.12 shows that the variation of reading range by changing the

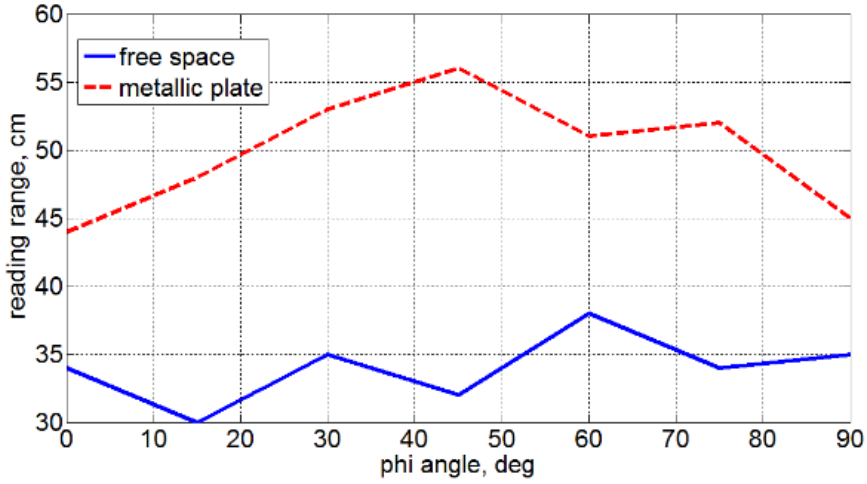


**Fig. 5.12. Reading range of the tag in free space and on a 20×20 cm$^2$ metallic plate with different polarization angle.**

polarization angle is small for the proposed tag. In addition, the reading range increases by placing the metallic plate behind the tag as it was expected. The ratio of reading range on a metallic plate to reading range in free space for different $\varphi$ angles from 0° to 90° is determined and the average value is 1.47 which is very close to the predicted value of 1.46 from the result of simulation. The agreement of these two values confirms that the metallic plate increases the directivity but has little effect on the other characteristics of the antenna.

# 5.3. Conclusion

Two RFID tag designs were proposed in this chapter. In the first design, by proper analysis of the equivalent circuit of label-type tags, it was shown that the most sensitive parts of the antenna are the capacitive parts in the feed point and antenna body. The result of the analysis confirmed that bigger capacitance in the antenna body leads to less sensitivity to the host material whereas less capacitance in the feed point helps to have less sensitivity. According to the findings, a novel label-type RFID tag was proposed. The robustness of the proposed 3D design to host material is improved without increasing the overall dimension neither using costly dielectric substrates. A small piece of flexible paper substrate is used in the design for physical strength and the tag can be conformal in two dimensions. The thickness of the design in the feeding point is just 1.5 mm. The analysis and measurement results showed

that the proposed design offers an outstanding read range on a different range of material. The most significant characteristic of the design is the acceptable read range on the metallic objects whereas the commercial label-type dipole tags are not practical on metallic hosts.

In the second design, a new dual-polarized UHF RFID antenna design was proposed in this chapter. Cost effective fabrication on thin flexible substrates is possible with this design while eliminating the need for vias and complicated multilayer structures. The simulation and measurement results confirmed its robustness to metallic and non-metallic objects. Stability in the mutual polarization power efficiency between the tag and reader antennas is a special characteristic of the proposed design. This leads to insensitivity to the polarization angle which makes the tag suitable for tagging metallic objects which needs to be tracked by handheld readers with linear antennas.

# Chapter 6. A Hybrid UHF RFID Tag Robust to Host Material

The 3D tag proposed in Chapter 5 offers a good read range on different material but the reading range on metallic objects is limited compared with tags that employ patch antenna. The dual-polarized tag proposed in Chapter 5 offers stability to the antenna orientation but the read range is limited. The stability in performance and the optimum reading range on different materials are two important factors in tagging objects. The challenge is to have a single design which can fulfil these requirements. The label-type dipole tag offers a desirable omnidirectional radiation pattern perpendicular to the dipole axis but it is not functional on metallic bodies. On the other hand, the tags with a ground plane offer an outstanding read range on metallic bodies but lower read range on non-metallic objects. In addition, a directive radiation pattern is not desirable for tagging non-metallic materials. Therefore, none of the reviewed tags are efficient on all materials.

In this chapter, a new tag design is proposed that shows the advantages of both mentioned groups: Omnidirectional radiation pattern on non-metallic objects and improved directive gain on metallic host materials with an acceptable read range in both cases. The hybrid UHF RFID tag proposed in this chapter works in two different modes. In one mode, the tag works as a dipole antenna on non-metallic objects and in the other mode it works as a short-ended quarter wavelength patch antenna on metallic objects. The design and analysis in two different modes are presented in next section followed by the fabrication and measurement results.

# 6.1. Tag Design and Analysis

The structure of the proposed design is depicted in Fig. 6.1. A Monza 4 Dura RFID chip is used in the design. This chip has a dual port input which is basically provided for dual-polarized symmetric tag designs for having a uniform radiation pattern as introduced in Chapter 3. However, the chip can be used for other purposes as the two ports are working independently. For example, a dual band design is proposed using this chip in [51]. As discussed in Chapter 3, the antenna in passive RFID tag designs needs to be conjugate matched to the complex input impedance of the RFID chip [25]. According to the internal capacitive components for saving power, RFID chips have capacitive input impedance which demands antenna design with inductive input impedance. The complex input impedance of Monza 4 is $Z_{chip}$ = 13-j151 at 866 MHz. Thus the input impedance of the antenna should be $Z_{ant}$ = 13+j151 for perfect matching.

As mentioned earlier, the tag works in two different modes. Each port of the chip is activated in one mode. The horizontal port of Monza 4 chip which is in the direction of Y axis in Fig. 6.1 is activated in off-metal mode. The tag works as a matched dipole in this mode. The inductive loop connected to the chip provides the required inductance for conjugate impedance matching [30]. The design is supported by FR-4 substrate with 3.2 mm thickness. There is no ground plane in the back of the antenna as shown in Fig. 6.1. Therefore, the antenna can radiate freely around the dipole axis. The dipole is comprised of wide arms. This has two benefits. First, wide arms improve the robustness of the tag to the host material which is discussed in the next subsections. Second, the wide surface of the dipole arm can play the role of a patch antenna in on-metal mode.

The vertical port of Monza 4 chip which is in the direction of X axis in Fig. 6.1 is activated in on-metal mode. This port leads to a conductive strip at one side and to conductive walls at the other side which is shown in the top and bottom of Fig. 6.1. By placing the tag on a metallic object, these conductors are capacitively coupled to the surface of the host material which acts as the ground plane and the tag transforms from a dipole into a patch antenna. The analysis of the tag working in off-metal and on-metal mode is presented in the following subsections.

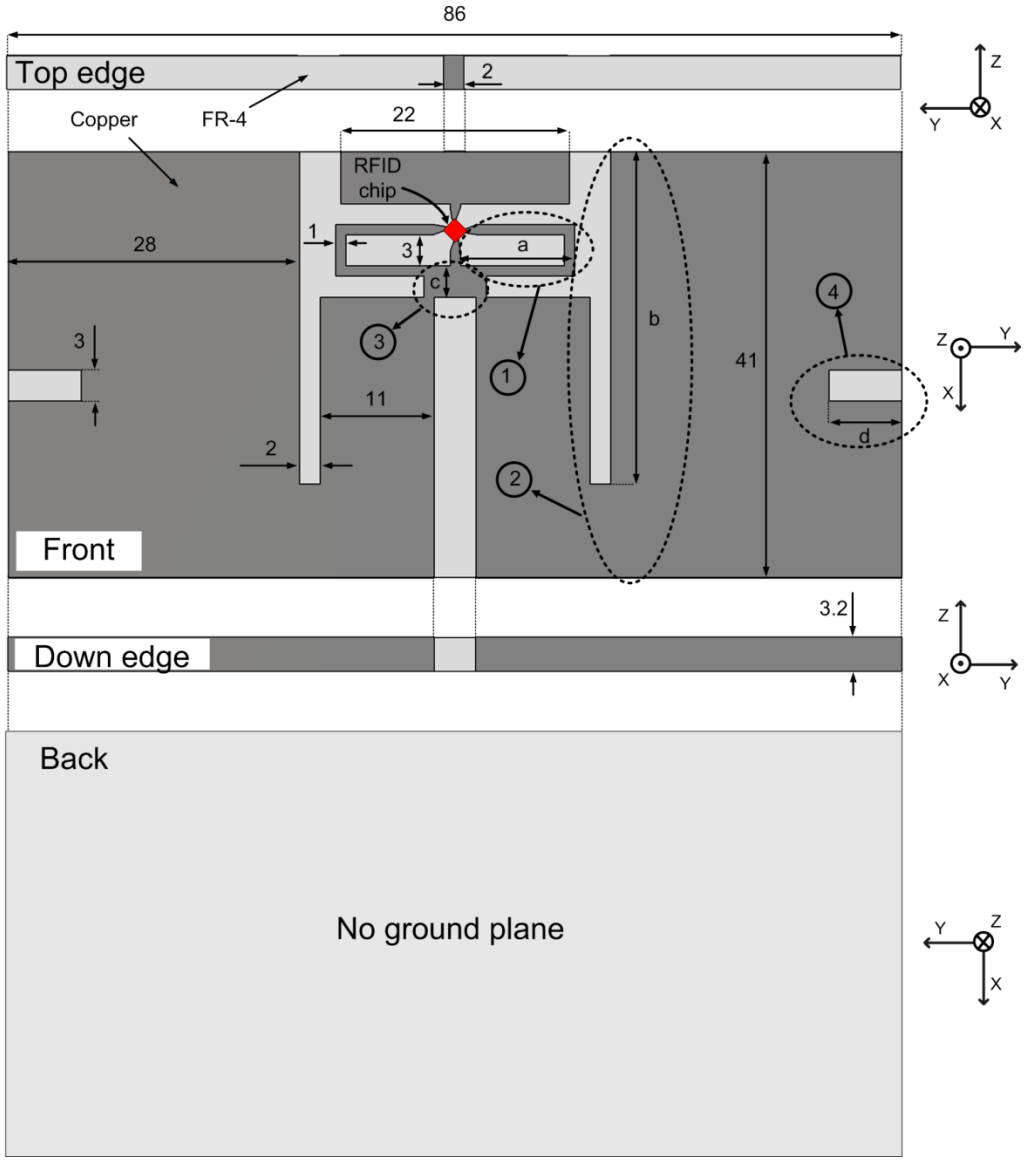


**Fig. 6.1. Structure of the proposed design. a = 11.5, b = 32, c = 2, and d = 9. All the values are in millimeters.**

## 6.1.1. Off-Metal Mode

The equivalent circuit of the tag in off-metal mode is shown in Fig. 6.2. This circuit is used for most dipole based tag designs [5]. The input impedance of Monza 4 is equivalent to 1.8 kΩ resistance in parallel to 1.21 pF capacitance as depicted in Fig. 6.2 (a). The position of the desired input impedance of the tag antenna for having a conjugate match ($Z_{ant}$ = 13+j151) would be close to the rim of the Smith chart normalized to 50 Ω [49], [58]. Studying the impedance matching is not easy at this point.

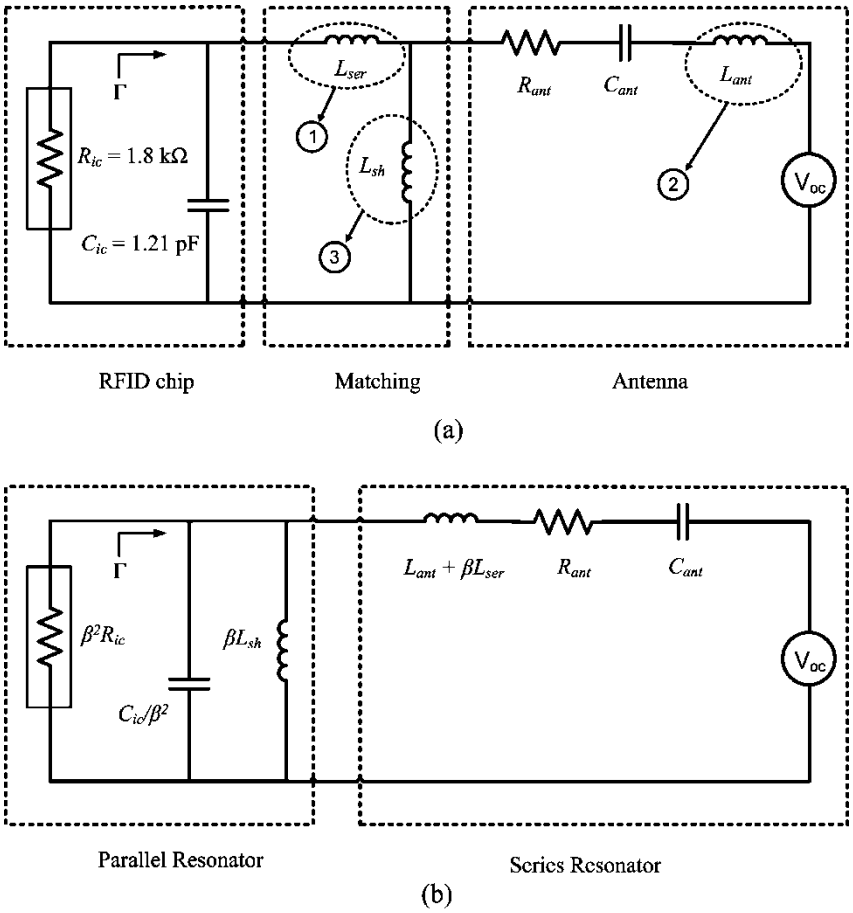


**Fig. 6.2. Equivalent circuits of the proposed tag design working in off-metal mode. (a) Primary equivalent circuit translated from physical structure. (b) Transformed equivalent circuit with parallel and series resonators.**

It is better to normalize the Smith chart to $Z_{ant}$ for having the match point at the center of the chart. The ADS software provides this facility but some simulation tools are not capable of normalizing the Smith chart to a complex load [82]. The proposed solution is to assume the capacitance of the chip as part of the antenna and consider the matching between the 1.8 kΩ resistor and the rest of the circuit as illustrated in Fig. 6.2 (a). The Smith chart should be normalized to 1.8 kΩ in this method. The equivalent circuit of Fig. 6.2 (a) can be transformed to the circuit of Fig. 6.2 (b). This circuit is a cascade of a parallel and series *RLC* resonator. The factor $\beta$ can be found by applying (4.3) as discussed in Chapter 4. The frequency response of the tuned physical structure in free space is shown in Fig. 6.3 by solid plot. There are two resonances in the plot representing the two parallel and series *RLC* resonators in the circuit.

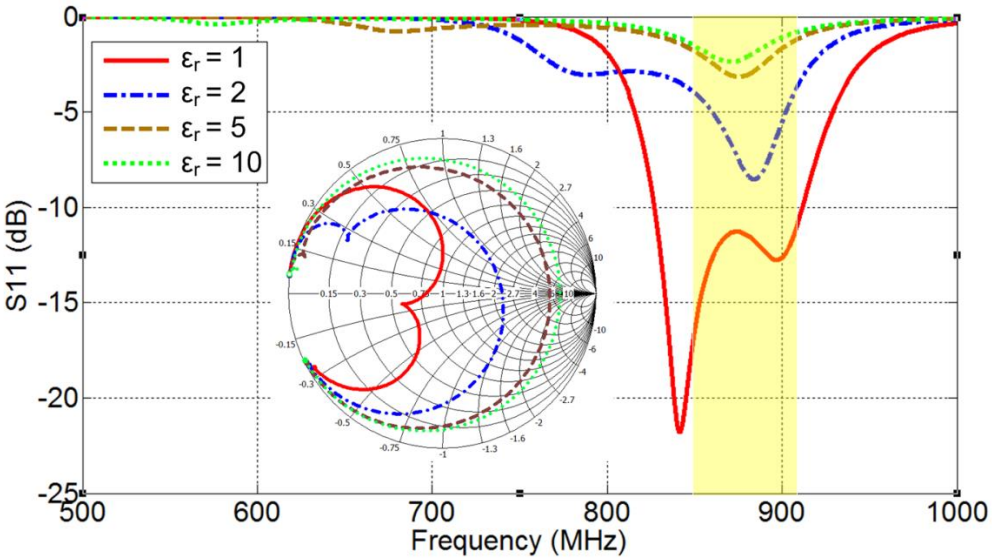


**Fig. 6.3. Frequency response of the tag in off-metal mode with different relative dielectric constant values of the host material. The Smith chart is normalized to 1.8 kΩ.**

The detuning effect occurs when the tag is placed on a material with a higher dielectric constant and this is mainly caused by changing the capacitance in the circuit.It is known that series *RLC* resonators with larger capacitance are less sensitive to dielectric constant variations as proved in Chapter 5. For that reason, the designed tag is comprised of wide arms. In parallel *RLC* resonators the smaller capacitance leads to less sensitivity. This can be shown by calculating the input admittance of a parallel *RLC* circuit and finding the derivative of it with respect to relative dielectric constant as follows:

$$Y_{in} = \frac{1}{R} + j\omega\varepsilon_{reff}C_0 - \frac{j}{\omega L} \tag{6.1}$$

$$\frac{\partial Y_{in}}{\partial \varepsilon_{reff}} = j\omega C_0 \tag{6.2}$$

where, $\varepsilon_{reff}$ is the effective relative dielectric constant of the background material and $C_0$ is the parasitic capacitance of the design which is in parallel with the chip capacitance. The internal chip capacitance is not contributing in the equation as it is not affected by host material. The parasitic capacitance should be as small as possible for making the derivative close to zero and having less sensitivity. This is guaranteed by having a thin matching loop and feed point. The detuning effect in

parallel resonator is less than the series one. Thus, one of the resonances in Fig. 6.3 is more robust to changes than the other one. The suggested method for having the optimum frequency response is to adjust the robust resonant frequency of the parallel resonator slightly higher than the desired working frequency and set the resonant frequency of the series resonator to lower close frequencies. By this way, the tag can cover the working frequency even after increasing the dielectric constant of the background material as shown in Fig. 6.3. Note that a -2 dB reflection coefficient is sufficient for running the chip in practice [28].

The elements of the parallel and series resonators in Fig. 6.2 (b) are related to each other by parameter $\beta$. Therefore, the two resonant frequencies cannot be tuned separately. Studying the impedance matching on a Smith chart can be helpful for tuning the frequency response of the tag. Different parts of the antenna and its effect on the impedance matching are analysed in the following. The result of this study can be generalized as a straightforward technic for fine tuning of any type of dipole based UHF RFID tag.

The tag structure of Fig. 6.1 is divided into different critical parts distinguished by the number and the corresponding elements in the equivalent circuit are illustrated in Fig. 6.2 (a). The effect of altering each part of the design on impedance matching is analysed. The effect of reducing the length of the matching loop in part one, which is equivalent to reducing the inductance $L_{ser}$, is investigated in Fig. 6.4. As can be

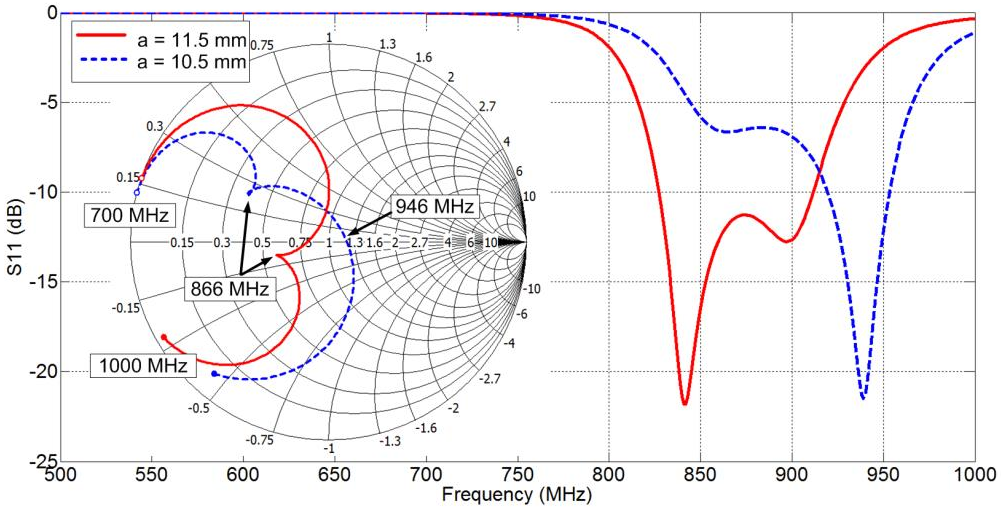


**Fig. 6.4. Reducing the length of part (1) in Fig. 6.1 and its effect on the frequency response and corresponding impedance matching in Smith chart.**

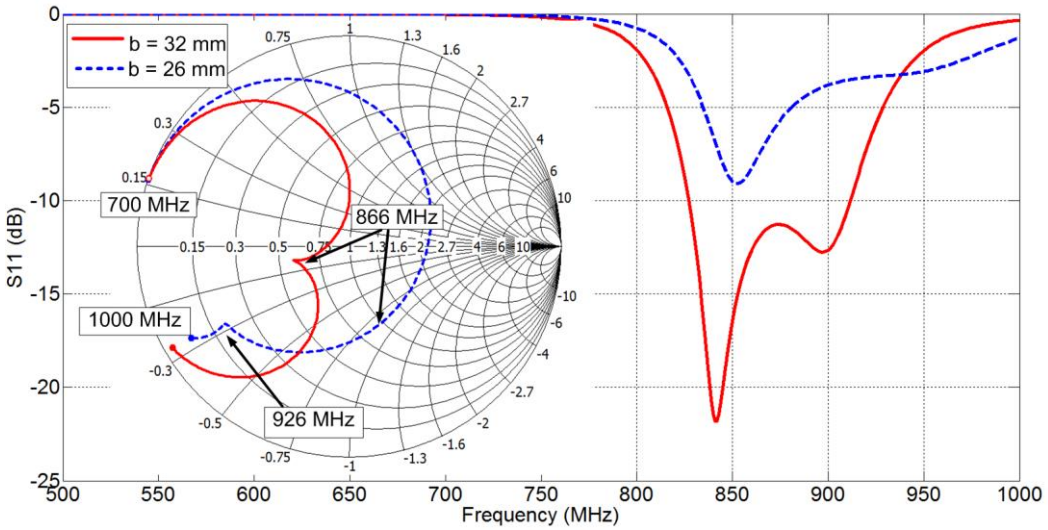


**Fig. 6.5. Reducing the length of part (2) in Fig. 6.1 and its effect on the frequency response and corresponding impedance matching in Smith chart.**

seen, the total plot in the Smith chart moves in a counter-clockwise direction which shifts the higher frequencies to the center of the chart.

Reducing the length of the slot in the second part of the antenna is mainly equivalent to reducing the inductance $L_{ant}$ in the circuit. The consequence of this change is moving the notch on the plot in Smith chart towards higher frequencies in a clockwise direction as shown in Fig. 6.5. Similar to inductance $L_{ant}$, reducing the capacitance $C_{ant}$ leads to a decrease in the inductive reactance of the series resonator [5]. Thus, the effect of reducing the capacitance $C_{ant}$, which is equal to reducing the area of the dipole, is almost similar to the plot of Fig. 6.5.

The third part of the antenna is equivalent to inductance $L_{sh}$. Reducing the thickness of this part increases the value of inductance. This transforms the notch on the plot in Smith chart to a loop as depicted in Fig. 6.6. The diameter of this loop can be further increased by increasing the value of inductance. The bandwidth of the frequency response can be controlled by this part. The radiation resistance $R_{ant}$ is mainly affected by the length of the dipole [5]. Decreasing $R_{ant}$, similarly increases the diameter of the loop in the plot of Fig. 6.6 which can be another way for controlling the bandwidth.

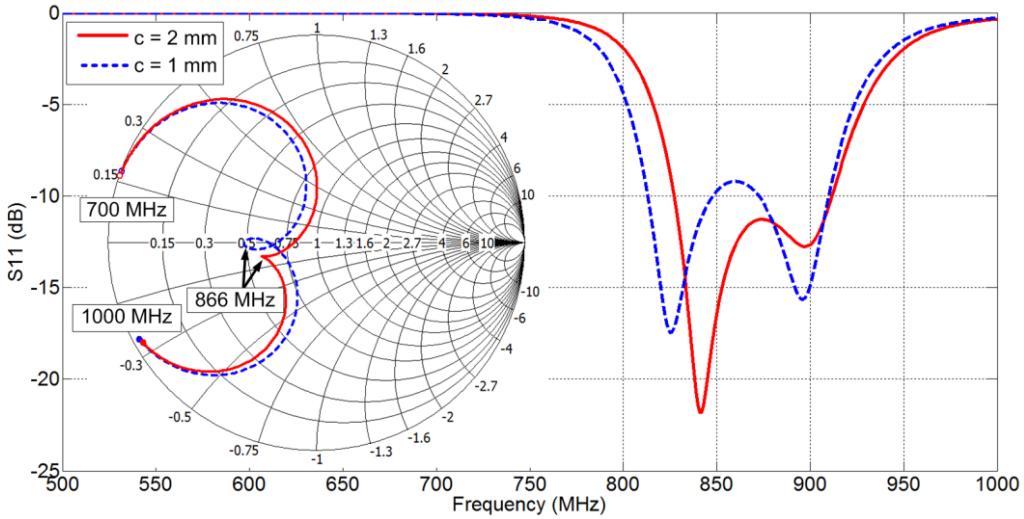


**Fig. 6.6. Reducing the width of part (3) in Fig. 6.1 and its effect on the frequency response and corresponding impedance matching in Smith chart.**

One of the advantages of the proposed tag is that there is no ground plane on the back of the substrate in off-metal mode. Thus, the radiation pattern is relatively uniform around the axis of the dipole as shown in Fig. 6.7. This makes the tag readable from different angles.

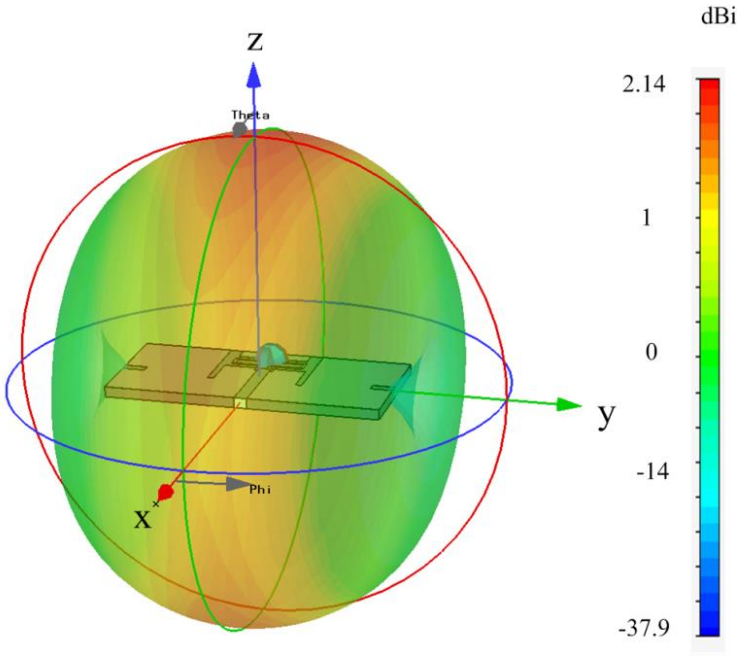


**Fig. 6.7. Radiation pattern of the tag in free space working in off-metal mode.**

## 6.1.2. On-Metal Mode

The hybrid tag transforms into a quarter wavelength patch antenna in on-metal mode as mentioned earlier. The patch is shorted to the ground using the conductive walls at one edge. Thus the radiation occurs at the opposite edge of the design. The excited electric field at this edge is the source of radiation in this antenna. According to the fringing effect, the length of the patch along X axis looks longer than the physical length. This difference can be found by (6.3) discussed in [26]:

$$\Delta l = 0.412h\frac{\left(\varepsilon_{reff}+0.3\right)\left(w/h+0.264\right)}{\left(\varepsilon_{reff}-0.258\right)\left(w/h+0.8\right)} \tag{6.3}$$

where, $h$ is the thickness of the FR-4 substrate, $w$ is the width of the patch along Y axis, and $\varepsilon_{reff}$ is the effective relative dielectric constant which can be found by (6.4):

$$\varepsilon_{reff} = \frac{\varepsilon_r+1}{2}+\frac{\varepsilon_r-1}{2\sqrt{1+12\,h/w}} \tag{6.4}$$

where, $\varepsilon_r$ is the relative dielectric constant of the substrate material which is 4.3 for FR-4. The physical length of a quarter wavelength patch resonating at frequency $f_0$ can be calculated by (6.5):

$$l = \frac{\lambda_0}{4\sqrt{\varepsilon_{reff}}}-\Delta l \tag{6.5}$$

where, $\lambda_0$ is the wavelength in free space at $f_0$. The calculated physical length using the defined formulas at 866 MHz is 41.7 mm which is close to the length of the proposed design. The difference is compensated by adding the slot in part (4) of Fig. 6.1.

The surface currents on the patch start from a low level at the location of the chip and reach a maximum after passing the quarter wavelength path as shown in Fig. 6.8. The high currents guarantee acceptable radiation efficiency despite the small thickness of the tag. The currents at the location of the chip are low and the voltage between the patch and the ground is high. This condition provides appropriate input impedance for matching with the chip [5].

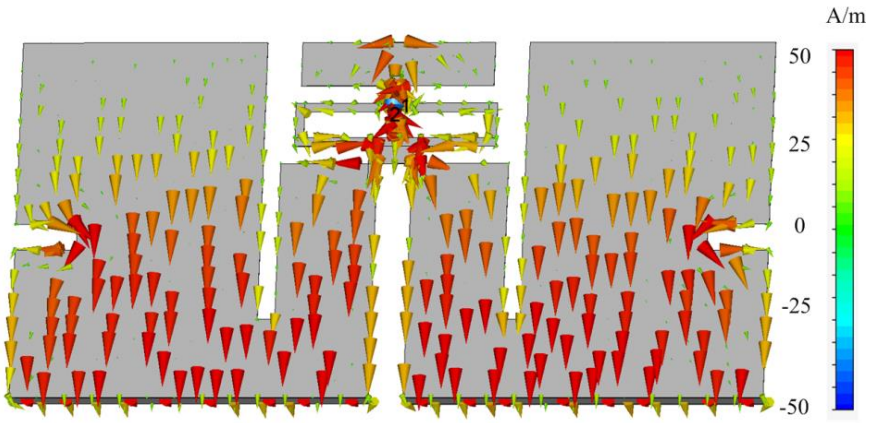


**Fig. 6.8. Surface currents of the design working in on-metal mode.**

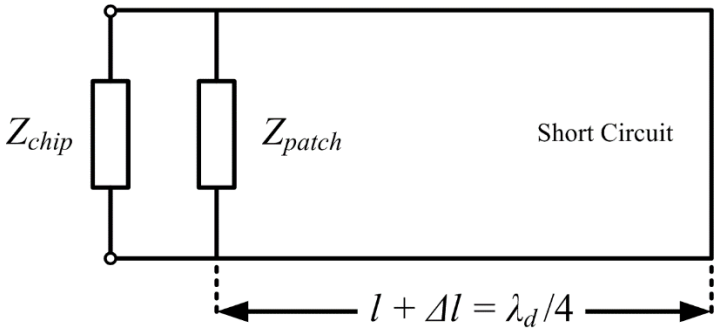


**Fig. 6.9. Equivalent circuit model of the tag working in on-metal mode.**

The equivalent circuit of the tag working in on-metal mode is shown in Fig. 6.9. The short circuit is seen as an open circuit from the location of the chip as the patch behaves like a quarter wavelength transformer. Similar to the off-metal mode, a conjugate impedance matching to the chip is required here. The input impedance of the patch is mainly dependent on the position of the chip port along X axis, the width of the patch along Y axis, and the slots in part (2) and (4) of the design shown in Fig. 6.1.

The frequency response of the tag is illustrated in Fig. 6.10 by solid line plot. Although the bandwidth of the tag in this mode is less than the off-metal mode but it is sufficient for running the chip at 866 MHz. The mutual coupling between the two ports is an undesirable factor that should be kept as low as possible. High degree of coupling causes a loss in the induced power which affects the performance. Symmetry of the design according to X axis helps to limit the coupling effect.

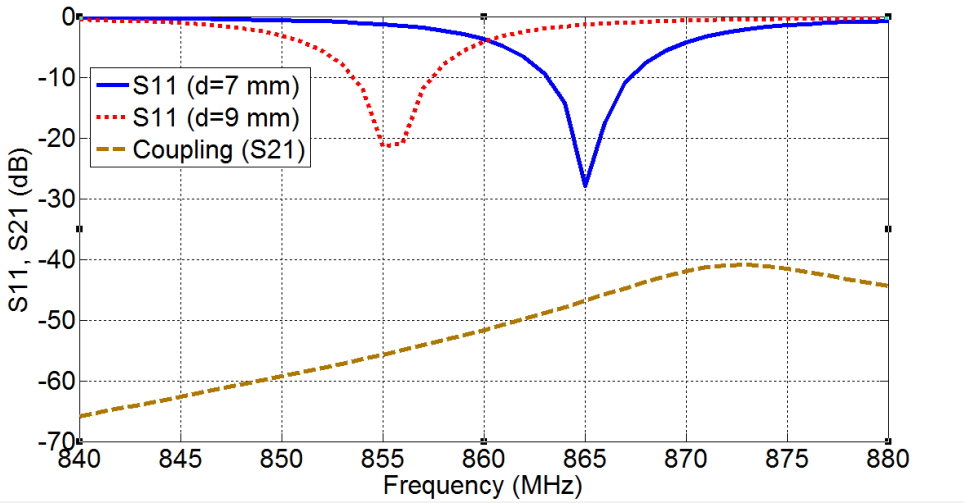


**Fig. 6.10. Frequency response of the tuned tag working in on-metal mode and the effect of increasing the length of the slot in part (4) of Fig. 6.1; Coupling between two ports of the chip.**

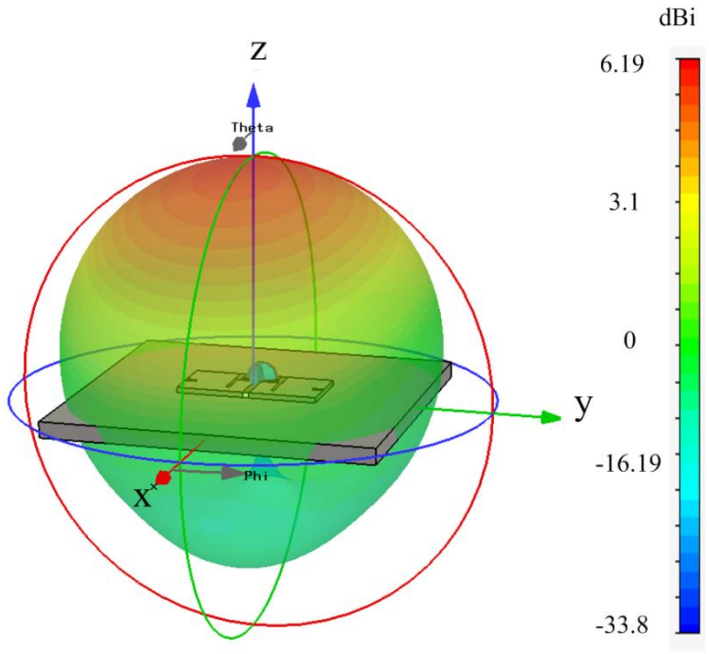


**Fig. 6.11. Radiation pattern of the tag on a 20 cm × 20 cm metallic plate.**

The surface currents shown in Fig. 6.8 are in symmetry with the vertical port of the chip. This induces the same voltage at both sides of the horizontal port and reduces the coupling effect consequently. The level of coupling between two ports in a tuned design is also plotted in Fig. 6.10. The slot located at part (4) of the design in Fig. 6.1 can be used for fine tuning of the tag in on-metal mode. The frequency response of the tag can be shifted by changing the length of this slot from 7 mm to 9 mm as

shown in Fig. 6.10 by dotted S11 plot. Increasing the length of this slot makes the surface currents to pass through a longer path which reduces the resonant frequency. This change does not have a significant effect on the frequency response of the tag in off-metal mode because the slot is located at the tip of the dipole where the currents are small at that mode.

The gain of the tag is dependent on the size of the metallic host material. The directivity of the design can reach up to 6.19 dBi by placing it on a 20×20 $cm^2$ metallic plate as shown in Fig. 6.11.

# 6.2. Fabrication and Measurement Results

The proposed design of Fig. 6.1 is etched on an FR-4 substrate and Monza 4 Dura chip is soldered to the two input ports of the tag as shown in Fig. 6.12. The theoretical read range of the tag can be predicted using Friis formula as introduced in Chapter 3 by equation (3.4). However, the calculated read range using this formula is not always accurate due to different errors in design simulation, fabrication and testing process. The practical approach for measuring the read range is the introduced method in Chapter 3 using equation (3.6). A Tagformance device is used for measuring the maximum read range. The fixed distance between the tag and the reader antenna which is $d_{ref}$ is specified by the spacer. A frequency sweep is done using the Tagformance unit.

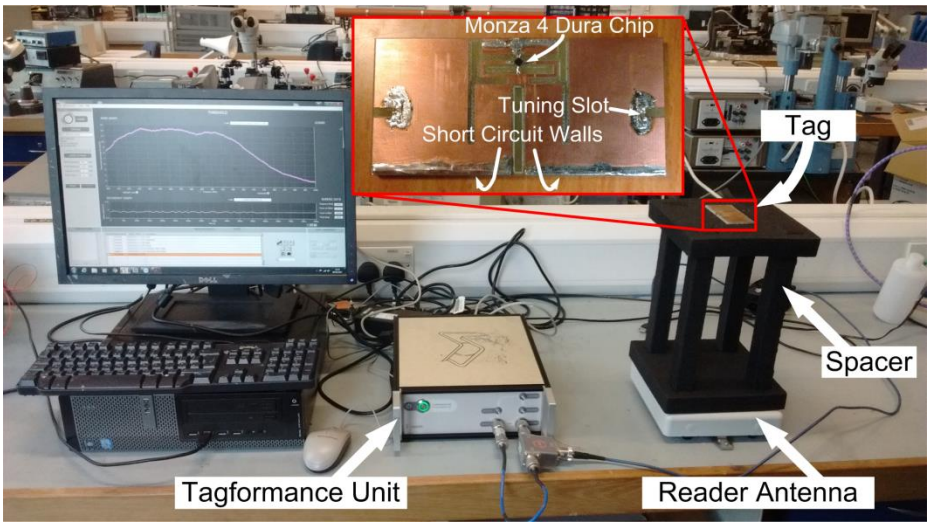


**Fig. 6.12. Prototype of the proposed design and measurement setup using Tagformance.**

The device finds the threshold required power for reading the tag in each frequency. Applying (3.6), the system software converts the threshold power value to the maximum read range which is also called theoretical read range forward. The measurement setup is illustrated in Fig. 6.12.

The theoretical read range of the tag which is defined in Chapter 3 is measured on a different range of materials with dimension of 200×200×6 $mm^3$. The result is plotted in Fig. 6.13. The read range of the tag in off-metal mode varies between 12 meters for low dielectric materials and 8 meters for high dielectric material like tempered glass. The presented result in Fig. 6.13 justifies the simulation result of Fig. 6.1.

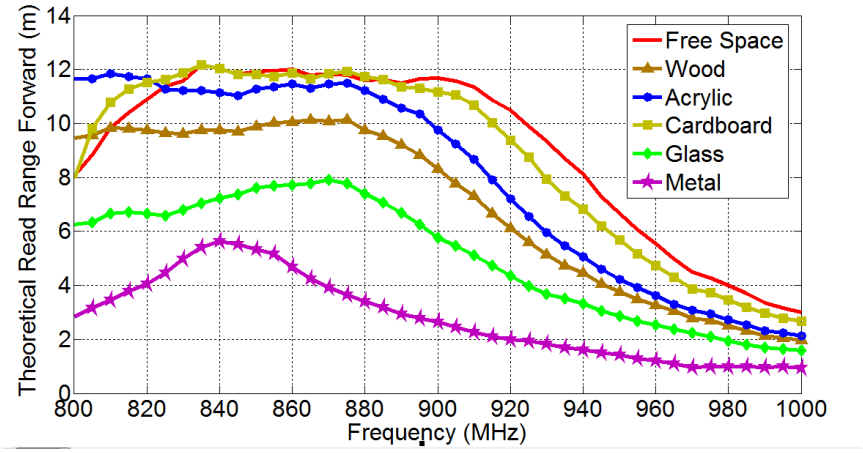


**Fig. 6.13. Theoretical read range of the tag on different materials measured using a Tagformance device.**

**Table 6.1. Comparison of the proposed tag with several other designs (EIRP = 4 W).**

| Reference | Tag Type | Tag Size (mm) | Metal Plate (cm) | On-metal Read Range (m) | Off-metal Read Range (m) |
|---|---|---|---|---|---|
| **This Work** | Hybrid | 86×41×3.2 | 20×20 | 5.6 | 12 (Free Space)<br>8 (Glass) |
| **[30]** | Dipole | 120×30×0.25 | N/A | 0 | 11 (Free Space) |
| **[49]** | Patch | 88×60×0.76 | 15×15 | 5.4 | 6.3 (Free Space)<br>5.7 (On-body) |
| **[83]** | Patch | 30×30×3 | 20×20 | 7.2 | 3.5 (Free Space)<br>4 (Glass) |
| **[62]** | Dipole with Decoupler | 95×25×3.6 | N/A | 6.2 | 7.1 (Free Space)<br>11.3 (Glass) |
| **[76]** | Groundless Patch | 80.5×74.5×1.5 | 31×23 | 7.9 | 4.4 (Free Space) |

There is degradation in the read range as the dielectric constant increases but it is limited because, there is a small frequency shift in the desired bandwidth. This means a limited detuning effect and can be referred to following reasons:

- The frequency response of the tag is optimally tuned and there is a good impedance matching between the chip and antenna.
- The FR-4 substrate prevents the dipole from a close contact to the host material and limits its effect on the dipole characteristics.
- The capacitive loaded wide dipole arms increase the bandwidth and robustness of the tag to high dielectric materials.

The maximum read range in on-metal mode is around 5.6 meters. There is a shift in the working frequency which is mainly caused by the fabrication errors. The proposed hybrid tag is compared with some other designs in terms of size and performance. The result is tabulated in Table 6.1. The dipole tag proposed in [30] offers high read range in free space but no study is done about its performance on different materials. In addition, it is not functional on metallic objects. The patch antenna proposed in [49] has less read range on different materials compared with this work. The patch in [83] has more read range on metallic plate but the performance on other materials is quite limited. The dipole proposed in [62] has slightly higher read range in on-metal mode but it offers less read range in off-metal mode. This design is equipped with a decoupler layer which makes it a complicated multilayer design compared with the simple single layer design proposed in this work. The groundless patch proposed in [76] offers more read range in on-metal mode but the read range is far less in free space and there is no study about its performance on other materials. Thus, considering different factors like: average read range on different materials, fabrication cost, and desired radiation pattern on different materials, the proposed hybrid tag outperforms other tag designs.

# 6.3. Conclusion

It was shown in this chapter that the proposed hybrid UHF RFID tag uniquely offered near omnidirectional radiation pattern of a dipole on non-metallic objects and directive pattern of a patch antenna on metallic objects which makes it capable of working efficiently on a wide range of materials. The measurement result showed

that the tag offered longer read range with less variation in performance on different materials wheras it has a simple single layer substrate. The hybrid tag is designed to have the maxmimum read range in free space. It is possible to tune the tag for materials with higher dielectric constant depending on the application. As mentioned earlier, the metallic surface of host material works as the ground plane in on-metal performance. Thus, for metallic materials with non-flat surface the read range might be degraded. In this case, a metallic sticker foil can be attached to the back of the design as a ground plane. This method can be also used for other challenging materials like water which absorbs the electromagnetic power and deteriorates the performance of the tag in off-metal mode.

# Chapter 7. Electromagnetic Band Gap Structures in Tag Design

Electromagnetic Band Gap (EBG) structures are introduced in this chapter and their application in protecting dipole antenna from metallic host material is considered. The performance of wire antenna close to the EBG ground plane in a horizontal position is considered as a suitable solution for RFID tags. It is shown that these EBG structures can maintain the radiation efficiency and matching of the antenna by offering proper reflection phase. The most common EBG is the high impedance mushroom structure which has been used usually for protecting RFID tags according to the literature. The presence of via in mushroom structure increases the cost of the design. It is shown in this chapter that a simple uni-planar structure can be developed by eliminating the via. This structure offers a desirable reflection phase for protecting the tag. Finally, a miniaturized uni-planar structure is designed and the performance of it in protecting the tag is examined. The result shows that the proposed design can protect the tag despite its smaller and simpler design compared to the previous works in the literature.

# 7.1. Introduction of EBG

"Generally speaking, electromagnetic band gap (EBG) structures are defined as artificial periodic (or sometimes non-periodic) structures that prevent/assist the propagation of electromagnetic waves in a specified band of frequency for all incident angles and all polarization states [84]". These structures have found lots of application in antenna design and in filtering the electromagnetic waves by offering interesting characteristic of reflection phase and also suppressing the surface waves which is going to be discussed more in this chapter.

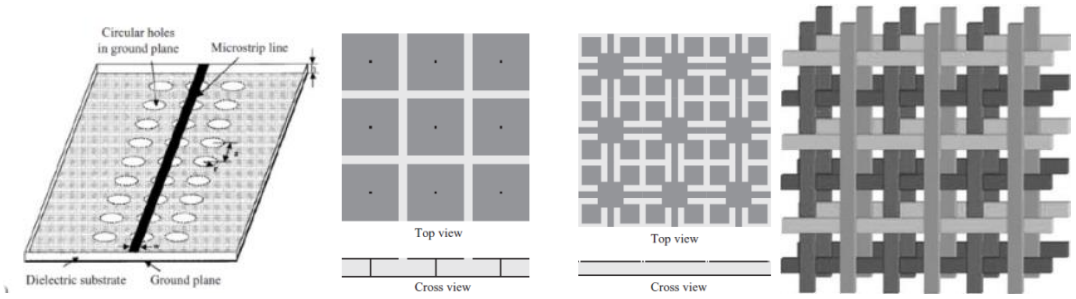


(a) (b) (c)

**Fig. 7.1. (a) 1D EBG structure in the shape of a transmission line [85], (b) two types of 2D EBGs [84], (c) 3D dimension EBG [84].**

There are different ways to categorize EBGs but a simple way is to divide them into groups based on their shape. As shown in Fig. 7.1, the periodic structure can be repeated in one dimension and make a 1D EBG. If the structure is repeated in two dimensions then a 2D EBG is produced which is the more common condition and at last the structure can also be repeated in three dimensions and create a 3D EBG. The second type of EBG (2D) that is shown in Fig. 7.1 (b) has more applications in antenna design and this chapter mainly focuses on this type of structure. Two different types of EBGs are shown in Fig. 7.1 (b). First the mushroom structure with via and second the uni-planar structure without via. Both of them have their own advantages and disadvantages which are going to be discussed in this chapter.

# 7.2. High Impedance Surface

High impedance surface is perhaps one of the most important and well known EBG structures which was introduced first time by Dan Sievenpiper in [86]. This structure is simply comprised of a ground plane covered by a dielectric material and on the top of the dielectric there are periodic square patches which are connected to the ground plane via holes as depicted in Fig. 7.2. This type of EBG is known as mushroom structure as mentioned earlier. The equivalent circuit of a unit cell of this EBG is also shown in Fig. 7.2. It is a parallel *LC* circuit that is carefully adjusted to resonate at the desired frequency. The input impedance of such a circuit can be found by applying (7.1):

$$Z = \frac{j\omega L}{1-\omega^2 LC} \tag{7.1}$$

$$\omega_0 = \frac{1}{\sqrt{LC}} \tag{7.2}$$

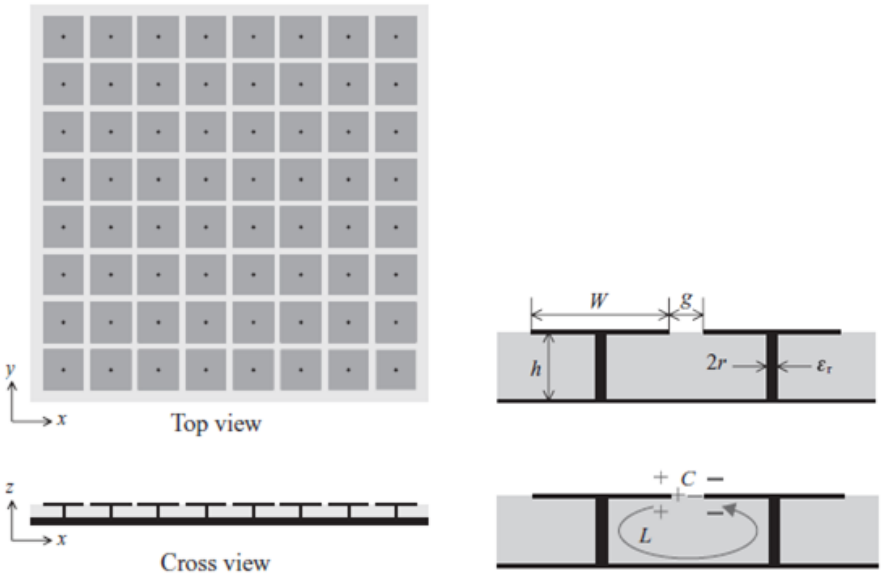


**Fig. 7.2. High impedance surface in the shape of a mushroom structure [84].**

In lower frequencies the impedance is inductive and it only supports TM surface waves. In higher frequencies the impedance is capacitive and the structure only supports TE surface waves and finally in resonance the input impedance is very big

that it stops any surface waves. That is the reason this type of structure is called high impedance surface. Suppressing the surface waves is not the only characteristic of this structure. It also reflects the wave in the phase between -180 to 180 degrees according to the frequency. It is known that a simple conductive plane as a ground plane reflects the wave by 180º difference in the phase and this makes some difficulty for antennas working close to the ground. A study is done in [84] to make the case clearer. The propagation of surface waves in different frequency and different wave numbers is studied and the results are shown in Fig. 7.3. The results show that in a certain bandwidth there is no surface current which certifies the existence of a band gap around the resonance frequency of the unit cell.

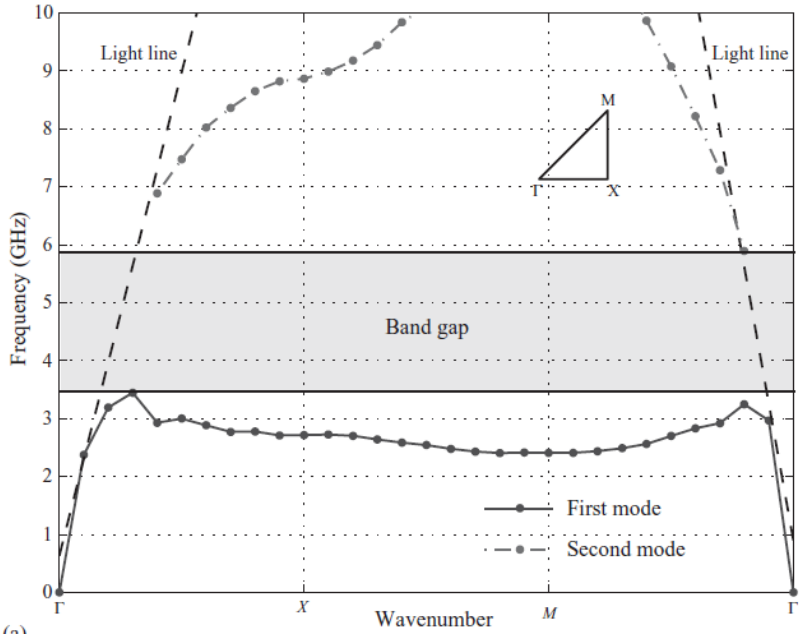


**Fig. 7.3. The presence of a surface wave band gap in the mushroom structure [84].**

Also the reflection phase of the incident wave is studied and the results are depicted in Fig. 7.4. It shows how the reflection phase changes by sweeping the frequency. The dimensions of the structure shown in Fig. 7.2 is as follows: $W$=0.1$\lambda$, $g$=0.02$\lambda$, $h$=0.04$\lambda$, $\varepsilon_r$=2.94 and $r$=0.005$\lambda$. The free space wavelength at 4 GHz is 75 mm. Thus, the size of a unit cell at this frequency would be 9×9×3 mm$^3$. The slope of the plot in Fig. 7.4 reflects the bandwidth of the design. A unit cell designed at the same frequency with larger thickness and dimension would show more bandwidth. This means the slope of the plot would be smaller.

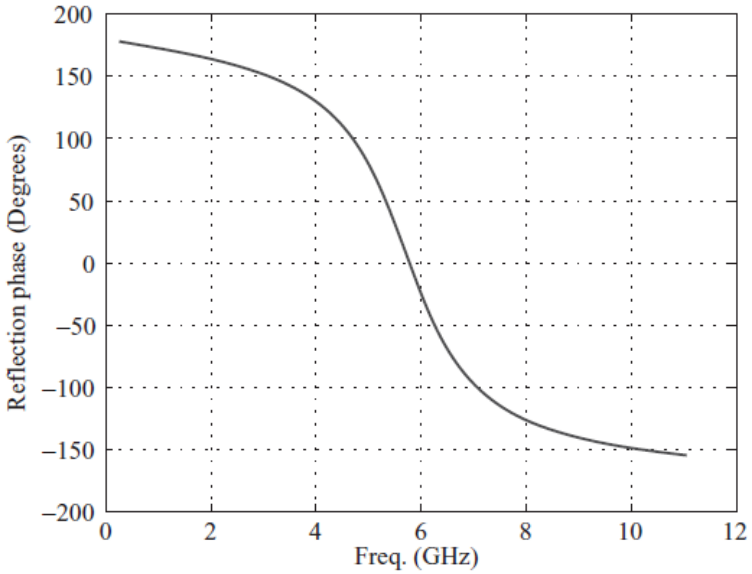


**Fig. 7.4. The reflection phase of the mushroom structure [84].**

# 7.3. EBG and Wire Antennas

EBG structures are used in improving the performance of patch and wire antennas. The surface current suppression characteristic of EBG is usually useful in improving the patch antenna performance [84]. Analysing the application of EBG in patch antenna is out of the scope of this thesis but the application of EBG for protecting wire dipoles is studied in this section because label-type tags can be considered as dipole antennas. Totally there are three different conditions when a wire antenna is facing a ground plane. These conditions are well demonstrated in Table 7.1. In the first case at top of the table the wire antenna is perpendicular to the ground plane which resembles a monopole antenna. The efficiency in this case is good but the antenna is quite big. In the second case the antenna is in parallel to the ground plane which makes a low profile structure but due to the currents with reverse phase on the ground plane the radiation efficiency and also the impedance matching are affected. The third condition is the solution offered by EBG ground plane. In this case the surface currents and the reflected wave from the ground plane are in the same phase of the wire antenna which is the desirable condition. So, there is a low profile system with high efficiency.

**Table 7.1. Comparison of conventional PEC and EBG ground plane in wire antenna designs [84].**

| Options | Efficiency | Low profile |
|---|---|---|
| J ↑ PEC ↑ I | ☺ | ☹ |
| J → PEC ← − | ☹ | ☺ |
| J → EBG − − → | ☺ | ☺ |

It is needed to realize the effect of different type of ground planes on the performance of a dipole antenna. In an experiment three different type of ground plane consisting of perfect electric conductor (PEC), perfect magnetic conductor (PMC), and EBG are compared to each other. The dipole is positioned at top of the ground in a horizontal condition as shown in Fig. 7.5. The system is designed to resonate around 12 GHz. The finite ground plane size is 25×25 $mm^2$ which is one wavelength at that frequency. The fundamental challenge in this type of low profile antenna is the coupling effect between the ground and the dipole. The ground affects both radiation efficiency and impedance matching of the antenna.

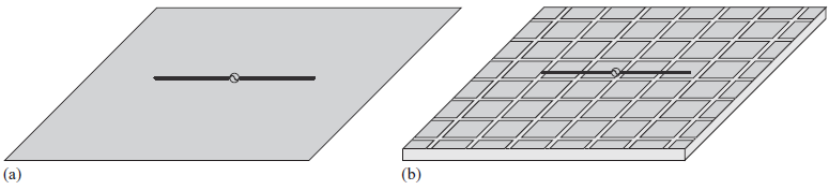


**Fig. 7.5. A dipole facing different type of ground plane [84].**

The result of S11 for the three different grounds is depicted in Fig. 7.6. It can be seen that the matching is totally affected for PEC. The reason is that the PEC surface has 180º reflection phase and the surface currents are in opposite direction of the currents in dipole which result in poor return loss. The reflection phase of PMC is the same as the dipole currents but because of the strong mutual coupling between them the impedance matching is affected.

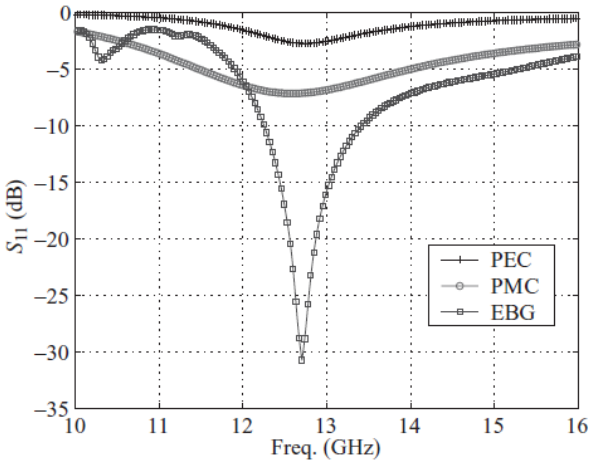


**Fig. 7.6. The effect of three different ground plane on the return loss of a dipole [84].**

It is possible to add a matching circuit to the antenna but it would make the design complicated. Furthermore, a PMC ground plane is possible in theory but cannot be found in nature. The best result is for EBG ground plane.

In simulating an infinite number of unit cells the reflection phase changes between -180º to 180º by frequency sweep with the zero reflection phase at the resonant frequency. Studies show the frequency band with the reflection phase 90±45º is the suitable band for protecting the dipole which means the resonant frequency of the dipole should be tuned at this band not the frequency with zero reflection phase [84]. The experiment which proves this fact is presented here. First of all the reflection phase result of an infinite number of unit cell of EBG is simulated. Then an EBG ground plane with finite dimension is designed and a dipole is positioned on top of it as shown in Fig. 7.7.

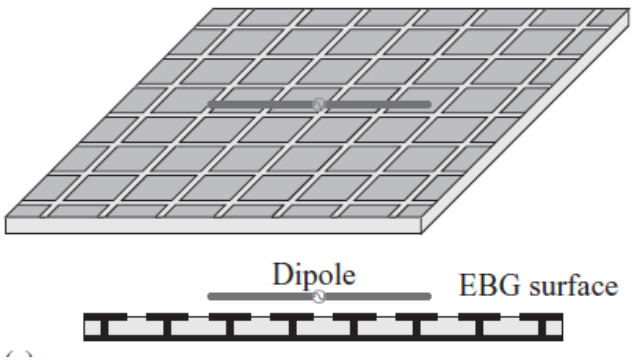


**Fig. 7.7. A dipole on top of finite dimension EBG ground [84].**

In the next step the length of the dipole is changed and the result for return loss is recorded in Fig. 7.8 (a). The reflection phase of the EBG in the same frequency band is depicted in Fig. 7.8 (b). This plot is achieved by designing a unit cell of EBG and applying the periodic boundary condition to model an infinite EBG surface [87] In certain frequencies the best radiation efficiency and impedance matching is achieved. That frequency is the suitable working frequency of the EBG as depicted in Fig. 7.8. By comparing the plots in top and bottom of the figure it can be concluded that the frequency corresponding to 90±45º reflection phase is the optimum point. It is shown in [84] that the frequency band with reflection phase around -90±45º is also suitable for designing dipole antenna but this frequency is located in higher band which leads to a design with bigger size but the same performance.

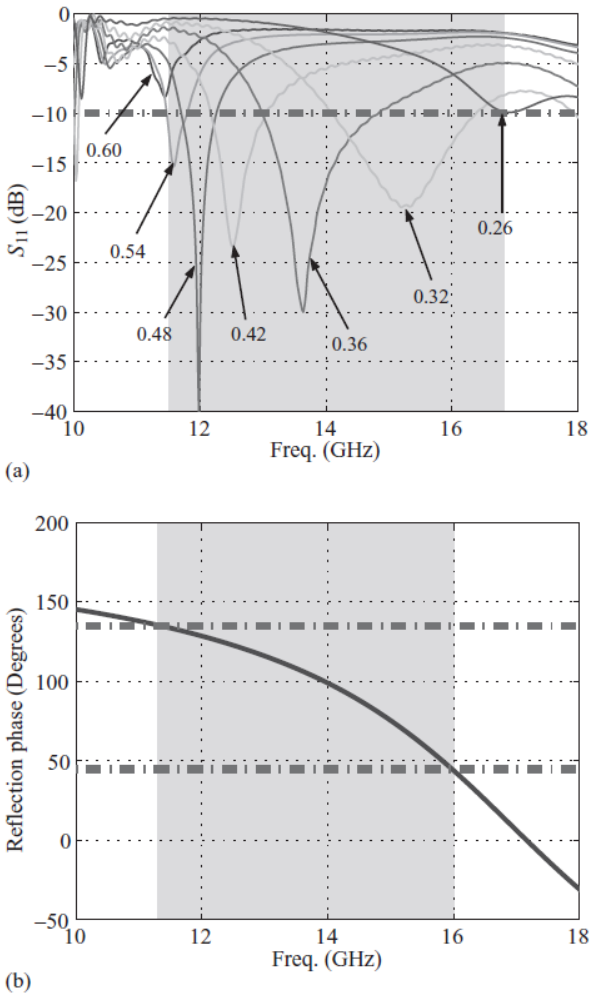


**Fig. 7.8. (a) The return loss of the dipole with different lengths on top of the EBG ground plane. (b) The reflection phase of the EBG in the same frequency band [87].**

So, the frequency band with 90±45º is usually preferred for designing the dipole antenna. A literature review about applying EBG structure in protecting RFID tags is presented in the next section.

# 7.4. EBG and UHF RFID Tags

There has been some works in the literature which introduce using EBG structure as a ground plane for UHF RFID dipole tags. In most of the designs the tag is a dipole antenna matched to the chip as explained in Chapter 3. The main idea is to make an artificial ground plane using finite number of EBG unit cells to protect the dipole tag from background metallic objects. One of the works done in [88] uses mushroom structure to protect a simple dipole as shown in Fig. 7.9. The design is comprised of 4×8 cells with total dimension of 142.5×70.5×4.8 $mm^3$. The dipole size with folded arms is 78×30 $mm^2$. A drawback of this design is the narrowband response of the tag. The designer could use a matching loop to cover the whole band.

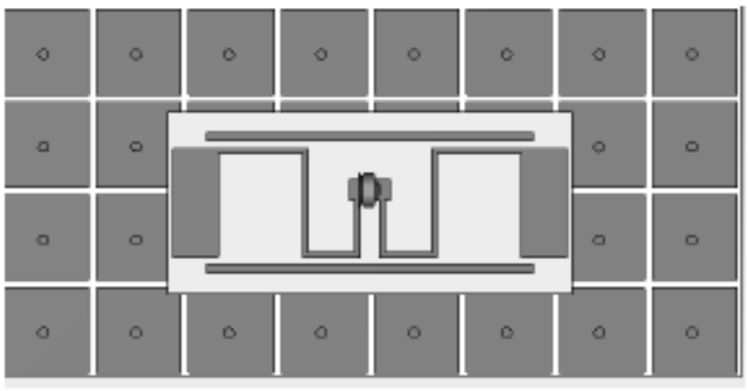

**Fig. 7.9. The EBG RFID tag proposed in [88].**

It is shown in another work that the presence of the EBG ground plane makes some changes in the impedance matching between the chip and antenna [89]. This means the antenna should be specially designed and tuned to work on the EBG. However the proposed solution in that work is to add some parasitic elements close to the tag for compensation as depicted in Fig. 7.10. There are 5×5 cells in the design and the overall dimension is 125×125×2 $mm^3$ which is usually applicable on large metallic objects.

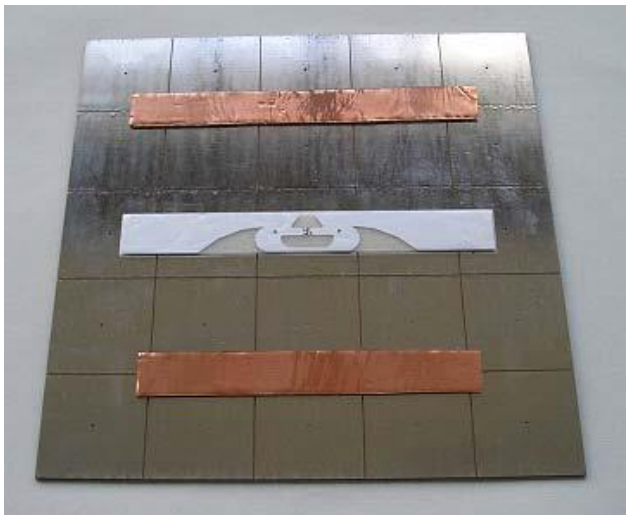

**Fig. 7.10. Correcting the impedance matching of an EBG supported tag using parasitic elements [89].**

A dipole antenna was studied on a three layer mushroom EBG structure in [90]. The design is depicted in Fig. 7.11. The square mushroom caps are etched on both sides of a 0.2 mm FR-4 substrate which is supported by another FR-4 substrate with 1.5 mm thickness. All the mushroom caps are connected to the common ground plane as shown in Fig. 7.11.

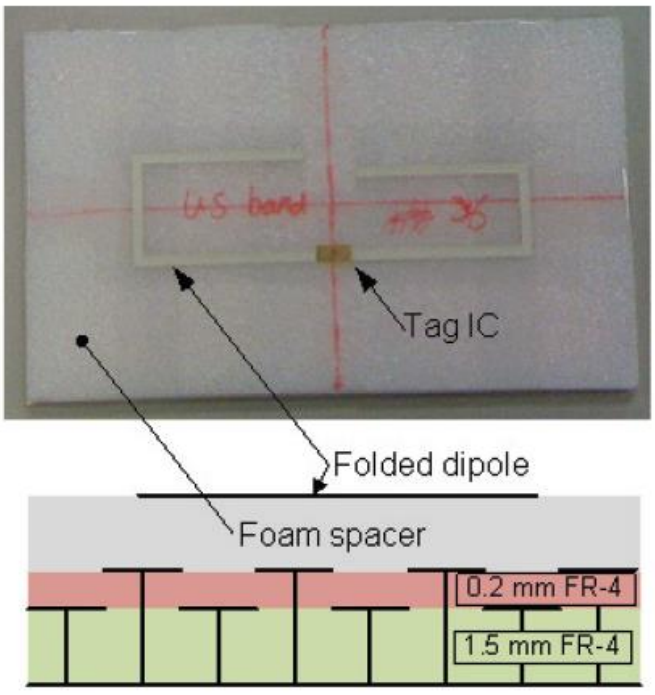


**Fig. 7.11. Dipole protected by dual mushroom EBG structure [2].**

A foam spacer with 3 mm thickness is placed on top of the mushroom structure and a dipole antenna with folded arms is placed on top of it. The size of the dipole is 82×22 $mm^2$ and the size of the overall design with 5×4 unit cells is 124×76×4.8 $mm^3$.

In summary, the mushroom EBG structures are useful in protecting dipole RFID tags from background objects. They improve the radiation efficiency and gain of the antenna by reflecting the wave with the same phase. However, these structures have two main drawbacks. First, the size of the design is more than conventional tag designs because there should be plenty number of unit cells to make the artificial ground plane effective. Second, the presence of vias makes the fabrication process difficult and costly.

# 7.5. Comparison of Mushroom and Uni-Planar Structure

Mushroom structures have shown good performance and they are already being used in many application. The presence of vias makes the structure complicated and costly. In this section the effect of eliminating vias is studied. A uni-planar EBG with the same period of the mushroom structure of Fig. 7.2 is depicted in Fig. 7.12 .

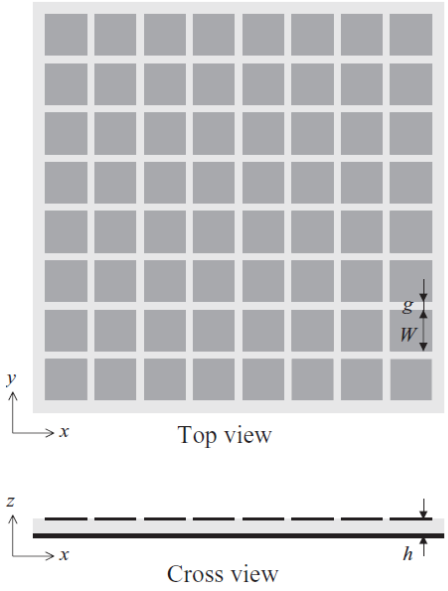


**Fig. 7.12. A grounded dielectric slab loaded with square patches [91].**

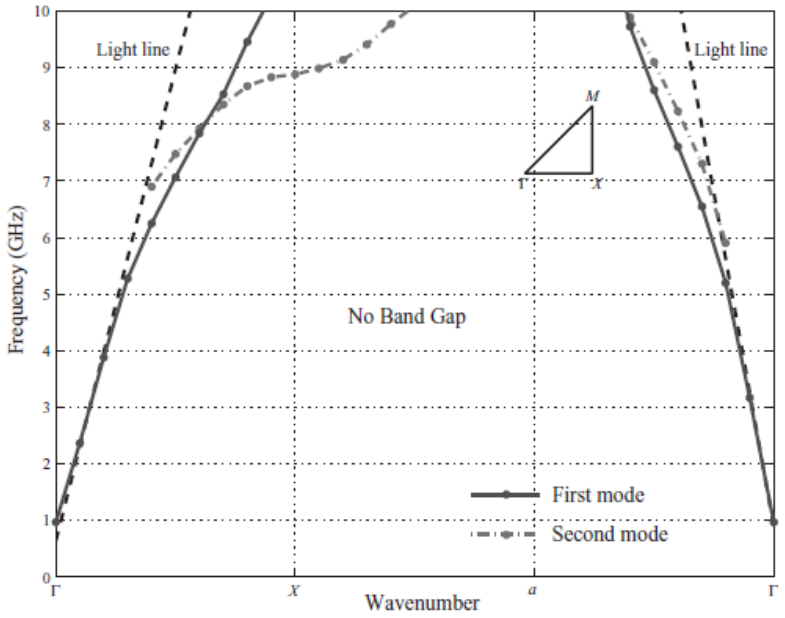


**Fig. 7.13. Lack of band gap in a uni-planar structure with square patches [92].**

The equivalent circuit of the surface of this uni-planar structure is a series *LC* circuit. This circuit shows low impedance at resonant frequency. Thus, the surface current is not suppressed in this structure and there is no band gap as illustrated in Fig. 7.13. The reflection phase of the uni-planar structure is similar to mushroom with less bandwidth. In a mushroom structure the incident wave faces a high impedance surface which is much higher than the impedance of the free space. This mismatch causes a reflection of the wave with the same phase at the resonant frequency. A uni-planar structure can be designed to show the same impedance as free space around 377 Ω. There is no mismatch in this case and the reflection of the incident wave is limited which means a low value of S11. Similar to mushroom structure the reflected wave has the same phase as the incident wave.

It can be concluded that the consequence of removing the via in a mushroom structure and converting it to a uni-planar design is transforming the parallel *LC* circuit to a series *LC* circuit. This eliminates the band gap in the surface current but the structure is still applicable as artificial ground plane for protecting tags. A specially designed uni-planar structure is proposed in the next section for protecting an RFID tag from background material.

# 7.6. Miniaturized Uni-Planar Structure for RFID Tags

A periodic structure for protecting the RFID tag is proposed in this section. The target is to eliminate the vias and create a structure similar to uni-planar design introduced in section 7.5. The problem of using a square shape uni-planar structure is the size limit. The overall size of an artificial ground plane made of uni-planar structure working at UHF RFID band is bigger than the given examples in previous section. A miniaturization is required to break down the size of the unit cell. One way for miniaturization is to apply a substrate with high dielectric constant between the square patch and the ground plane. However, this method increases the cost of the prototype. The second way is to increase the inductance of the square patch by applying thin and meandered conductive tracks [84]. The third way for miniaturizing and lowering the resonant frequency of the structure is to increase the capacitance between the adjacent patches. This can be done by using inter-digital capacitors in unit cells [93, 94].

As mentioned above increasing the capacitance or inductance can miniaturize the unit cell. The question is which method is preferred in the design. The equivalent circuit of a uni-planar square patch can be used for finding the answer. The circuit is a series *RLC*. The quality factor of this circuit can be found by:

$$Q = \frac{1}{R}\sqrt{\frac{L}{C}} \tag{7.3}$$

which indicates: more capacitance in the circuit gives less quality factor that leads to higher bandwidth. Thus, applying the inter-digital capacitor to the square patch seems to be a suitable solution. The proposed unit cell is illustrated in Fig. 7.14. The dimension of the unit cell is 24×14×2.2 $mm^3$. The width of the arms is 1 mm with 0.5 mm of gap between them. The frequency response is shown in Fig. 7.15. The desired working frequency is 866 MHz. The reflection phase of the unit cell is adjusted in the range of 90±45º at this frequency. The corresponding S11 plot shows a small reflection at this point which means the surface impedance of the designed structure is close to the impedance of the free space at that frequency.

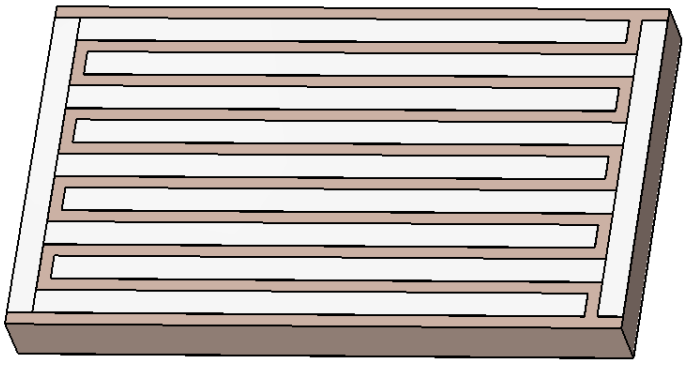

**Fig. 7.14. Unit cell of inter-digital structure.**

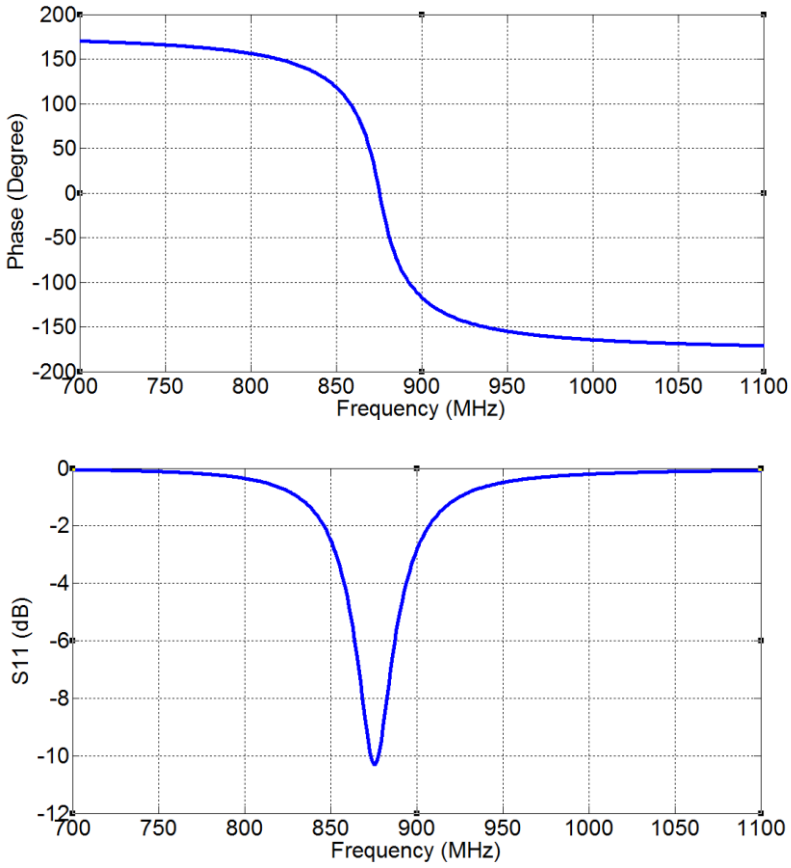


**Fig. 7.15. Frequency response of the unit cell.**

This is completely different from a mushroom structure where there is a high reflection caused by high impedance surface.

The tag is placed on top of an array of the inter-digital unit cell with 6×4 cells as shown in Fig. 7.16. The tag design used for this test is ALN-9768 that was studied in Chapter 4. The tag is placed within 1 mm distance from the designed ground and

the S11 result of the antenna input is plotted in Fig. 7.17. As can be seen the frequency response of the input impedance of the tag remains unchanged at 866 MHz frequency which means the artificial ground plane is not affecting the impedance matching of the antenna. The radiation pattern of the structure is shown in Fig. 7.18. The directivity of the dipole is increased to 4.5 dBi and the radiation efficiency is -0.6 dB that is equal to 87 % which is much higher than the result of Fig. 3.23.

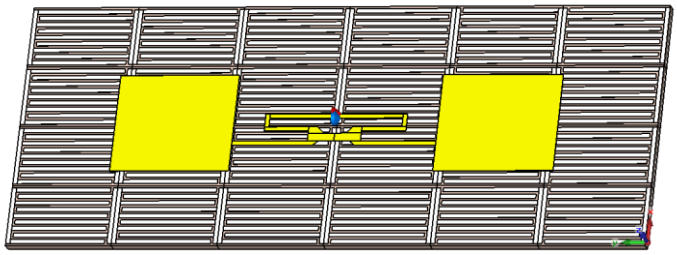

**Fig. 7.16. The tag is placed above a 6 × 4 array of unit cells with 1 mm distance.**

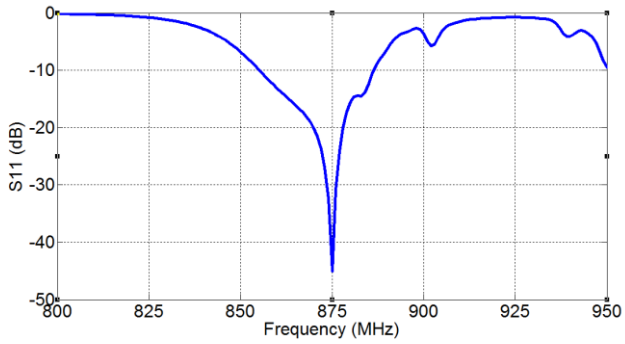


**Fig. 7.17. The S11 of the system with 1 mm distance between the tag and the designed ground.**

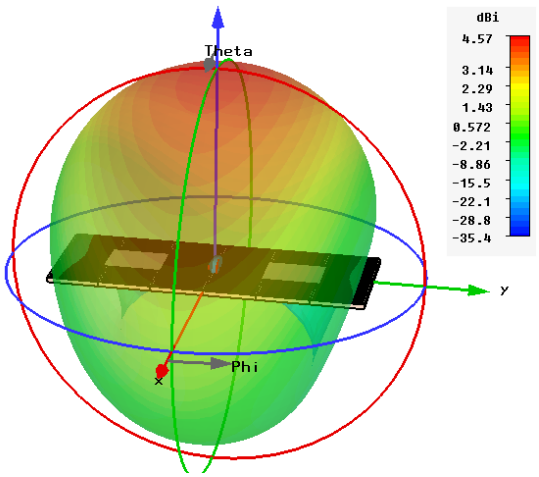


**Fig. 7.18. Radiation pattern of the system.**

The designed structure is placed on a host material in the next step as depicted in Fig. 7.19. The size of the host material is 200×100×10 $mm^3$. The effect of the host material on the impedance matching between the antenna and chip is studied next. The host material is changed from free space to FR-4 in the first experiment to evaluate the effect of increasing the relative dielectric constant from 1 to 4.3. In the next step, the host material is changed to Alumina which has relative dielectric constant around 9.4. Finally, the host material is changed to a perfect electric conductor (PEC). The result of this simulation is presented in Fig. 7.20. As can be seen, increasing the dielectric constant of the host material does not leave a destructive effect on the impedance matching of the antenna and chip but the use of PEC tends to have more effect on the frequency response.

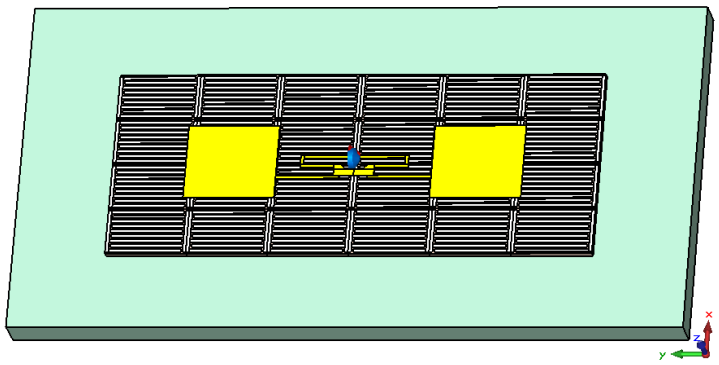

**Fig. 7.19. Designed tag located on a host material.**

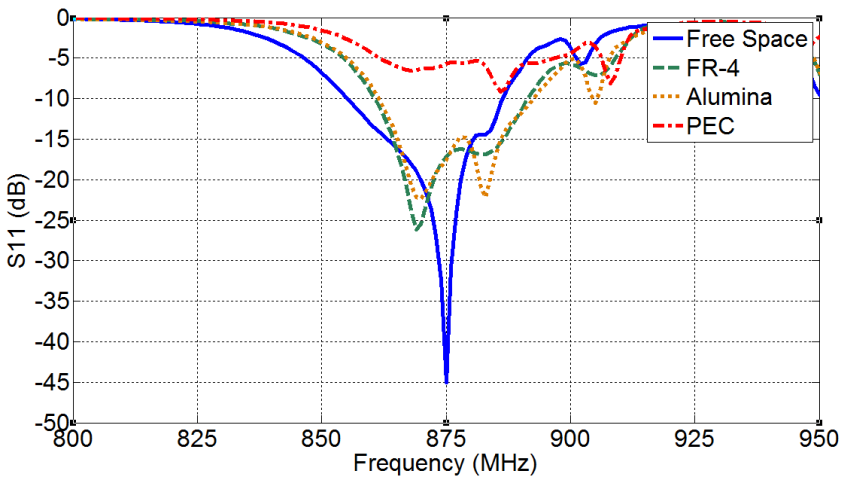


**Fig. 7.20. The effect of changing the host material on the impedance matching of the antenna and chip**

This is completely acceptable as the ground plane is finite therefore there is some interaction between the top layer and the host metallic material which changes the frequency response of the tag. The S11 around -5 dB is acceptable for a passive RFID tag in practice [28].

# 7.7. Conclusion

EBG structures as a solution for protecting the RFID tag from host material was introduced in this chapter. The high impedance surface is the most common choice for designing artificial ground in the literature but the designs suffer from large size and complexity as reviewed in this chapter. The uni-planar structure offers simpler design as it does not need any via. The reflection phase of this structure is similar to the HIS but the reflection coefficient is less than HIS as the surface impedance is small and can be close to the impedance of free space which means a perfect impedance matching and a small amount of reflection. The proposed inter-digital uni-planar structure showed an acceptable performance in protecting ALN-9768. The overall dimension of the designed tag with 1 mm distance from the periodic ground plane is 144×56×3.2 $mm^3$. The size of the proposed design is smaller than the reviewed works in this chapter. In addition, all the reviewed works employ complex mushroom structure whereas the proposed structure is free from any via holes and connections between the layers.

# Chapter 8. Conclusions and Future Work

Passive UHF RFID tags were studied in this thesis. The main target was to investigate and propose tag designs robust to metallic and challenging material. There has been many works revolving around this subject in the literature during the past years. Although, interesting designs were proposed with outstanding performance but designing a tag with optimum performance which can satisfy the factors of low profile and low cost is a challenging task. There is a compromise between these factors usually. All of the proposed tag designs in this thesis offer an optimum performance according to the mentioned factors which are comparable to the most significant recent works. In addition to proposed new designs in this thesis, analysis and studies that was not covered in the literature before was conducted. Including analysis of the effect of the background material and liquid bottle on the different parts of a tag and suggesting a straightforward method for designing optimum matched tags using Smith chart. As the final part of this thesis, a comprehensive review on the conclusions of the research and the possible future work is given in this chapter.

# 8.1. Conclusions

In **Chapter 1**, the problem was defined, and the motivation of this research was discussed. A passive UHF RFID tag was introduced as a rival for traditional optical barcode system in tracking and tagging objects. The main obstacles hindering the progress of replacing optical barcode system with RFID tags is the sensitivity of the tag antenna to the host material and the production cost. The objectives of the study were defined with the goal of solving the current problem of tags and contributing to the growth of this technology.

In **Chapter 2**, the basics of the RFID technology was introduced. It was learned the communication in RFID is based on modulated backscatter principle which was basically practiced for the first time during World War II. Different types of RFID tags and operating frequency which are suitable for a variety of applications were reviewed. The high data capacity of RFID system was revealed after studying the communication protocols. After getting familiar with RFID technology and its advantages it was understood why RFID is more demanding than optical barcode system.

In **Chapter 3**, the main subject of the thesis: passive UHF RFID tags was studied. The two main parts of a passive tag: antenna and chip was reviewed. It was learned how the advances in semiconductor technology have helped to increase the sensitivity of the chip which improved the read range of the system. Delivering the maximum energy from reader to the tag is known as a vital factor for passive tags as they rely on this energy for running the internal circuitry of the chip. Conjugate impedance matching between the antenna input and the chip is the principle that guarantees the maximum energy delivering. However, it was shown that conjugate impedance matching is not a straightforward task in short dipoles as they have capacitive input impedance similar to RFID chips and extra inductive elements are needed in the design. The detuning effect on two commercial tags was examined and it was concluded that the robust tag offers more bandwidth in the impedance matching. More analysis showed that the detuning effect actually is equivalent to the change in the value of the capacitances in the antenna. A comprehensive literature review about the tags robust to challenging objects was performed. It was found that there is a lack of study on the effect of the liquid bottle on the tag in terms of circuit

analysis. Different designs robust to metallic objects were reviewed and discussed. In most of the cases, a suitable performance is achieved with the cost of a complicated design.

In **Chapter 4**, the study was focused on the design of a tag robust to liquid bottles. It was learned how to convert a tag design to the equivalent circuit and calculate the values of the elements in the circuit. The result of the analysis showed that the effect of the liquid bottle is equivalent to reducing the radiation resistance and increasing the loss resistance of the antenna which leads to an increase in the total value of the resistance in the equivalent circuit of the antenna. In fact, the liquid bottle has two destructive effects on the performance of the tag. First, reducing the radiation efficiency of the antenna and second, altering the input impedance of the antenna which affects the impedance matching between the antenna and RFID chip. The first problem is related to the physics of the liquid which absorbs the electromagnetic energy. The second problem was solved by adding extra compensating elements to the design. The impedance matching was fixed without increasing the overall size of the design. The read range test confirmed that the proposed solution is effective.

In **Chapter 5**, two new designs were proposed. In the first design, the research was focused on identifying the most sensitive elements in a typical label-type tag. It was known from Chapter 3 that the detuning effect is caused by the change in the value of the capacitances in the antenna. Totally, there are two capacitances in a tag design: First, the capacitance in parallel to the chip and second, the capacitance of the dipole arm. The first capacitance was found to be more sensitive. Thus, a novel 3D design was suggested that protects this capacitance from the background material. As the production cost is an important factor, a small portion of the proposed design is supported with flexible paper substrate. For increasing the robustness of the second capacitance in the dipole arm it was shown theoretically that bigger capacitance leads to more robustness which means it is better to have a dipole loaded with capacitive parts at the tip. The proposed design showed robustness to materials with high dielectric constant. In addition, it is applicable on metallic objects with acceptable read range. In the second design, a dual-polarized tag mountable on different material was proposed. The tag employs a Monza 4 chip which was introduced in Chapter 3. The two independent port of this chip makes it a

suitable option for dual-polarized antenna and any other design with two ports. Most of the RFID readers employ circularly polarized or dual-polarized antenna which increases the readability of the tag. In some small handheld readers a linearly polarized antenna is used. A dual-polarized tag is more reliable to use with this type of readers. The test results showed an outstanding read range and the tag was insensitive to the polarization angle of the reader antenna.

In **Chapter 6**, a universal tag with optimum performance on a wide range of material was presented. It is known that dipole antenna tags are the best option for non-metallic objects. They offer high radiation efficiency and a uniform radiation pattern which is desirable for reading the tag from different angles. In addition, they are low profile and cost effective. Dipole tags are not applicable on metallic objects. Patch antennas are usually used for this purpose. Although patch antenna is applicable on non-metallic objects but the performance is limited in terms of read range and radiation pattern. The novel design proposed in Chapter 6 is a hybrid of both dipole and patch antenna. The tag converts from a dipole to a patch as soon as it is placed on a metallic object. The simulation and lab experiment showed an outstanding performance on different materials. Another important result of this chapter is the study of different parts of the tag and its effect on the impedance matching. The study was done using the Smith chart with the target of reaching the optimum impedance matching. The expected plot of an optimum design was introduced which passes close to the center of the chart at the desired frequency. By knowing the effect of changing each part of the antenna on the optimum plot, the designer can decide which part of the design needs to be modified to reach a perfect impedance matching. The result of this study gives a straightforward method for designing a tag in a logical strategy instead of doing multiple blind simulations.

In **Chapter 7**, EBG structures were introduced and their application in protecting dipole antenna from metallic objects was reviewed. It was learned that mushroom structure is the most common design in the literature. This structure protects the antenna by reflecting the wave with the same phase as it approaches the surface. In addition, there is no surface current on this structure as the wave faces a high impedance plane. The mushroom structure is useful and effective but it suffers from complex design as it has a via connecting the two layers. Studies showed that by eliminating the via and reaching a uni-planar structure still a desired zero reflection

phase can be achieved. However, there is surface current in the uni-planar structure but the result showed that the zero reflection phase is the important factor in protecting the tag from the metallic object. The proposed inter-digital structure can be designed at any other frequency for protecting different dipoles.

Finally, the main achievements of the thesis can be summarized as follows:

- Proposing a novel RFID tag with improved read range on liquid bottles: Tagging and tracking liquid filled bottles is demanded by different industries such as wine and medicine. The existing commercial RFID tags offer a limited rad range when placed on a liquid bottle. The analysis performed in Chapter 4 revealed the reason of this phenomenon. The proposed solution to tackle the negative effect of the liquid on the performance of the tag led to a novel design with improved read range. This enables a reliable tracking of liquid bottles. The working principle of the proposed design can be used to design new robust tags.
- Designing a label-type dipole tag mountable on metallic and non-metallic objects: Most of the thin label-type dipole tags are sensitive to the dielectric constant of the host material and are not practical on metallic objects. The existing robust tags in the market are costly compared to the thin label-type dipole tags. The proposed tag design in Chapter 5 is mountable on both metallic and non-metallic objects. The novel dipole design is low cost and flexible which can be used for tagging a wide range of objects with different shapes.
- Designing a dual-polarized cavity-backed tag mountable on metallic and non-metallic objects: The proposed design in Chapter 5 employs a low cost FR-4 substrate. There is no via in the design which facilitates the fabrication process. Dual-polarized characteristic of the antenna improves the reliability of the reading using a handheld RFID reader.
- Proposing a hybrid tag robust to host material: The existing UHF RFID tags are normally designed to work on either metallic or non-metallic objects. A tag which is specially designed for one group of material cannot offer the optimum read range and radiation pattern when it is placed on the other group of material. The groundless hybrid tag introduced in Chapter 6

offers an optimum read range and radiation pattern on a wide range of materials including metallic objects. This saves the cost for both producers and costumers of the UHF RFID tags.

- Introducing a novel method for reaching an optimum tag design: The method introduced in Chapter 6 is a straightforward solution using Smith chart and equivalent circuit for designing and fine tuning UHF RFID tags. This method saves the designing time and guarantees the perfect impedance matching and maximum read range.
- Designing a novel periodic structure for protecting UHF RFID tags from background material: The most common periodic structure for protecting antennas from host material is the mushroom structure. The presence of via in this structure makes the fabrication process costly and complicated. The proposed periodic structure in Chapter 7 eliminates the need for via which makes the design simple and cost effective. The novel design showed that there is no need to have a high impedance surface for protecting the tag but a low impedance surface which is matched to the impedance of the free space can protect the tag with zero reflection phase characteristics.

# 8.2. Future Work

The outstanding advantage of RFID systems has made it a fast growing technology since its inception. The main obstacle hindering the widespread adoption of this technology is the tag price [1]. However, the growth of semiconductor technology and manufacturing methods has reduced the price in the past years. Studies and development in antenna designs has also helped this improvement by offering low profile simple designs. This thesis contributed to this progress by offering low cost tags robust to host material. The result of this study can be used for further investigation in future work. A few possible scenarios are reviewed in this section.

The result of the investigation in Chapter 4 showed that the liquid bottle interacts with the performance of the tag as the water absorbs the electromagnetic energy caused by its high conductivity. This conductivity was used for correcting the

impedance matching between the antenna and chip without considering the radiation properties of the liquid. On the other hand, there has been some works about employing water as a monopole antenna [95]. The result of those studies can be applied to a tag design for liquid bottle. The tag can be a monopole design embedded to the cork or lid of the bottle with the radiating arm connected to the liquid. In this special arrangement the liquid inside the bottle plays an important role as the main radiating part of the tag. According to the typical height of a bottle which is comparable to the wavelength at the design frequency, a high read range is expected from the proposed work. However, more study is required for this work.

The hybrid tag introduced in Chapter 6 is equipped with Monza 4 which is a dual port chip as introduced in Chapter 3. The two ports are independent and one of them works when the tag is in off-metal mode and the other works for on-metal mode. A challenging problem for the future work is to eliminate the need for a dual port chip. In this case the antenna structure should be completely changed to a single port prototype which can be matched to any typical RFID chip. The main challenge in this work is to have a hybrid design matched to the same chip in both on-metal and off-metal scenarios. Rigorous studies are required in future to achieve this goal.

In Chapter 7 it was shown that having a high impedance surface unit cell in the artificial ground plane is not necessary for protecting the tag from the metallic surface. This means unlike the previous designs which used mushroom structure, the proposed design supports the surface currents. These surface currents can contribute to radiation which means the artificial ground plane becomes part of the antenna. The idea for the future work is to simplify the design by embedding the tag into the artificial ground plane. The tag might be converted to a small feed point which can excite the artificial ground plane to radiate the wave. This can remove one layer from the prototype and reduce the production cost.

The future work in UHF RFID tag design is not limited to the works proposed in this thesis. According to different applications of this technology discussed in Chapter 2, development is taking place in many areas. Integrating the RFID tags to the environmental sensors is one of the hot areas in recent years. There has been different type of passive and active designs so far. The works can be divided into two groups. The first group are the tags with a distinct sensor. The RFID system is integrated to an electronic sensor system which reports the sensed data to the RFID

chip and the tag reports this data to the reader [96-101]. The second group are systems with combined sensor antenna. These designs are usually passive tags with extra sensing elements that changes the characteristic of the antenna when one of the environment characteristics changes. For example, a temperature sensor can shift the frequency response of the tag and the reader can decide the value of the temperature by detecting this frequency shift. These types of works are reported in [80, 102-104]. The tags in second group are low cost and the working principle is related to the subject covered in this thesis. By studying the frequency response of the tag, interesting simple sensor designs can be proposed for future work.

Finally, with the fast growth of Internet of Things (IoT) and evolution of Near Field Communication (NFC) systems and integrating this technology to mobile phones, each person would carry an RFID reader system that connects the person to the global network. There is no doubt an exciting future is waiting for this technology.

# References


[1] V. D. Hunt, A. Puglia, and M. Puglia, *RFID : a guide to radio frequency identification*, Hoboken, N.J.: Wiley-Interscience, 2007.

[2] T. Bjorninen, L. Sydanheimo, L. Ukkonen, and Y. Rahmat-Samii, "Advances in Antenna Designs for UHF RFID Tags Mountable on Conductive Items," *IEEE Antennas and Propagation Magazine,* vol. 56, no. 1, pp. 79-103, Feb, 2014.

[3] K. Finkenzeller, *RFID handbook : fundamentals and applications in contactless smart cards and identification*, 2nd ed., Chichester, England ; Hoboken, N.J.: Wiley, 2003.

[4] L. Brown, *A radar history of World War II : technical and military imperatives*, Bristol ; Philadelphia: Institute of Physics Pub., 1999.

[5] D. M. Dobkin, *The RF in RFID: UHF RFID in practice*: Newnes, 2012.

[6] H. Stockman, "Communication by means of reflected power," *Proceedings of the IRE,* vol. 36, no. 10, pp. 1196-1204, 1948.

[7] C. L. R, "Folded dipole having a direct current output," Google Patents, 1960.

[8] C. Walton, "Electronic identification & recognition system," Google Patents, 1973.

[9] A. R. Koelle, S. W. Depp, and R. W. Freyman, "Short-range radio-telemetry for electronic identification, using modulated RF backscatter," *Proceedings of the IEEE,* vol. 63, no. 8, pp. 1260-1261, 1975.

[10] J. Landt, "The history of RFID," *IEEE potentials,* vol. 24, no. 4, pp. 8-11, 2005.

[11] "Readers and a Printer for the RFID and Sensor Solution," http://www.fujitsu.com/global/solutions/business-technology/intelligent-society/ait/readers/.

[12] IDTechEx, P. Harrop, and R. Das, *RFID Forecasts, Players and Opportunities 2014-2024*: IDTechEx, 2014.

[13] D. D. Deavours, "Analysis and Design of Wideband Passive UHF RFID Tags Using a Circuit Model," *IEEE Rfid: 2009 IEEE International Conference on Rfid*, pp. 275-282, 2009.

[14] N. A. Mohammed, K. R. Demarest, and D. D. Deavours, "Analysis and synthesis of UHF RFID antennas using the embedded T-match," in *2010 IEEE International Conference on RFID (IEEE RFID 2010)*, 2010, pp. 230-236.

[15] M. T. Reich, and C. Bauer-Reich, "UHF RFID impedance matching: When is a T-match not a T-match?," in *2014 IEEE International Conference on RFID (IEEE RFID)*, 2014, pp. 23-30.

[16] S. Zuffanelli, J. Bonache Albacete, and F. Martín Antolín, "Antenna design solutions for radio frequency identification (RFID) tags based on metamaterial-inspired resonators and other resonant structures," 2015.

[17] P. Nikitin, K. Rao, and S. Lam, "UHF RFID tag characterization: overview and state-of-the-art," in *Antenna Measurement Techniques Association Symposium (AMTA)*, 2012.

[18] E. Bergeret, J. Gaubert, P. Pannier, and J. M. Gaultier, "Modeling and Design of CMOS UHF Voltage Multiplier for RFID in an EEPROM Compatible Process," *IEEE Transactions on Circuits and Systems II: Express Briefs,* vol.

54, no. 10, pp. 833-837, 2007.
[19] G. D. Vita, and G. Iannaccone, “Design criteria for the RF section of UHF and microwave passive RFID transponders,” *IEEE Transactions on Microwave Theory and Techniques,* vol. 53, no. 9, pp. 2978-2990, 2005.
[20] "Monza 4 tag chip datasheet "; https://support.impinj.com/hc/en-us/articles/202756908-Monza-4-RFID-Tag-Chip-Datasheet.
[21] D. B. Miron, *Small antenna design*: Newnes, 2006.
[22] "Alien Technology RFID Tags," http://www.alientechnology.com.
[23] "Tag Factory On-metal UHF RFID Tags," http://thetagfactory.com/Products/ultra-high-frequency/on-metal.
[24] D. M. Pozar, *Microwave engineering*, 4th ed., Hoboken, NJ: Wiley, 2012.
[25] K. V. S. Rao, P. V. Nikitin, and S. F. Lam, “Antenna design for UHF RFID tags: A review and a practical application,” *IEEE Transactions on Antennas and Propagation,* vol. 53, no. 12, pp. 3870-3876, Dec, 2005.
[26] Y. Huang, and K. Boyle, "Popular Antennas," *Antennas*, pp. 129-213: John Wiley & Sons, Ltd, 2008.
[27] D. M. Dobkin, and S. M. Weigand, “Environmental effects on RFID tag antennas,” *2005 IEEE MTT-S International Microwave Symposium, Vols 1-4*, pp. 135-138, 2005.
[28] S. Shao, R. J. Burkholder, and J. L. Volakis, “Design Approach for Robust UHF RFID Tag Antennas Mounted on a Plurality of Dielectric Surfaces,” *IEEE Antennas and Propagation Magazine,* vol. 56, no. 5, pp. 158-166, Oct, 2014.
[29] T. G. Tang, Q. M. Tieng, and M. W. Gunn, “Equivalent circuit of a dipole antenna using frequency-independent lumped elements,” *IEEE Transactions on Antennas and Propagation,* vol. 41, no. 1, pp. 100-103, 1993.
[30] G. Zamora, S. Zuffanelli, F. Paredes, F. Martin, and J. Bonache, “Design and Synthesis Methodology for UHF-RFID Tags Based on the T-Match Network,” *IEEE Transactions on Microwave Theory and Techniques,* vol. 61, no. 12, pp. 4090-4098, Dec, 2013.
[31] T. Bjorninen, A. Z. Elsherbeni, and L. Ukkonen, “Low-Profile Conformal UHF RFID Tag Antenna for Integration With Water Bottles,” *IEEE Antennas and Wireless Propagation Letters,* vol. 10, pp. 1147-1150, 2011.
[32] J. T. Xi, and T. T. Ye, “Conformal UHF RFID Tag Antenna Mountable on Winebottle Neck,” *2012 IEEE Antennas and Propagation Society International Symposium (Apsursi)*, 2012.
[33] R. Goncalves, S. Rima, R. Magueta, A. Collado, P. Pinho, N. B. Carvalho, and A. Georgiadis, “RFID Tags on Cork Stoppers for Bottle Identification,” *2014 IEEE Mtt-S International Microwave Symposium (Ims)*, 2014.
[34] R. Goncalves, N. B. Carvalho, R. Magueta, A. Duarte, and P. Pinho, “UHF RFID tag antenna for bottle labeling,” *2014 IEEE Antennas and Propagation Society International Symposium (Apsursi)*, pp. 1520-1521, 2014.
[35] R. Quiroz, T. Alves, B. Poussot, and J. M. Laheurte, “Combined RFID tag antenna for recipients containing liquids,” *Electronics Letters,* vol. 49, no. 4, pp. 240-242, Feb 14, 2013.
[36] S. R. Aroor, and D. D. Deavours, “Evaluation of the State of Passive UHF RFID: An Experimental Approach,” *IEEE Systems Journal,* vol. 1, no. 2, pp. 168-176, 2007.
[37] J. D. Griffin, G. D. Durgin, A. Haldi, and B. Kippelen, “RF Tag Antenna

Performance on Various Materials Using Radio Link Budgets," *IEEE Antennas and Wireless Propagation Letters,* vol. 5, no. 1, pp. 247-250, 2006.
[38] R. S. Elliot, *Antenna theory and design*: John Wiley & Sons, 2006.
[39] P. Raumonen, L. Sydanheimo, L. Ukkonen, M. Keskilammi, and M. Kivikoski, "Folded dipole antenna near metal plate," in *IEEE Antennas and Propagation Society International Symposium. Digest. Held in conjunction with: USNC/CNC/URSI North American Radio Sci. Meeting (Cat. No.03CH37450)*, 2003, pp. 848-851 vol.1.
[40] C. A. Balanis, *Modern antenna handbook*, Hoboken, NJ: Wiley, 2008.
[41] T. Björninen, K. E. Delzo, L. Ukkonen, A. Z. Elsherbeni, and L. Sydänheimo, "Long range metal mountable tag antenna for passive UHF RFID systems," in *RFID-Technologies and Applications (RFID-TA), 2011 IEEE International Conference on*, 2011, pp. 202-206.
[42] H. D. Chen, Y. H. Tsao, and C. Y. Kuo, "Low-profile radio frequency identification tag antenna using a trapezoid patch mountable on metallic surfaces," *Microwave and Optical Technology Letters,* vol. 52, no. 8, pp. 1697-1700, 2010.
[43] T. V. Koskinen, H. Rajagopalan, and Y. Rahmat-Samii, "A thin multi-slotted dual patch UHF-band metal-mountable RFID tag antenna," *Microwave and Optical Technology Letters,* vol. 53, no. 1, pp. 40-47, 2011.
[44] S. J. Kim, B. Yu, Y. S. Chung, F. J. Harackiewicz, and B. Lee, "Patch-type radio frequency identification tag antenna mountable on metallic platforms," *Microwave and Optical Technology Letters,* vol. 48, no. 12, pp. 2446-2448, 2006.
[45] S.-J. Kim, B. Yu, H.-J. Lee, M.-J. Park, F. J. Harackiewicz, and B. Lee, "RFID tag antenna mountable on metallic plates," in *Microwave Conference Proceedings, 2005. APMC 2005. Asia-Pacific Conference Proceedings*, 2005, pp. 3 pp.
[46] B. Lee, and B. Yu, "Compact structure of UHF band RFID tag antenna mountable on metallic objects," *Microwave and Optical Technology Letters,* vol. 50, no. 1, pp. 232-234, 2008.
[47] J.-S. Kim, W.-K. Choi, and G.-Y. Choi, "Small proximity coupled ceramic patch antenna for UHF RFID tag mountable on metallic objects," *Progress In Electromagnetics Research C,* vol. 4, pp. 129-138, 2008.
[48] K. H. Lin, S. L. Chen, and R. Mittra, "A Looped-Bowtie RFID Tag Antenna Design for Metallic Objects," *IEEE Transactions on Antennas and Propagation,* vol. 61, no. 2, pp. 499-505, Feb, 2013.
[49] M. Polivka, and M. Svanda, "Stepped Impedance Coupled-Patches Tag Antenna for Platform-Tolerant UHF RFID Applications," *IEEE Transactions on Antennas and Propagation,* vol. 63, no. 9, pp. 3791-3797, Sep, 2015.
[50] S. L. Chen, and K. H. Lin, "A Slim RFID Tag Antenna Design for Metallic Object Applications," *IEEE Antennas and Wireless Propagation Letters,* vol. 7, pp. 729-732, 2008.
[51] G. H. Du, T. Tang, and Y. Deng, "Dual-band metal skin UHF RFID tag antenna," *Electronics Letters,* vol. 49, no. 14, pp. 858-859, Jul 4, 2013.
[52] A. G. Santiago, J. R. Costa, and C. A. Fernandes, "Broadband UHF RFID Passive Tag Antenna for Near-Body Applications," *IEEE Antennas and Wireless Propagation Letters,* vol. 12, pp. 136-139, 2013.

[53] L. Xu, B. J. Hu, and J. Wang, "UHF RFID tag antenna with broadband characteristic," *Electronics Letters,* vol. 44, no. 2, pp. 79-80, 2008.
[54] J. Zhang, and Y. Long, "A Dual-Layer Broadband Compact UHF RFID Tag Antenna for Platform Tolerant Application," *IEEE Transactions on Antennas and Propagation,* vol. 61, no. 9, pp. 4447-4455, 2013.
[55] M. Hirvonen, P. Pursula, K. Jaakkola, and K. Laukkanen, "Planar inverted-F antenna for radio frequency identification," *Electronics Letters,* vol. 40, no. 14, pp. 848-850, 2004.
[56] M. A. Jensen, and Y. Rahmat-Samii, "EM interaction of handset antennas and a human in personal communications," *Proceedings of the IEEE,* vol. 83, no. 1, pp. 7-17, 1995.
[57] K. L. Virga, and Y. Rahmat-Samii, "Low-profile enhanced-bandwidth PIFA antennas for wireless communications packaging," *IEEE Transactions on Microwave Theory and Techniques,* vol. 45, no. 10, pp. 1879-1888, 1997.
[58] M. Hirvonen, K. Jaakkola, P. Pursula, and J. Saily, "Dual-band platform tolerant antennas for radio-frequency identification," *IEEE Transactions on Antennas and Propagation,* vol. 54, no. 9, pp. 2632-2637, Sep, 2006.
[59] W. Choi, H. W. Son, J.-H. Bae, G. Y. Choi, C. S. Pyo, and J.-S. Chae, "An RFID tag using a planar inverted-F antenna capable of being stuck to metallic objects," *ETRI journal,* vol. 28, no. 2, pp. 216-218, 2006.
[60] H. Kwon, and B. Lee, "Compact slotted planar inverted-F RFID tag mountable on metallic objects," *Electronics Letters,* vol. 41, no. 24, pp. 1308-1310, 2005.
[61] L. Mo, and C. Qin, "Tunable compact UHF RFID metal tag based on CPW open stub feed PIFA antenna," *International Journal of Antennas and Propagation,* vol. 2012, 2012.
[62] J. Choo, and J. Ryoo, "UHF RFID Tag Applicable to Various Objects," *IEEE Transactions on Antennas and Propagation,* vol. 62, no. 2, pp. 922-925, Feb, 2014.
[63] A. Hamani, M. C. E. Yagoub, T. P. Vuong, and R. Touhami, "A Novel Broadband Antenna Design for UHF RFID Tags on Metallic Surface Environments," *IEEE Antennas and Wireless Propagation Letters,* vol. 16, pp. 91-94, 2017.
[64] J. D. Kraus, "Antennas," 1988.
[65] C. Lindberg, "A shallow-cavity UHF crossed-slot antenna," *IEEE Transactions on Antennas and Propagation,* vol. 17, no. 5, pp. 558-563, 1969.
[66] C. Jui-Ching, N. I. Dib, and L. P. B. Katehi, "Theoretical modeling of cavity-backed patch antennas using a hybrid technique," *IEEE Transactions on Antennas and Propagation,* vol. 43, no. 9, pp. 1003-1013, 1995.
[67] N. C. Karmakar, "Investigations into a cavity-backed circular-patch antenna," *IEEE Transactions on Antennas and Propagation,* vol. 50, no. 12, pp. 1706-1715, 2002.
[68] H. Sun, B. Tao, and O. M. Ramahi, "Proximity Coupled Cavity Backed Patch Antenna for Long Range UHF RFID Tag," *IEEE Transactions on Antennas and Propagation,* vol. 64, no. 12, pp. 5446-5449, Dec, 2016.
[69] D. Kim, and J. Yeo, "A Passive RFID Tag Antenna Installed in a Recessed Cavity in a Metallic Platform," *IEEE Transactions on Antennas and Propagation,* vol. 58, no. 12, pp. 3814-3820, 2010.

[70] A. Dubok, and A. B. Smolders, “Miniaturization of Robust UHF RFID Antennas for Use on Perishable Goods and Human Bodies,” *IEEE Antennas and Wireless Propagation Letters,* vol. 13, pp. 1321-1324, 2014.

[71] Y. F. Lin, M. J. Chang, H. M. Chen, and B. Y. Lai, “Gain Enhancement of Ground Radiation Antenna for RFID Tag Mounted on Metallic Plane,” *IEEE Transactions on Antennas and Propagation,* vol. 64, no. 4, pp. 1193-1200, 2016.

[72] S. R. Best, “Improving the performance properties of a dipole element closely spaced to a PEC ground plane,” *IEEE Antennas and Wireless Propagation Letters,* vol. 3, no. 1, pp. 359-363, 2004.

[73] S. Genovesi, and A. Monorchio, “Low-Profile Three-Arm Folded Dipole Antenna for UHF Band RFID Tags Mountable on Metallic Objects,” *IEEE Antennas and Wireless Propagation Letters,* vol. 9, pp. 1225-1228, 2010.

[74] M. Polivka, M. Svanda, and P. Cerny, "Multiple-Arm folded monopole antenna operating extremely close to a conductive plane." pp. 1-5.

[75] M. Švanda, and M. Polívka, “Horizontal five-arm folded dipole over metal screening plane for UHF RFID of dielectric objects,” *Microwave and Optical Technology Letters,* vol. 52, no. 10, pp. 2291-2294, 2010.

[76] J. Dacuna, and R. Pous, “Low-Profile Patch Antenna for RF Identification Applications,” *IEEE Transactions on Microwave Theory and Techniques,* vol. 57, no. 5, pp. 1406-1410, May, 2009.

[77] A. A. Babar, T. Bjorninen, V. A. Bhagavati, L. Sydanheimo, P. Kallio, and L. Ukkonen, “Small and Flexible Metal Mountable Passive UHF RFID Tag on High-Dielectric Polymer-Ceramic Composite Substrate,” *IEEE Antennas and Wireless Propagation Letters,* vol. 11, pp. 1319-1322, 2012.

[78] T. Björninen, A. A. Babar, L. Ukkonen, L. Sydanheimo, A. Z. Elsherbeni, and J. Kallioinen, “Compact metal mountable UHF RFID tag on a barium titanate based substrate,” *Progress In Electromagnetics Research C,* vol. 26, pp. 43-57, 2012.

[79] T. W. Koo, D. Kim, J. I. Ryu, H. M. Seo, J. G. Yook, and J. C. Kim, “Design of a Label-Typed UHF RFID Tag Antenna for Metallic Objects,” *IEEE Antennas and Wireless Propagation Letters,* vol. 10, pp. 1010-1014, 2011.

[80] A. A. Babar, S. Manzari, L. Sydanheimo, A. Z. Elsherbeni, and L. Ukkonen, “Passive UHF RFID tag for heat sensing applications,” *IEEE Transactions on Antennas and Propagation,* vol. 60, no. 9, pp. 4056-4064, 2012.

[81] S. Shao, R. J. Burkholder, and J. L. Volakis, “Physics-Based Approach for Antenna Design Optimization of RFID Tags Mounted on and Inside Material Layers,” *2014 IEEE Antennas and Propagation Society International Symposium (Apsursi)*, pp. 1676-1677, 2014.

[82] "Term (Port Impedance for S-parameters) used in Advanced Design System," http://edadocs.software.keysight.com/pages/viewpage.action?pageId=5918331.

[83] F. L. Bong, E. H. Lim, and F. L. Lo, “Flexible Folded-Patch Antenna With Serrated Edges for Metal-Mountable UHF RFID Tag,” *IEEE Transactions on Antennas and Propagation,* vol. 65, no. 2, pp. 873-877, Feb, 2017.

[84] F. Yang, and Y. Rahmat-Samii, *Electromagnetic band gap structures in antenna engineering*, Cambridge, UK ; New York: Cambridge University Press, 2009.

[85] V. Radisic, Y. Qian, R. Coccioli, and T. Itoh, “Novel 2-D photonic bandgap

structure for microstrip lines," *IEEE Microwave and guided wave letters,* vol. 8, no. 2, pp. 69-71, 1998.

[86] D. Sievenpiper, L. J. Zhang, R. F. J. Broas, N. G. Alexopolous, and E. Yablonovitch, "High-impedance electromagnetic surfaces with a forbidden frequency band," *IEEE Transactions on Microwave Theory and Techniques,* vol. 47, no. 11, pp. 2059-2074, Nov, 1999.

[87] F. Yang, and Y. Rahmat-Samii, "Reflection phase characterizations of the EBG ground plane for low profile wire antenna applications," *IEEE Transactions on Antennas and Propagation,* vol. 51, no. 10, pp. 2691-2703, 2003.

[88] C. Phatra, P. Krachodnok, and R. Wongsan, "Design of a RFID tag using dipole antenna with Electromagnetic Band Gap," in *2012 9th International Conference on Electrical Engineering/Electronics, Computer, Telecommunications and Information Technology*, 2012, pp. 1-4.

[89] T. Konishi, T. Miura, Y. Numata, S. Sato, A. Sanada, and H. Kubo, "An impedance matching technique of a UHF-band RFID tag on a high-impedance surface with parasite elements," in *Radio and Wireless Symposium, 2009. RWS'09. IEEE*, 2009, pp. 67-70.

[90] B. Gao, and M. M. Yuen, "Passive UHF RFID packaging with electromagnetic band gap (EBG) material for metallic objects tracking," *IEEE Transactions on Components, Packaging and Manufacturing Technology,* vol. 1, no. 8, pp. 1140-1146, 2011.

[91] A. Al-Zoubi, F. Yang, and A. Kishk, "A low-profile dual-band surface wave antenna with a monopole-like pattern," *IEEE Transactions on Antennas and Propagation,* vol. 55, no. 12, pp. 3404-3412, 2007.

[92] F. Yang, A. Aminian, and Y. Rahmat-Samii, "A novel surface-wave antenna design using a thin periodically loaded ground plane," *Microwave and Optical Technology Letters,* vol. 47, no. 3, pp. 240-245, 2005.

[93] A. Presse, X. Zhang, M. Mantash, A.-C. Tarot, and J. M. Floc'h, "Miniaturization of an artificial magnetic conductor with interdigital capacitances," in *Antennas & Propagation Conference (LAPC), 2015 Loughborough*, 2015, pp. 1-4.

[94] Y. Yamashita, Y. Toyota, K. Iokibe, K. Kondo, S. Yoshida, and T. Kaneko, "Miniaturization of a planar EBG structure using interdigital electrodes," in *Electrical Design of Advanced Packaging and Systems Symposium (EDAPS), 2015 IEEE*, 2015, pp. 39-42.

[95] L. Xing, Y. Huang, Y. Shen, S. Al Ja'afreh, Q. Xu, and R. Alrawashdeh, "Further investigation on water antennas," *IET Microwaves, Antennas & Propagation,* vol. 9, no. 8, pp. 735-741, 2015.

[96] A. E. Abdulhadi, and R. Abhari, "Multiport UHF RFID-Tag Antenna for Enhanced Energy Harvesting of Self-Powered Wireless Sensors," *IEEE Transactions on Industrial Informatics,* vol. 12, no. 2, pp. 801-808, 2016.

[97] L. Catarinucci, R. Colella, and L. Tarricone, "Enhanced UHF RFID sensor-tag," *IEEE Microwave and Wireless Components Letters,* vol. 23, no. 1, pp. 49-51, 2013.

[98] D. De Donno, L. Catarinucci, and L. Tarricone, "Enabling self-powered autonomous wireless sensors with new-generation I 2 C-RFID chips," in *Microwave Symposium Digest (IMS), 2013 IEEE MTT-S International*, 2013, pp. 1-4.

[99] D. De Donno, L. Catarinucci, and L. Tarricone, “A battery-assisted sensor-enhanced RFID tag enabling heterogeneous wireless sensor networks,” *IEEE Sensors Journal,* vol. 14, no. 4, pp. 1048-1055, 2014.

[100] A. P. Sample, D. J. Yeager, P. S. Powledge, A. V. Mamishev, and J. R. Smith, “Design of an RFID-based battery-free programmable sensing platform,” *IEEE Transactions on Instrumentation and Measurement,* vol. 57, no. 11, pp. 2608-2615, 2008.

[101] A. Vaz, A. Ubarretxena, I. Zalbide, D. Pardo, H. Solar, A. Garcia-Alonso, and R. Berenguer, “Full passive UHF tag with a temperature sensor suitable for human body temperature monitoring,” *IEEE Transactions on Circuits and Systems II: Express Briefs,* vol. 57, no. 2, pp. 95-99, 2010.

[102] T. Björninen, and F. Yang, “Signal strength readout and miniaturised antenna for metal-mountable UHF RFID threshold temperature sensor tag,” *Electronics Letters,* vol. 51, no. 22, pp. 1734-1736, 2015.

[103] J. Gao, J. Siden, and H.-E. Nilsson, “Printed electromagnetic coupler with an embedded moisture sensor for ordinary passive RFID tags,” *IEEE Electron Device Letters,* vol. 32, no. 12, pp. 1767-1769, 2011.

[104] S. Kim, Y. Kawahara, A. Georgiadis, A. Collado, and M. M. Tentzeris, “Low-cost inkjet-printed fully passive RFID tags for calibration-free capacitive/haptic sensor applications,” *IEEE Sensors Journal,* vol. 15, no. 6, pp. 3135-3145, 2015.

# Appendix A

**Equivalent circuit transformation:** The transforming of the equivalent circuit in Fig. 4.6 to the equivalent circuit of Fig. 4.8 is explained in this Appendix. The transformation takes place in two steps. For the first step please refer to [13]. For the second step, it is shown here how the circuit of Fig A. 1(a) can be transformed to the circuit of Fig A. 1(b) and the values of *x* and *y* in equation (4.4) are derived.

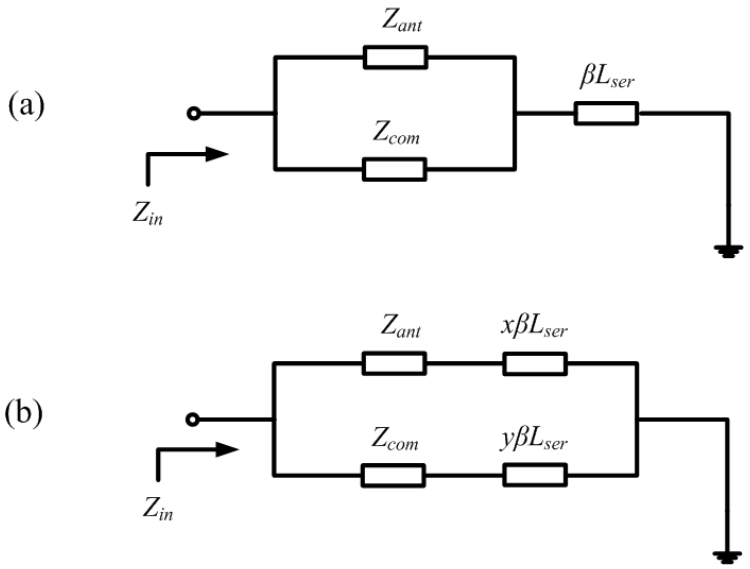


**Fig. A. 1. Equivalent circuit transformation from circuit topology (a) to (b).**

The input impedance of the circuit in Fig A. 1(a) can be found by:

$$Z_{in} = \frac{Z_{ant} Z_{com}}{Z_{ant} + Z_{com}} + \beta L_{ser} \tag{A.1}$$

The input impedance of the transformed circuit of Fig A. 1(b) can be found by:

$$Z_{in} = \frac{\left(Z_{ant} + x\beta L_{ser}\right)\left(Z_{com} + y\beta L_{ser}\right)}{Z_{ant} + Z_{com} + \beta\left(x + y\right)L_{ser}} \tag{A.2}$$

The input impedance of the two circuits should be equal in all conditions. When $Z_{com}$ is reaching infinity, the input impedance of the first circuit is equal to:

$$\lim_{Z_{com}\to\infty} Z_{in} = Z_{ant} + \beta L_{ser} \tag{A.3}$$

and the input impedance of the second circuit is:

$$\lim_{Z_{com}\to\infty} Z_{in} = Z_{ant} + x\beta L_{ser} \tag{A.4}$$

The equations (A.3) and (A.4) should be equal. The following condition should stand to satisfy this:

$$\lim_{Z_{com}\to\infty} x = 1 \tag{A.5}$$

When $Z_{ant}$ is reaching infinity, it can be concluded with the similar assumption:

$$\lim_{Z_{ant}\to\infty} y = 1 \tag{A.6}$$

When $Z_{ant}$ is equal to zero, equation (A.1) is equal to:

$$\lim_{Z_{ant}\to 0} Z_{in} = \beta L_{ser} \tag{A.7}$$

and equation (A.2) is equal to:

$$\lim_{Z_{ant}\to 0} Z_{in} = \frac{x\beta L_{ser}\left(Z_{com} + y\beta L_{ser}\right)}{Z_{com} + \beta\left(x+y\right)L_{ser}} \tag{A.8}$$

For making (A.7) and (A.8) equal to each other, the following relations should stand:

$$\lim_{Z_{ant}\to 0} x = 1 \tag{A.9}$$

$$\lim_{Z_{ant}\to 0} y = \infty \tag{A.10}$$

When $Z_{com}$ is equal to zero, with similar assumption:

$$\lim_{Z_{com}\to 0} y = 1 \tag{A.11}$$

$$\lim_{Z_{com}\to 0} x = \infty \tag{A.12}$$

According to the achieved conditions for $x$ and $y$, it can be concluded:

$$x = 1 + \frac{Z_{ant}}{Z_{com}} \quad , \quad y = 1 + \frac{Z_{com}}{Z_{ant}} \tag{A.13}$$

All the conditions for x and y are satisfied in equation (A.13). The accuracy of this relation can be investigated by considering any desired value for the elements of the circuit in Fig. A. 1 and calculating the input impedance.

# Appendix B

ALIEN

## HIGGS™ 4 SOT

### DATASHEET ADDENDUM

The Higgs-4 SOT is a highly integrated single chip UHF RFID Tag IC packaged in a JEDEC SOT-323 SOT. The chip conforms to the EPCglobal Class-1 Gen-2 specification and provides state-of-the-art performance for a broad range of UHF RFID tagging applications. The Higgs-4 IC is implemented in a low cost CMOS process and uses proven and cost effective EEPROM technology.


Application Diagram

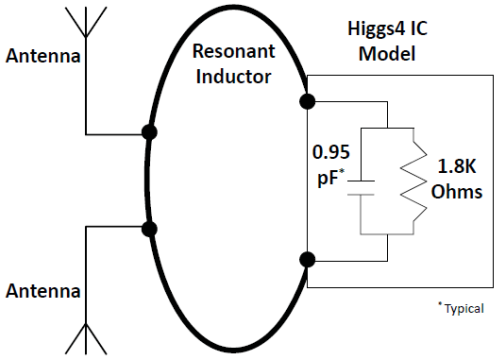


Pin Configuration and Soldering Footprint

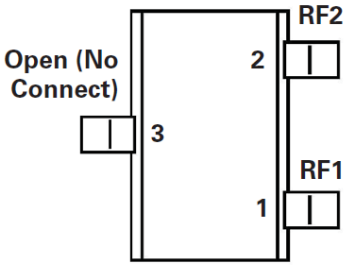


**Pin Configuration**

| Pin # | Pin Name | Description |
|---|---|---|
| 1 | RF1 | RFID antenna RF connection |
| 2 | RF2 | RFID antenna RF connection for differential antenna or GND for single ended designs |
| 3 | Open | Do not connect |

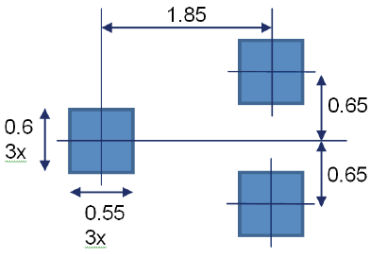

Higgs™4 SOT
Datasheet Addendum

Physical Dimensions
**JEDEC SOT-323**

All dimensions in millimeters unless specified otherwise

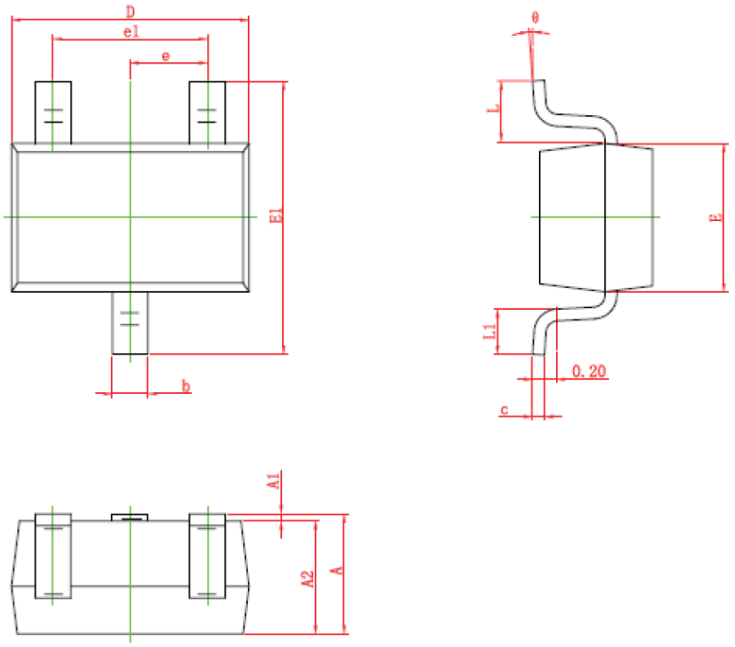


| Symbol | Dimensions In Millimeters | | Dimensions In Inches | |
|---|---|---|---|---|
| | Min | Max | Min | Max |
| A | 0.900 | 1.100 | 0.035 | 0.043 |
| A1 | 0.000 | 0.100 | 0.000 | 0.004 |
| A2 | 0.900 | 1.000 | 0.035 | 0.039 |
| b | 0.200 | 0.400 | 0.008 | 0.016 |
| c | 0.080 | 0.150 | 0.003 | 0.006 |
| D | 2.000 | 2.200 | 0.079 | 0.087 |
| E | 1.150 | 1.350 | 0.045 | 0.053 |
| E1 | 2.150 | 2.450 | 0.085 | 0.096 |
| e | 0.650 TYP | | 0.026 TYP | |
| e1 | 1.200 | 1.400 | 0.047 | 0.055 |
| L | 0.525 REF | | 0.021 REF | |
| L1 | 0.260 | 0.460 | 0.010 | 0.018 |
| θ | 0° | 8° | 0° | 8° |

## Tape Dimensions

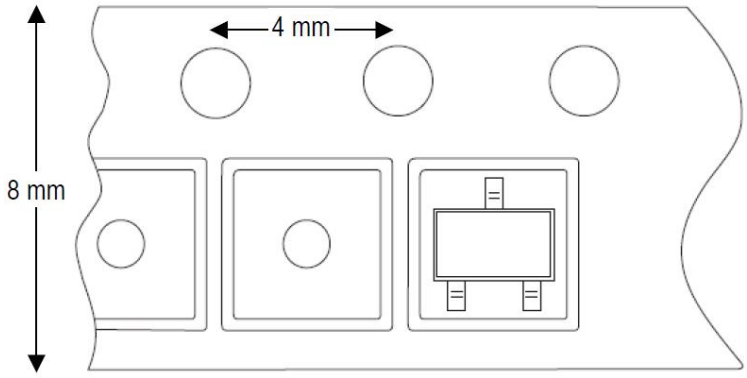


## Reel Dimensions

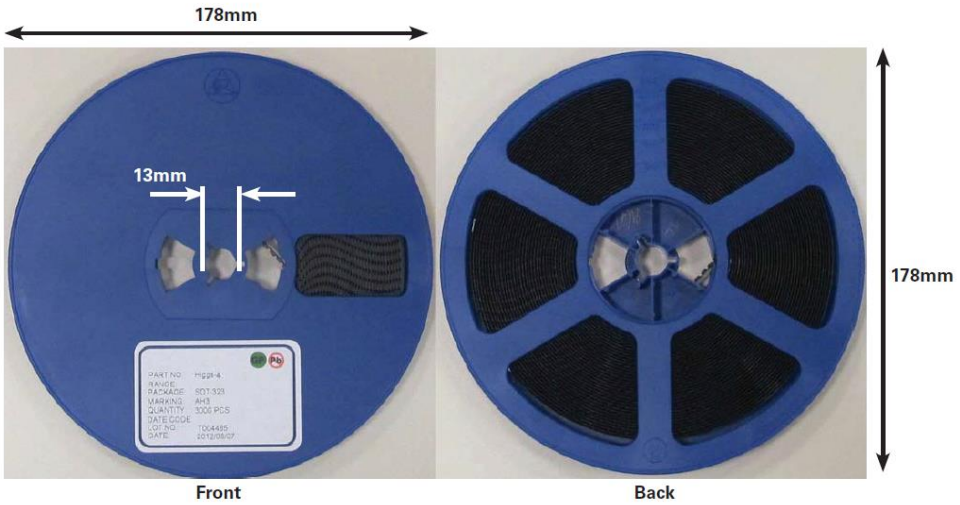

# Higgs™ 4 SOT Datasheet Addendum

## Absolute Maximum Ratings

Absolute maximum ratings are those values beyond which the device could be permanently damaged. Absolute maximum ratings are stress ratings only and functional device operation is not implied. Operating the device beyond the absolute maximum ratings may permanently degrade device performance and/or shorten operating lifetime.

| Parameter | Rating |
|---|---|
| Input Current Across Input Pads | 10mA |
| Maximum RF Input Power | +20dBm |
| Power Dissipation (TAMB = 25°C) | 100mW |
| Storage Temperature Range | -40°C to +85°C |
| Assembly Survival Temperature (60 seconds) | +235°C |
| ESD Immunity (HBM) | 2kV |

## Operating Conditions and Electrical Characteristics

| Symbol | Parameter | Conditions / Capability | Min | Typ | Max | Units |
|---|---|---|---|---|---|---|
| **Operating Conditions** | | | | | | |
| $T_A$ | Operating Temperature | | -50 | | +85 | °C |
| $f_{in}$ | Operating Frequency | | 840 | | 960 | MHz |
| **Electrical Characteristics** | | | | | | |
| $S_R$ | Sensitivity during Read | With 2dBi directivity of dipole | | -20.5 | | dBm |
| $I_S$ | Interference Signal Suppression | | | -4 | | dB |
| $R_P$ | Equivalent input parallel resistance | At -20.5 dBm input power | | 1800 | | Ohms |
| $C_P$ | Equivalent input parallel Capacitance | At -20.5 dBm input power | | 0.95 | | pF |
| $D_{ret}$ | Data Retention | | | 50 | | Years |
| $P_{cycl}$ | Programming Cycles at 25°C | | | 100,000 | | Cycles |

## Ordering Information

| Part | Model Number | Description |
|---|---|---|
| Higgs™ 4 IC | ALC-370-SOT | SMD Package: SOT-323 |



June 24, 2014

Alien Technology
18220 Butterfield Blvd.
Morgan Hill, CA 95037
866-RFID NOW
www.alientechnology.com

# Appendix C

UHF Gen 2 RFID Tag Chip (IPJ-P5003, IPJ-P5005)

## Monza® 4 Dura Product Brief

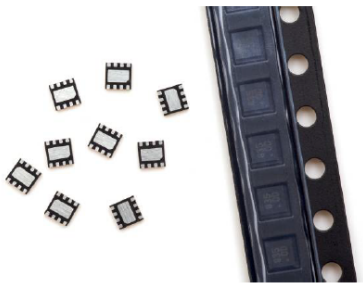

## Overview

With availability of Monza® 4 tag chips in a packaged format (Monza 4 Dura), Impinj extends the advantages of fully EPCglobal-compliant, high-performance, Monza-powered tags to printed circuit board (PCB) applications and enables ruggedized tag designs.

Monza 4 Dura is supported by standard PCB surface mount assembly techniques, meaning easy integration into products designed with PCBs, as well as other electronic applications where soldered connections are preferred. Impinj encased the Monza 4 tag chips in a µDFN package, making it the industry's smallest and lowest profile tag chip part.

Electronics manufacturers can leverage RFID to monitor work in progress, track inventory, follow board revision history, and prevent counterfeiting. The protection the package offers enables many new opportunities to use UHF RFID in the industrial marketplace.

Monza is supported by a family of innovative antenna designs that not only optimize tag performance for wide-ranging requirements and specific market applications, but also enable whole new categories of use.

## Features

- **True3D antenna technology**—patented, dual-differential antenna ports enable compact omni-directional tags, improving read reliability
- Superior read sensitivity of –17.4 dBm (with single port operation, 19.9 dBm with True3D) combined with excellent interference rejection yields a read range of 16 meters (21 meters with True3D)
- Industry-leading write sensitivity of -14.6 dBm for unparalleled commissioning and bulk encoding reliability.
- Available memory options to support large user-memory applications
- **Block permalocking** adds flexibility in memory usage
- Field-rewritable NVM provides programming flexibility and 100,000-cycle/50-year retention reliability
- Write rate of 5 ms for 32-bit writes enables 2500 tags/minute programming
- 8-pin uDFN package accommodates surface-mount assembly
- Industrial temperature range (–40 °C to +85 °C) yields reliable performance under harsh conditions

## Applications

- PCB Tracking
- Ruggedized tag designs
- Asset inventory and management, especially those with high reliability requirements
- Item-level tracking
- Work-in-progress tracking

Revision 4.0, 2011-11-18

www.impinj.com

## Operating Conditions and Electrical Characteristics

| Parameter | Min | Typ | Max | Units | Comments |
|---|---|---|---|---|---|
| Operating Frequency | 860 | | 960 | MHz | |
| Read Sensitivity Limit (Single Port) | | -17.4 | | dBm | |
| Read Sensitivity Limit (True3D) | | -19.9 | | dBm | |
| Write Sensitivity Limit (Single Port) | | -14.6 | | dBm | |
| Write Sensitivity Limit (True3D) | | -17.1 | | dBm | |
| Operating Temperature | -40 | | 85 | ºC | |
| Data Retention | | 50 | | Years | |
| Programming Cycles | | 100,000 | | Cycles | |
| Recommended Source Admittance | | 0.6 – j7.2 | | mS | Single Antenna Port |
| Package Intrinsic Inductance | | 24 | | nH | Parallel RL model of recommended Admittance |
| Package Intrinsic Resistance | | 1650 | | Ω | |
| ESD | | | 2000 | V | Human Body Model |
| DC Input Voltage | | | ± 3.5 | Volts | Applied across two pins |
| DC Input Current | | | ± 0.5 | mA | Into any input pin |

## Package Dimensions

| Parameter | Min | Typ | Max | Units | Comments |
|---|---|---|---|---|---|
| Package Length ($P_l$) | 1.9 | 2.0 | 2.1 | mm | |
| Package Width ($P_w$) | 1.9 | 2.0 | 2.1 | mm | |
| Package Height ($P_h$) | 0.45 | 0.50 | 0.55 | mm | |

## Package Pin Out

| Pin Name | Pin No. | Description |
|---|---|---|
| RF1+ | 8 | **Differential RF Input Pads for Antenna 1**—isolated from the RF Input Pads for Antenna 2 |
| RF1- | 4 | |
| RF2+ | 1 | **Differential RF Input Pads for Antenna 2**—isolated from the RF Input Pads for Antenna 1 |
| RF2- | 5 | |
| — | 2,3,6,7 | No connects (NC) |

## Tape and Reel Format

| Parameter | Value | Comments |
|---|---|---|
| Reel Size | 7 in (17.8 cm) | Outside diameter |
| Hub Size | 2.16 in (5.5 cm) | Inside hub diameter |
| Quantity/reel | 3000 | Units |

Monza® 4 Dura

## Detailed Package Drawing

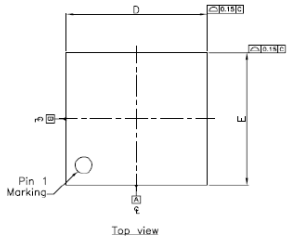


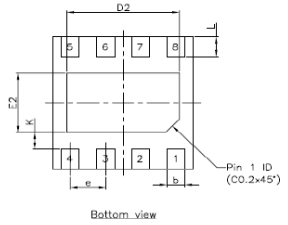


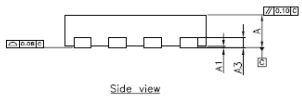


| SYMBOL | MIN. | NOM. | MAX. |
|---|---|---|---|
| A | 0.45 | 0.50 | 0.55 |
| A1 | 0.00 | 0.02 | 0.05 |
| A3 | | 0.152 REF | |
| b | 0.18 | 0.25 | 0.30 |
| D | 1.90 | 2.00 | 2.10 |
| D2 | 1.50 | 1.60 | 1.70 |
| E | 1.90 | 2.00 | 2.10 |
| E2 | 0.80 | 0.90 | 1.00 |
| e | | 0.50 BSC | |
| K | 0.20 | | |
| L | 0.20 | 0.30 | 0.45 |

NOTES:
1. ALL DIMENSIONS IN MILLIMETER ANGLES IN DEGREE.
2. COPLANARITY APPLIES TO THE EXPOSED PAD AS WELL AS THE TERMINALS. COPLANARITY SHALL NOT EXCEED 0.08 MM.
3. WARPAGE SHALL NOT EXCEED 0.10 MM.
4. PACKAGE LENGHT/PACKAGE WIDTH ARE NOT CONSIDERED AS SPECIAL CHARACTERISTIC.
5. REFER JEDEC MO-229.
6. MARKING IS FOR PACKAGE ORIENTATION REFERENCE ONLY.

## Tape And Reel Drawing

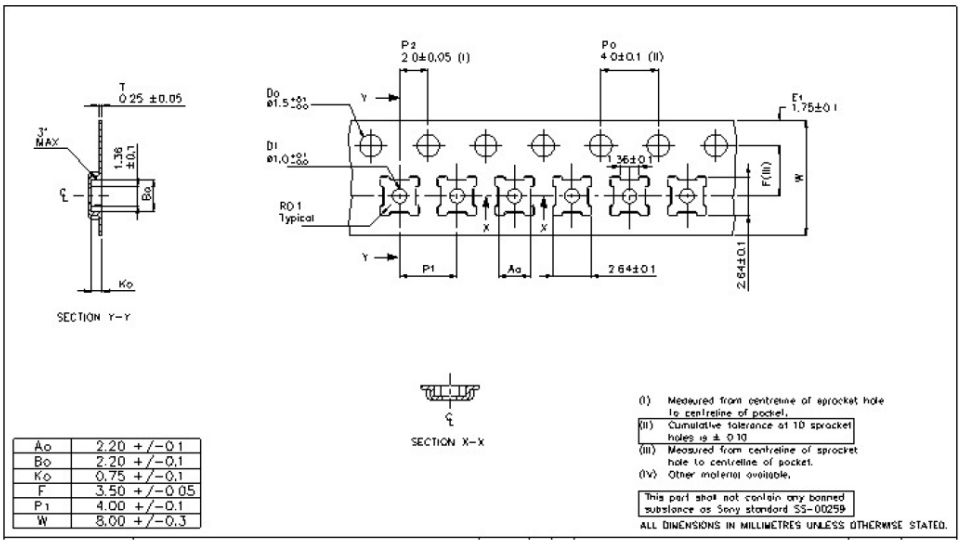


| | |
|---|---|
| Ao | 2.20 +/-0.1 |
| Bo | 2.20 +/-0.1 |
| Ko | 0.75 +/-0.1 |
| F | 3.50 +/-0.05 |
| P1 | 4.00 +/-0.1 |
| W | 8.00 +/-0.3 |

## Ordering Information

| Part | Description |
|---|---|
| IPJ-P5003 | Monza 4QT Dura (packaged silicon), industrial temperature range |
| IPJ-P5005 | Monza 4E Dura (packaged silicon), industrial temperature range |

## Notices:



This product is covered by one or more of the following U.S. patents. Other patents pending. 7283037, 7026935, 7049964, 7501953, 7030786, 7246751, 7245213, 7408466, 7187290, 7215251, 7116240, 7183926, 7312622, 7307528, 7388468, 7394324, 7120550, 7253719, 7380190, 7403122, 7307529, 7472835, 7561866, 7405659, 7307534, 7528728, 7423539, 7123171, 7420469, 7541843, 7448547, 7525438, 7482251

# List of Publications

1. **A. P. Sohrab**, Y. Huang, M. Hussein, M. Kod and P. Carter, "A UHF RFID Tag With Improved Performance on Liquid Bottles," *IEEE Antennas and Wireless Propagation Letters*, vol. 15, pp. 1673-1676, 2016.

2. **A. P. Sohrab**, Y. Huang, M. Kod, M. Hussein and P. Carter, "Label-type 3D RFID tag mountable on metallic and non-metallic objects," *2016 Loughborough Antennas & Propagation Conference (LAPC)*, Loughborough, pp. 1-3, 2016.

3. **A. P. Sohrab**, Y. Huang, M. N. Hussein and P. Carter, "A Hybrid UHF RFID Tag Robust to Host Material," *IEEE Journal of Radio Frequency Identification*, vol. 1, no. 2, pp. 163-169, June 2017.